SMALL MOLECULE PHOTORESIST MATERIALS FOR NEXT GENERATION LITHOGRAPHY

A Dissertation

Presented to the Faculty of the Graduate School

of Cornell University

In Partial Fulfillment of the Requirements for the Degree of

Doctor of Philosophy

By

Marie Elyse Krysak

January 2013

© 2013 Marie Elyse Krysak

SMALL MOLECULE PHOTORESIST MATERIALS FOR NEXT GENERATION LITHOGRAPHY

Marie Elyse Krysak, Ph.D.

Cornell University, 2013

Photolithography remains the most efficient method to create semiconductor devices. Moore's law states that the number of transistors per integrated circuit will double every four years. In order to successfully continue this trend of miniaturizing feature sizes, new, smaller sized patterning materials must be studied. Small molecule photoresists are being developed for high resolution patterning. Low molecular weight amorphous materials, or molecular glasses (MGs), have emerged as alternatives to polymeric resist materials. They combine the benefits of small molecular size with the favorable aspects of polymers, such as a high glass transition temperature (Tg) and the ability to form thin films. Inorganic-based nanoparticles are currently being explored as next generation photoresists. These materials are similar in architecture to MGs, but are comprised of an inorganic core that provides excellent thermal stability and resistance to plasma etching.

This research focuses on the synthesis and characterization both MG and nanoparticle resist materials for high resolution patterning. The materials studied are designed for use with Extreme Ultraviolet Lithography (EUV-L), using a wavelength of

13.5 nm. This next-generation technique is believed to be the key to extending patterning capabilities to sub 30 nm and beyond.

Small molecule resists materials have been specifically designed for use with alternative lithographic processing techniques. Small, rigid structures were designed for vapor deposition, which has been examined as an alternative to spin-coating. This process has been shown to deposit a uniform film, free from defects and impurities, without the use of solvent. Sub-millisecond laser heating is a relatively new technique that is studied as an alternative the post exposure bake. This method has shown the ability to reduce line edge roughness while simultaneously improving resist sensitivity. Systematically designed MG photoacid generators have been used to characterize the acid diffusion behavior during laser heating as compared to traditional hotplate heating. The development of resist materials for these new processes is a critical step in the preparation of these processes for widespread use in lithographic processing.

BIOGRAPHICAL SKETCH

Marie Krysak was born in Johnson City, NY in March 1986. From an early age, she knew that science and math were her favorite subjects. Of course, that didn't stop her from trying her hand at almost anything that came her way. Junior high and high school were a big blur of basketball, track and field, dance classes, regional and national competitions, voice lessons and school musicals. Performing was her great passion and she never passed up an opportunity to be on stage. Around 11th grade, she could see her life taking one of two paths. Either she would go to college to major in science, or she would go to a music school to major in performing or music education. After much soul searching, and some very good advice to not turn a great hobby into work, she decided science was the way to go.

In the fall of 2004, Marie enrolled at the Rochester Institute of Technology as a chemistry major. From the very first quarter, she knew she had made the right decision, as she thoroughly enjoyed the classes in her major. Unsatisfied by even the smallest block of free time, she joined the dance team, the rugby team, and overloaded her class schedule every quarter. She was approached by Prof. Gerald Takacs and was offered a summer research position after her freshman year, which she enthusiastically accepted. It was then that she really started to take an interest in research. She continued to work in the lab throughout the rest of her time in college. She took a job in the chemistry stockroom during her second year, and had the opportunity to chat with the professors running lab sections. It was during these chats that the professors had convinced her to consider graduate school. Right around spring quarter of her second year, she also

realized that she was on track to graduate the following year. As the thought of getting a job seemed almost terrifying, graduate school applications started rolling. She was accepted into Cornell University before Christmas, and immediately knew that Cornell was the place she wanted to be. It is located in a beautiful area, and is a highly reputable school. She finished her undergraduate studies and enthusiastically waited for the start of the Teaching Assistant Training Program.

The three-week program filled with name-games, safety trainings and valuable teaching classes was a light schedule, allowing for plenty of time to make friends with the other students. As she happily explored Ithaca during the beautiful summer months with her new friends, excitement brewed for the year ahead.

Despite this easygoing introduction to graduate school, she was in no way, shape or form prepared for what lay ahead. Fall semester quickly divulged into perpetual all-nighters, teaching, and endless grading, all while searching for a research group during what seemed like non-existent free time. However, the other graduate students became some of her best friends, and significantly eased the stresses of first year. She met with Prof. Ober towards the end of the semester, after talking with a few professors and not finding the right fit. During their first meeting, she knew this was the group for her. She thoroughly enjoyed her research, even though it could be frustrating at times. She was also presented with many opportunities to travel and work in various labs around the world, and gained invaluable knowledge in doing so. During the summer of her 4th year, she was fortunate to receive the opportunity to complete a summer internship at Intel in Portland, Oregon. She felt right at home there, and decided to return for a full-time position on completion of her degree.

This thesis is dedicated to my mother and father, who never stopped believing in me no matter how rough the road, as well as my brother, Dan and sister, Nikki, for their endless support

ACKNOWLEDGEMENTS

I would first and foremost like to sincerely thank Prof. Ober for giving me the opportunity to pursue my research, as well as all the guidance and support he has given me these past five years. I'm also thankful for all the opportunities to travel and network with professionals connected to my area of research. I would also like to thank my committee members, Prof. Giannelis and Prof. Dichtel for their guidance during my graduate work and for reviewing my thesis. The staff at CNF and CCMR are also gratefully acknowledged for the assistance in running tools and experiments.

I would like to thank my collaborators, Prof. Hans-Werner Schmidt, as well as Christian Neuber and Tristan Kolb for their hospitality during my visits to Bayreuth, as well as their guidance during the vapor deposition process. Prof. Reyes Sierra and Wenjie Sun at the University of Arizona, and the staff at Lawrence Berkeley National Lab are thanked for their discussions and their efforts during various collaborations.

I especially would like to thank the Semiconductor Research Corporation Education Alliance and Intel for giving me a fellowship to support my research, as well as GlobalFoundries and SEMATECH for providing funding for my various projects. Kenji Yoshimoto, Paul Zimmerman and Warren Montgomery in particular are thanked for their guidance and support of my research.

I would like to thank my parents for their everlasting support and encouragement, especially during these last five years. Thank you for always listening, especially to the phone calls with more sobs than actual words. Thank you for giving me one of the many

places I used to write as I practiced the art of Thesis Feng Shui – change location, change motivational energy.

To my friends in graduate school, I would have never gotten through this without your support. Srikant, my office neighbor who I can always count on for a lunch companion and a shoulder to cry on, thank you for always being there, especially at 2:00 am before group meeting day. Erika, I know I've told you many times, but our Thursday dinners always kept me sane. Thank you for always knowing exactly what I am thinking and always being supportive, even if my decisions weren't always rational. To Ryan, for always keeping me laughing no matter how ridiculous the topic. I will be counting the days until you get to Portland. To Joni, who started as my recruitment weekend roommate; I guess it's only fitting that we end grad school as roommates. Thank you and Kieli for letting me stay with you as I finished my thesis. I will miss our girl time and can't wait for a reunion at the wedding! To Chin, thank you for being such a great friend these past several years. To Taz and Ry, thank you for so many fun nights at the Taz Mahal.

To the Ober group members, past and present, thank you all for your help and support. To Christine, my conference buddy and office mate, I will very much miss sitting next to you. Thank you to Anuja and Jing who trained me when I was a lost, scared, and generally confused first-year. To Markos, Evan and Yeon Sook, thank you for working so hard on those late nights at RIT and Berkeley Lab. So many of you have helped me through this process and were vital to my success.

TABLE OF CONTENTS

BIOGRAPHICAL SKETCH…………………………………………………………..iii

DEDICATION…………………………………………………………………..……v

ACKNOWLEDGEMENTS…………………………………………………………vi

TABLE OF CONTENTS…………………………………………………………viii

LIST OF FIGURES……………………………………………………………...xv

LIST OF TABLES………………………………………………………………….xx

CHAPTER 1: SMALL MOLECULE PHOTORESISTS FOR HIGH RESOLUTION LITHOGRAPHY

Abstract………………………………………………………………………………1

1.1 Introduction…………………………………………………...……………………2

1.1.1 Chemical Amplification

1.1.2 Photoacid Generators (PAGs)

1.2 Molecular Glasses……………...…………………………………………………11

1.2.1 Planar MG Architecture

1.2.2 Branched MG Architectures

1.2.3 Ring MG Architectures

1.2.4 Spiro and Fused MG Architectures

1.2.5 MGs for 193 nm Lithography

1.3 Hybrid Organic-Inorganic Small Molecule Photoresists……………….……….24

1.4 Alternative Lithographic Processing Steps……………………..………………..28

1.4.1 Vapor Deposition

1.4.1.1 MGs for Vapor Deposition

1.4.2 Sub-Millisecond Laser Post Exposure Bake

1.5 Summary………………………….……..………………………………..32

Acknowledgements……………………………………………………………32

References………..………………………………………………………………33

CHAPTER 2: SYNTHESIS AND CHARACTERIZATION OF MOLECULAR GLASS PHOTOACID GENERATORS

Abstract……………………………………………………………………..44

2.1 Introduction……………………...……………………………………………..44

2.2 Experimental……………………………...…………………………………....46

2.2.1 Materials

2.2.2 Characterization

2.2.3 Synthesis

2.2.4 Lithographic Characterization of Photoacid Generators

2.2.5 Constructing Bilayers to Measure Acid Diffusion

2.3 Results and Discussion………………………..………………………………54

2.3.1 Synthesis and Design Strategy of Molecular Glass Photoacid Generators

2.3.2 Thermal Properties

2.3.3 Optical Properties

2.3.4 Lithographic Characterization

2.3.5 Acid Diffusion Analysis

2.3.6 Patterninng by E-beam Lithography

2.3.7 Environmental Compatibility Evaluation

2.4 Conclusions…………………………………………………………………………70

Acknowledgements…………………………………………………………...…………70

References………………………………………………………………………………..72

CHAPTER 3: INORGANIC-ORGANIC HYBRID NANOPARTICLE PHOTORESISTS FOR NEXT GENERATION LITHOGRAPHY

Abstract……………………………………………………………………………..76

3.1 Introduction…………………………………………………………………….....77

3.2 Experimental……………………………………………………………………...79

3.2.1 Materials

3.2.2 Nanoparticle Synthesis

3.2.3 Negative Tone Processing

3.2.4 Positive Tone Processing

3.2.5 Characterization

3.3 Results and Discussion……………………………………………………………..83

3.3.1 Synthesis

3.3.2 Structural Characterization

3.3.3 Effect of Ligand on Nanoparticle Solubility

3.3.4 Patternability

3.3.5 EUV Lithography

3.3.5.1 Absorbance at EUV wavelength

3.3.5.2 Additive Concentration

3.3.6 Etch Resistance

3.4 Conclusions……………………………………………………………...…102

Acknowledgements…………………………………………………………..……104

References……………………………………………………………………….....105

CHAPTER 4: INVESTIGATION OF THE PATTERNING MECHANISM OF ORGANIC/INORGANIC HYBRID NANOPARTICLE PHOTORESISTS

Abstract…………………………………………………………………...…….109

4.1 Introduction…………………………………………………………………...110

4.2 Experimental………………………………………………………………….112

4.2.1 Materials

4.2.2 Synthesis

4.2.3 Negative Tone Processing

4.2.4 Positive Tone Processing

4.2.5 Characterization

4.3 Results and Discussion……………………………………………………….115

4.3.1 Investigation of Patterning Mechanism During UV Irradiation

4.3.1.1 Optical Absorbance

4.3.1.2 Nuclear Magnetic Resonance Analysis

4.3.1.3 Scanning Transmission Electron Microscopy (TEM) Analysis

4.3.1.4 In-Film Fourier Transform-Infrared (FT-IR) Spectroscopy Analysis

4.3.2 Investigation of Patterning Mechanism During Post Exposure Bake

4.3.2.1 Thermogravimetric Analysis

4.3.2.2 In-Film FT-IR Analysis

4.3.2.3 Film Thickness Changes After Various Process Steps

4.3.2.4 Particle Size after PEB

4.3.3 Patterning Mechanism

4.3.3.1 Negative Tone Patterning

4.3.3.2 Positive Tone Mechanism

4.4 Conclusions……………………………………………………………...…134

Acknowledgements…………………………………………………………..……137

References……………………………………………………………………...…….138

CHAPTER 5: USING SMALL MOLECULE RESIST MATERIALS TO INVESTIGATE THERMAL INDUCED BEHAVIORS DURING SUB-MILLISECOND LASER POST EXPOSURE BAKE

Abstract……………………………………………………………………………143

5.1 Introduction……………………………………………………………….…..144

5.2 Experimental……………………………………………………………….....147

5.2.1 Materials

5.2.2 PAG Synthesis and Characterization

5.2.3 Molecular Glass Resist Synthesis

5.2.4 Characterization

5.2.5 Bilayer Fabrication Procedure

5.2.6 Lithographic Processing

5.3 Results and Discussion……………………………………………………………150

5.3.1 Series 1 PAGs

5.3.1.1 Acid Diffusion Behavior

5.3.1.2 Lithographic Performance

5.3.2.1 Thermal Characterization

5.3.2.2 Lithographic Characterization

5.3.2.3 Relative Acid Diffusion Behavior

5.3.2.4 Diffusivity and Activation Energy

5.3.2.4 Lithographic Patterning

5.3.3 Low Tg Molecular Glasses

5.3.3.1 Thermal Decomposition

5.3.3.2 Lithographic Patterning of Low Tg MG Resists with Laser-PEB

5.4 Conclusions……………………………………………………………...……170

Acknowledgements…………………………………………………………………..170

References……………………………………………………………………...…..172

CHAPTER 6: INVESTIGATION OF SINGLE-COMPONENT MOLECULAR GLASSES FOR ALL-DRY LITHOGRAPHY

Abstract……………………………………………………………………………....176

6.1 Introduction………………………………………………………………...….177

6.2 Experimental……………………………………………………………………180

6.2.1 Synthesis of Molecular Glasses

6.2.2 Characterization

6.2.3 Film Deposition

6.2.3.1 Vapor Deposition

6.2.3.2 Spin-coating

6.2.4 Lithographic Processing

6.2.5 Dissolution Rate Measurements

6.3 Results and Discussion……………………………………………………...……..186

6.3.1 Design Strategy and Synthesis

6.3.2 Thermal Analysis

6.3.3 Vapor Deposition

6.3.4 Dissolution properties

6.3.5 Lithographic patterning with solvent developer

6.3.6 In-film investigation of cross-linking reaction

6.3.7 All-Dry Lithographic Processing

6.4 Conclusions……………………………………………………………...……197

Acknowledgements……………………………………………………………..200

References…………………………………………………………………………201

SUMMARY AND FUTURE WORK…………………………………………...…..205

LIST OF FIGURES

CHAPTER 1

Figure 1.1 Process of patterning by photolithography 4

Figure 1.2 Decomposition of t-BOC upon exposure to acid 7

Figure 1.3 Structures of APEX and ESCAP resists 8

Figure 1.4 Acid generation mechanism of triphenylsulfonium salt PAGs 10

Figure 1.5 Planar MG derivatives 14

Figure 1.6 Branched MG structures 17

Figure 1.7 Calix[4]resorcinarene MG photoresists 19

Figure 1.8 Cholic acid and cyclodextrin derivatives for 193 nm MG photoresists 23

Figure 1.9 Silane MG derivatives 25

Figure 1.10 Nanoparticle and MG photoresist structures 27

Figure 1.11 Scheme of physical vapor deposition and thermal development 30

CHAPTER 2

Figure 2.1 Molecular glass PAG structures 55

Figure 2.2 UV absorbance spectra for each MG PAG 59

Figure 2.3 Plot of intensity at the maximum absorbance as a function of UV dose and the calculated quantum yields 60

Figure 2.4 The effect of PAG concentration on the sensitivity of the MG resist- MG PAG system

Figure 2.5 Comparison of acid diffusion behavior of the MG PAGs 64
Figure 2.6 Actual feature size as a function of exposure dose for TPS-Nonaflate (TPS-NF) and 3P3A MG PAG with a MG resist 66
Figure 2.7 SEM image of 100 nm line/space patterns with low LER obtained by patterning with e-beam lithography 68

CHAPTER 3
Figure 3.1 Structures of the inorganic-organic hybrid nanoparticles 81
Figure 3.2 Size distribution plots of nanoparticle systems via dynamic light scattering 84
Figure 3.3 In-film FT-IR spectra of HfO_2-MAA and HfO_2-IBA 85
Figure 3.4 1H NMR spectra for a) HfO_2-IBA and b) HfO_2-MAA 87
Figure 3.5 TGA curves of the hybrid nanoparticle systems 88
Figure 3.6 Solubility testing of HfO_2 nanoparticles functionalized with various ligands 90
Figure 3.7 a) Positive and b) negative-tone patterns with HfO_2-IBA nanoparticle resist mixed with a photo-radical initiator (DPAP) c) positive and b) negative-tone patterns with HfO_2-IBA nanoparticle resist mixed with a photoacid generator 92
Figure 3.8 Relative photo-absorption cross section of atoms at EUV wavelengths 94
Figure 3.9 SEM images of HfO_2-MAA (negative tone) containing varied concentrations of PAG and free methacrylic acid 97
Figure 3.10 SEM image of 25 nm line-space patterns with ZrO_2-MAA (negative tone) obtained with EUV lithography with a dose of 4.2 mJ/cm^2 99
Figure 3.11 Top: Relative etch rates of HfO_2-MAA with and without a post-development

bake compared to PHOST. Bottom: SEM image of resist profiles a) before and b) after the post-development bake 100

Figure 3.12 Top: Bottom: SEM images of A) Side view of 1:1 line/space patterns transferred by etching with SF_6/O_2 plasma, B) Side view of 1:1 line/space patterns transferred by etching with CF_4 plasma 101

Figure 3.13 a) AFM image showing pattern surface after O_2 plasma treatment and b) height measurement of remaining patterns 103

CHAPTER 4

Figure 4.1 Nanoparticle resist structures 114

Figure 4.2 UV absorbance of HF-MAA and HF-propionic acid nanoparticles 117

Figure 4.3 UV Absorbance of nanoparticles with different exposure doses 118

Figure 4.4 ^{1}H NMR spectra of HfO_2–MAA films a) before and b) after UV exposure 121

Figure 4.5 TEM images of HfO_2-MAA resist a) before and b) after UV exposure 123

Figure 4.6 Particle size distribution with and without UV exposure as measured by dynamic light scattering 124

Figure 4.7 a) In-film FT-IR spectrum of HfO_2-MAA resist b) In-film FT-IR spectrum of HfO_2-MAA resist after exposure, referencing the unexposed spectrum as a background 126

Figure 4.8 Thermogravimetric analysis of unexposed HfO_2-MAA before and after PEB 128

Figure 4.9 In-film FT-IR of unexposed and exposed films after PEB 130

Figure 4.10 Particle size distributions after a post exposure bake with and without UV

exposure as measured by dynamic light scattering 133

Figure 4.11 Patterning mechanism during UV exposure 135

Figure 4.12 Patterning mechanism during the PEB 136

CHAPTER 5

Figure 5.1 PAG and molecular glass resist structures 148

Figure 5.2 Relative acid diffusion length of the Series 1 PAGs after hotplate and laser-PEB 152

Figure 5.3 Contrast curves of Series 1 PAGs after hotplate and laser PEB 153

Figure 5.4 SEM images of 200 nm line/space patterns by e-beam lithography using a) hotplate PEB and b) laser PEB 155

Figure 5.5 Weight loss percentages as a function of temperature of the Series 2 PAGs 157

Figure 5.6 Contrast curves of the Series 2 PAGs using laser-PEB 158

Figure 5.7 Relative acid diffusion behaviors of Series 2 PAGs with hotplate and laser PEB 159

Figure 5.8 Diffusivity as a function of PEB temperature of the Series 2 PAGs using hotplate and laser PEB 162

Figure 5.9 SEM image of 100 nm dense and isolated lines of the TrisPhenol PAG and CR-15 resist patterned with e-beam lithography 164

Figure 5.10 ^{1}H NMR analysis of tris-t-BOC and tri-HPB-mp-t-BOC after thermal treatment with the CO_2 laser 166

Figure 5.11 Optical images of patterned tris-t-BOC and TrisPhenol PAG with hotplate and laser PEB 168

Figure 5.12 SEM image of tri-HPB-mp-t-BOC and TrisPhenol PAG patterned with e-beam lithography using laser-PEB 169

CHAPTER 6

Figure 6.1 Molecular glass structures 183

Figure 6.2 Synthetic schemes for CM-Binaphthyl and CM-CR2 188

Figure 6.3 All-dry lithography process 190

Figure 6.4 HPLC graph of CM-calix and TPO before vapor deposition and the resulting film after co-deposition of the materials 193

Figure 6.5 Dissolution rates of CM-CR15 in various developers 194

Figure 6.6 SEM image of high resolution patterns obtained by e-beam lithography of CM-CR15 with a dose of 200 $\mu C/cm^2$ and development in isopropanol 196

Figure 6.7 In-film IR spectra of CM-Calix and CM-CR2 198

Figure 6.8 SEM of 1:1 (left) and 1:2 and 1:3 (right)100 nm line/space patterns obtained after all-dry e-beam lithographic processing of CM-Calix 199

LIST OF TABLES

CHAPTER 2

Table 2.1 Thermal Characterization of MG PAGs 57

Table 2.2 Summary of inhibitory concentrations determined for the molecular glass in different toxicity assays 69

CHAPTER 4

Table 4.1 Resist film thickness after various lithographic process steps 131

CHAPTER 5

Table 5.1 Activation energies of Series 2 PAGs with hotplate and laser PEB 163

CHAPTER 6

Table 6.1 Thermal Characterization of Molecular Glasses 191

CHAPTER 1

SMALL MOLECULE PHOTORESISTS FOR HIGH RESOLUTION LITHOGRAPHY

Abstract

The semiconductor industry continues to move forward with the development of technology enabling the fabrication of hundreds of million devices on a single chip. Lithography has been the process used to fabricate such devices, and is constantly evolving to meet the demands of the industry. Material development must keep up with the process changes, and new photoresist design is needed to further push the limits of resolution. This chapter will discuss the lithographic process and give a brief summary of past resist development. Emphasis is placed on small molecule molecular glass photoresists as alternatives to polymeric resists, and their potential for sub-30 nm resolution and beyond. A comprehensive overview of resist structures will be presented, as well as a new resist design based on metal oxide nanoparticles. In addition, recent advances in the resist deposition and post exposure bake processes will also be discussed.

1.1. Introduction

Photolithography is the current method of patterning thin films for nanofabrication in the semiconductor industry. The performance of semiconductors has improved dramatically over the past 30 years due to the reduction of feature sizes. The industry is driven by Moore's Law[1], which states that the number of transistors that can be placed on an integrated circuit will double approximately every two years. The diminution of transistor size has increased processing speed and decreased the power required to run each transistor. In order to keep up with industry demands, both materials and lithography tools must evolve. According to Rayleigh's law, $R = k*\lambda/NA$, the resolution, R, of feature sizes is dictated by the wavelength, λ, of the light used to pattern the film. The constant, k, can be decreased by modifying both the lithographic materials and the exposure tools. As described throughout this text, the reduction of feature sizes has been achieved over time by reducing the patterning wavelength. Recently, efforts to increase the numerical aperture, NA, have been made by the introduction of 193 nm immersion lithography, which is discussed later in detail.

The modern use of the term lithography refers to the selective removal of areas of a thin film. This is usually done with a photoresist, or a photosensitive organic material. UV light is passed through a mask with a master pattern, and the pattern is transferred to the underlying photoresist. A photo-chemical change occurs during this exposure, allowing selective removal of the film during development. Patterning of semiconductors begins with spin-coating a resist solution onto a silicon substrate. The wafer is then baked to remove residual solvent in the film. During exposure, UV light is passed through a mask, where the mask pattern is transferred to the underlying substrate. The photo-labile film undergoes a chemical transformation which, when aided by a post-exposure bake, changes the solubility properties of the exposed portion. The film

is then subject to a developer, which will remove the exposed portion of a positive tone resist, or the unexposed portion of a negative tone resist. Finally, this pattern can be transferred to the silicon substrate by reactive ion etching. Many factors must be addressed when designing a photoresist so that it is compatible with every step of this process, depicted in Figure 1.1. The resist must be soluble in the spinning solvent, and produce an amorphous thin film. Good adhesion to the substrate can be promoted by tailoring the polarity of the polymer so it shows affinity towards the hydrophilic silicon wafer[2]. To ensure the UV light passes through the entire film during exposure, high transparency at the desired wavelength is crucial. A glass transition temperature (Tg) in the desired range is essential, since an optimal PEB temperature is usually just below the Tg[3]. A Tg below the PEB temperature can yield distorted patterns due to reflow of the polymer[4], while a high Tg would require PEB temperatures beyond the point of thermal decomposition. The polymer must have sufficient resistance to the reactive ion etch process in order to effectively transfer the pattern into the silicon substrate. The relative etch resistance of a polymer can be roughly determined by the Ohnishi parameter, $N/(N_c-N_o)$ [5]. N represents the totals number of atoms in the molecule; Nc and No are the total number of carbon and oxygen atoms, respectively. The equation indicates that a high carbon to oxygen ratio is a requisite for high etch resistant resists. As atomic composition is not the only factor that determines etch rates, the ring parameter was also established, which states that cyclic or ring moieties will increase the etch resistance of the polymer[6].

Designing resists to meet the needs of the current patterning technology has been a main component of semiconductor research in the past three decades. Polymer structures have been extensively researched and modified for compatibility with the lithography process. One of the most important structural features of a resist or resist components is the photo-labile portion. The

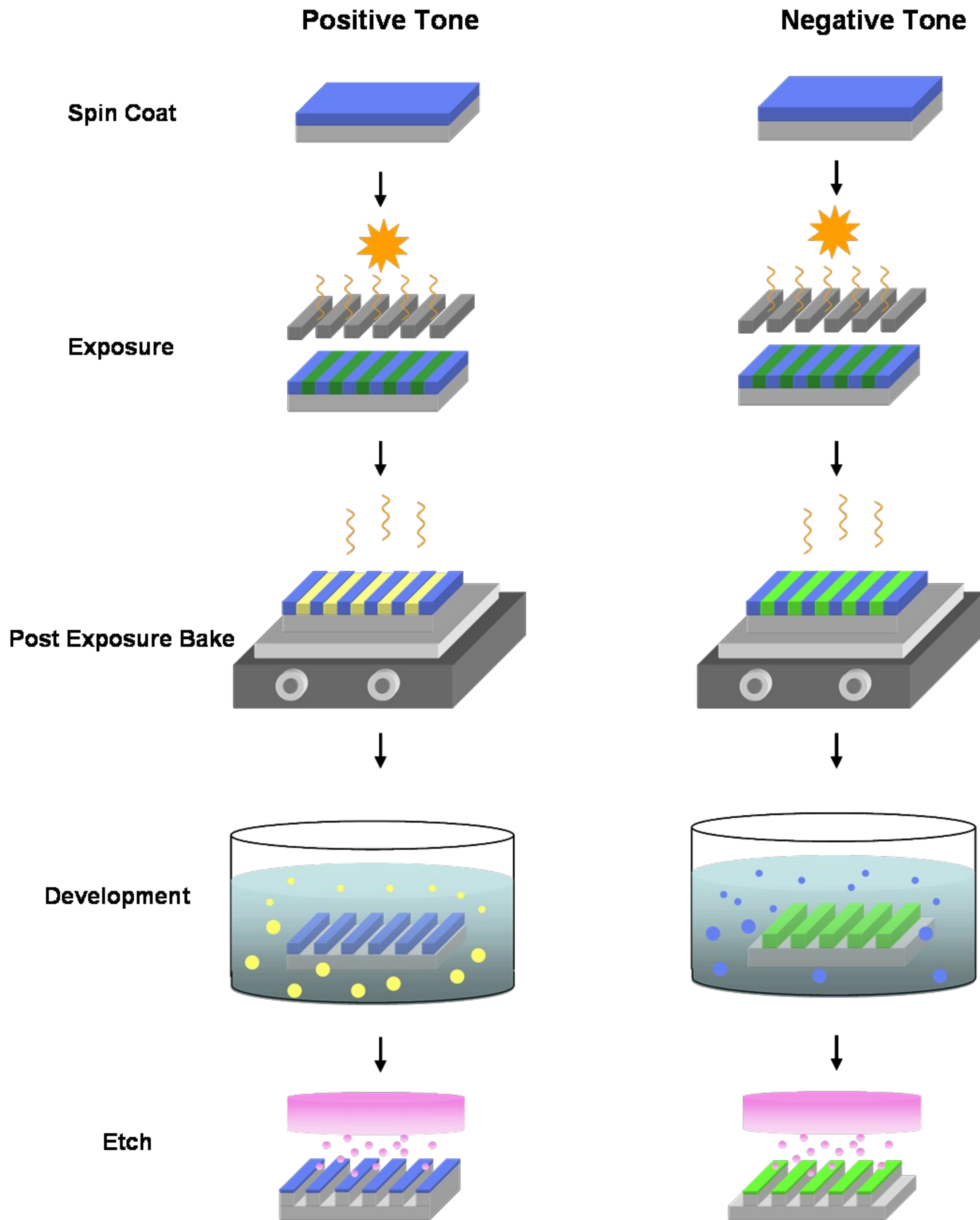

Figure 1.1 Process of patterning by photolithography

chemical transformation that occurs must alter the solubility properties of the material, through a polarity or molecular weight change.

In the early 1980's, polyisoprene-based structures were investigated as positive type resists. It has been shown that cis-1,4-polybutadiene can be cyclized by Lewis acid catalysts[7], and when mixed with a cross-linking agent and exposed to UV light[8]. The two-component diazonaphthoquinone (DNQ)-novolac resist system was a step forward, patterning sub-micron features with i-line (365 nm) technology. DNQ is a photoactive compound that acts as a dissolution inhibitor to the novolac resin when unexposed to UV light. During exposure, DNQ is converted to indene carboxylic acid through a series of chemical transformations. The resulting molecule acts as a dissolution promoter, enabling the novolac resin to dissolve in 0.26 N tetramethylammonium hydroxide (TMAH), the industry standard developer[9]. The development of the xenon-helium (Xe-He) lamps with 254 nm emission and the krypton-fluorine (KrF) laser with 248 nm emission enabled resolution targets beyond the capabilities of the i-line technology[10]. At the lower wavelength, the DNQ/novolac system showed significant performance issues. The resist is highly absorbing in this region, and patterning attempts showed low sensitivity and poor resolution. Some efforts were made to design base-soluble polymers that were more transparent at 250 nm, as well as bleachable photoactive dissolution inhibitors[11], but these were not successful. Other photochemistries were also researched, including main-chain scissionable polymers. When exposed to UV irradiation, methacrylate-based polymers have been shown decompose into smaller units, thus increasing its dissolution rate in various developers[12]. While these polymers had some advantages, they were ultimately abandoned for 248nm exposure due to their low sensitivity.

1.1.1. Chemical Amplification

With the shift to DUV with the KrF laser, the optics required to use this new technology significantly lowered the power of the laser. An entirely new resist chemistry was developed by Ito, Willson and Fréchet in 1982 which drastically increased sensitivity[13]. The resist is decorated with acid-labile groups, and a photoacid generator (PAG) is included in the matrix[14]. When exposed, the PAG produces acid. When baked, the acid will cause a chemical reaction, switching the solubility of the resist and enabling either the exposed or unexposed regions to be developed. Instead of requiring one photon for only a few chemical reactions, the acid is regenerated after each deprotection step, allowing one photon to initiate a large number of reactions, Figure 1.2.

The first chemically amplified resist system was based on poly(4-hydroxystyrene) (PHOST)[13]. The hydroxyl groups were protected with a non-polar *tert*-butoxycarbonyl (t-BOC) functional group. With exposure to acid and heat from the PEB step, the t-BOC group is decomposed, and the remaining PHOST molecule is rendered soluble in 0.26 N TMAH.
Other resists based on the PHOST structure were developed for use with the KrF laser, which improved upon the properties of PBOCST. ESCAP (environmentally stable chemically amplified photoresist)[15] and APEX were developed with free hydroxyl groups to promote solubility in spinning solvents and adhesion to the hydrophilic substrate[16], Figure 1.3. ESCAP features an acid-labile ester monomer, which will reveal a carboxylic acid upon deprotection. This carboxylic acid promotes solubility in the aqueous base developer and improves development contrast between the exposed and unexposed portions. The styrene monomer was added to increase the etch resistance.

Chemically amplified resists have been the workhorse of the semiconductor industry, and much research has been devoted to its understanding. While polymer structures have previously

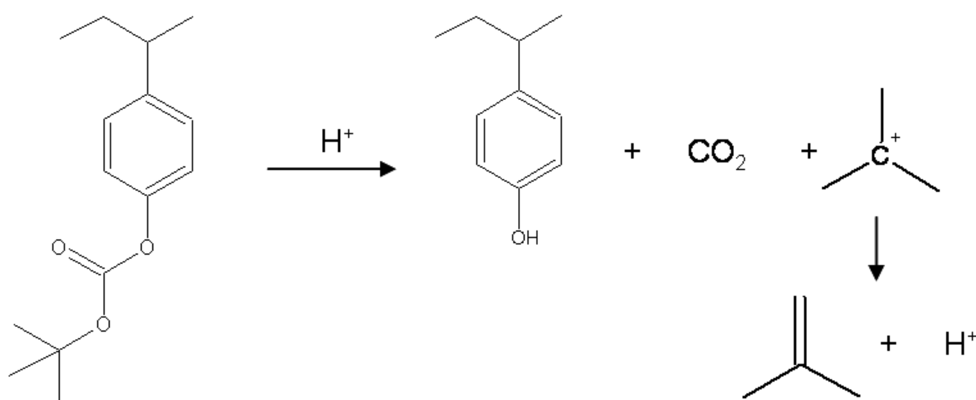

Figure 1.2 Decomposition of t-BOC upon exposure to acid

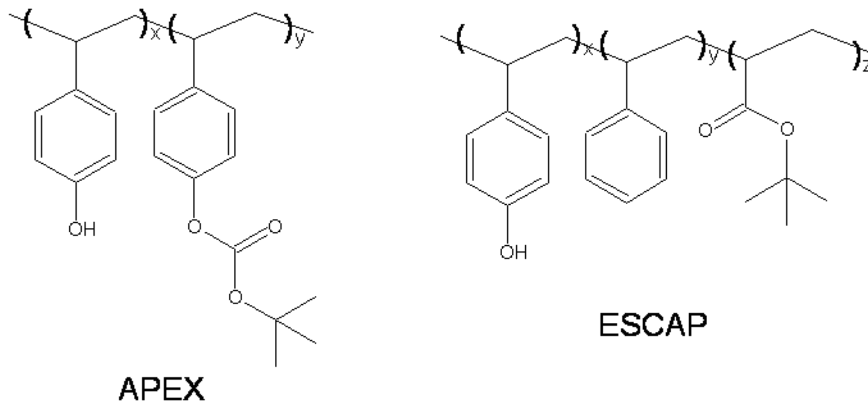

Figure 1.3 Decomposition of t-BOC upon exposure to acid

been considered and are still in development today, this chapter will focus on alternative architectures for photoresist materials.

1.1.2 Photoacid Generators (PAGs)

PAGs are the foundation of chemically amplified resists, and their structures can significantly impact lithographic performance. PAG performance can be quantified by the quantum yield, or a number expressing how many photons are required to convert one acid-labile molecule. Before the concept of chemical amplification, a new set of photons were required for every conversion reaction. Once a PAG molecule has generated acid, the acid is regenerated every time a deprotection or crosslinking event occurs, meaning one set of photons can initiate a cascading set of reactions. The acid generation mechanism for triphenylsulfonium salts is shown in Figure 1.4. Miscibility, acid strength and size, solubility, toxicity and thermal stability are also important factors to consider when designing and choosing a PAG system.

PAGs can either be ionic or non-ionic. The non-ionic molecules are typically based on sulfone or sulfonate esters[17, 18]. While some non-ionic PAGs have shown promising results, ionic PAGs have outshined the non-ionic molecules in terms of performance. Ionic PAGs are typically based on onium salts, such as triphenylsulfonium and diphenyliodonium salts[19]. When combined with a fluorinated counterion, these PAGs show outstanding quantum efficiency and generate quite strong acids. One of the first ionic PAGs to be used in a chemically amplified resist was triphenylsulfonium hexafluoroantimonate[19], but due to toxicity concerns, metallic acid generators have been phased out. Fluorinated sulfonates were used in place of the antimonite, which produces an incredibly strong organic acid. Longer fluorinated chains, such as octaflate and nonaflate substituents, produced stronger acid and showed better lithographic performance than shorter fluorinated chains (ref). Other research has been conducted on the effect of

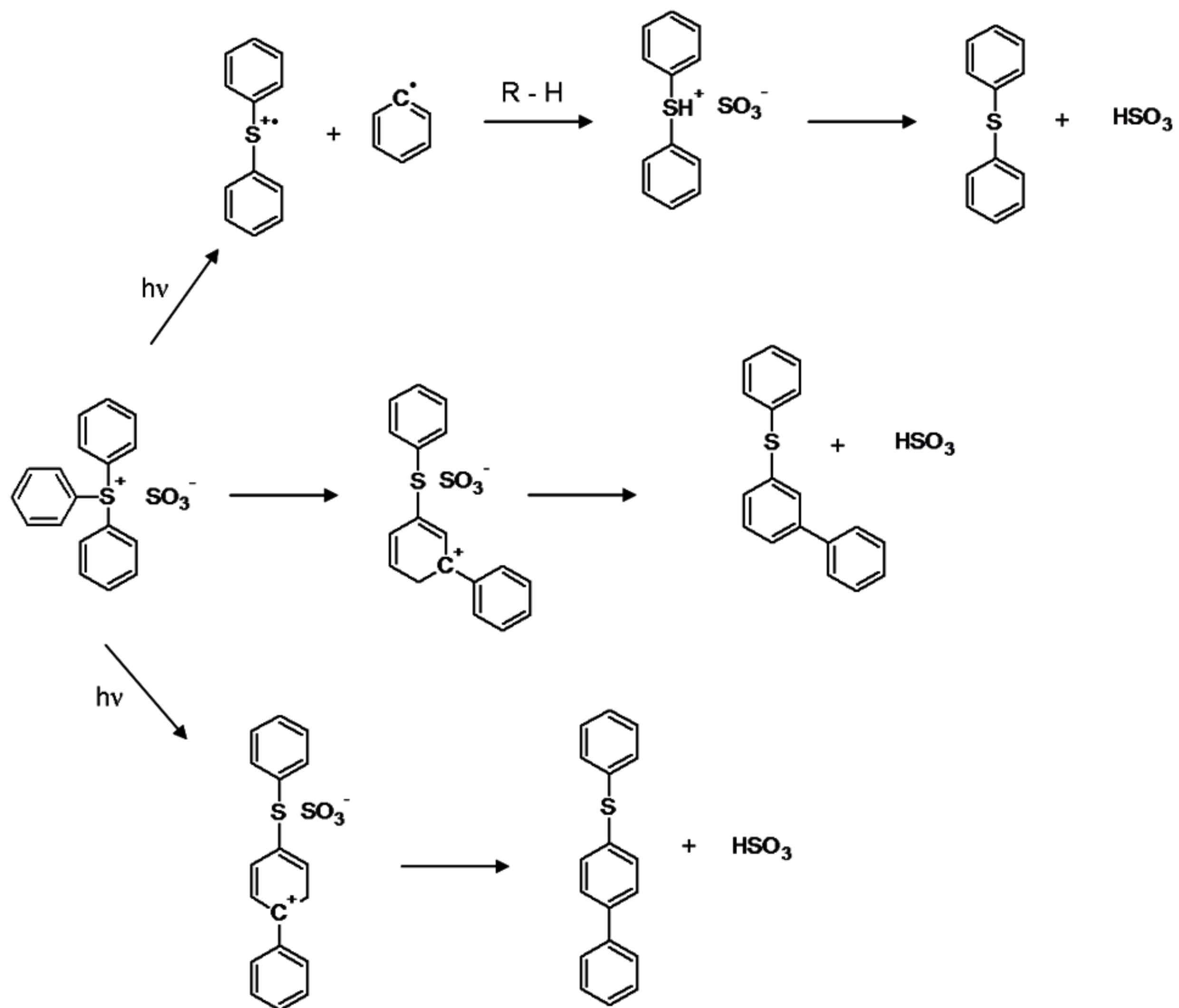

Figure 1.4 Acid generation mechanism of triphenylsulfonium salt PAGs

the size of the acid anion[20]. With a larger anion, the photogenerated acid diffusion length is shorter. The importance of controlling acid diffusion will be discussed later in the chapter.

Recently, however, perfluorooctane sulfonates (PFOS) were found to be global pollutants, and a strong effort ensued to design a new generation of PFOS free PAGS. Ober and co workers have developed a “sweet” PFOS-free PAG based on biocompatible and biodegradable sugars to promote environmentally friendly lithography materials[21].

1.2 Molecular Glasses

As feature sizes are pushed to the 22 nm node and beyond, reducing LER remains a critical challenge that must be addressed. The resists mentioned above are widely based on random copolymer structures. These polymers are polydisperse, relatively large in size and have molecular weights in the range of 5-15 kg/mol. Characteristics such as these can have a negative impact on resist performance[22], and therefore it is necessary to explore other architectures for new resist platforms. Molecular glass (MG) photoresists, or low molecular weight amorphous materials, have emerged as viable alternatives to polymeric structures[23-25].

According to the Tammann rule, every molecule will encounter the glassy state when cooled below its melting temperature. However, small molecules usually have an affinity for crystallization, and will typically crystallize before the Tg is reached. MGs possess certain structural features that inhibit crystallization and promote the formation of a glassy state. Rigid, bulky, asymmetrical substituents can promote vitrification, because of their ability to decrease the free volume of the material and restrict intramolecular mobility. The molecular structure of early MGs has been based on the structures of PHOST and ESCAP, with etch resistant phenolic rings decorated with acid-labile protecting groups. Instead of attaching these functional groups to

a polymer backbone, they are bound to an etch resistant MG core, with a total molecular size of around 5 nm.

MGs have the ability to combine the benefits of polymers such as an amorphous structure, thin-film forming ability and thermal stability with the characteristics of small molecules, such as high purity and a well-defined structure. The glass transition temperature, or Tg of these materials needs to be sufficiently high to withstand elevated temperatures during the PEB. If heated beyond the molecule's Tg after exposure, the material will relax, causing the exposed and unexposed regions to blur together, significantly affecting the shape and size of the desired features.

The main attraction of these molecules is their relatively small size, which is about an order of magnitude smaller than polymer photoresists. The radius of gyration of a MG is smaller than that of a polymer, which can translate to lower LER values of patterned MG resists[22]. In comparison to polymers, the distribution of free volume in MGs is confined to much smaller units[26], which can have an effect on the acid diffusion kinetics in the resist film. The small size of the free volume units can potentially limit the diffusion length of the photogenerated acid, thereby reducing LER[27]. The importance of understanding acid diffusion kinetics in resist matrices will be discussed later in the chapter.

1.2.1 Planar MG Architectures

The first MGs used as photoresists were reported by Shirota and co-workers[28]. These were branched structures based on phenylbenzene derivatives. The MGs were patterned with e-beam lithography, but showed very poor sensitivity compared to other resist using chemically amplified acidolysis photochemistry. The structures were later modified with t-BOC protecting groups, which will deprotect upon contact with acid leaving pendant hydroxyls, rendering the

molecule soluble in aqueous base developer. This MG proved to have sufficient sensitivity, and was the first MG system to demonstrate 100nm line-space patterns.

Ober and coworkers have examined MG structures based on a hydroxyphenylbenzene core. The effect of molecular size and isomeric forms on Tg and lithographic performance have been researched[29]. Figure 1.5 shows the library of planar MGs synthesized for this study. The MGs with all *meta* or all *para* substituents consistently exhibited a lower Tg than those with a mixture of *meta* and *para* substituents. This is because of the increased asymmetry of the MGs with mixed *meta* and *para* substituents. Hydrogen bonding will also significantly affect the Tg of the material. Structures with large amounts of hydroxyl groups exhibit a higher Tg than those with few hydroxyls, because of the increased hydrogen bonding. As the t-BOC protection ratio increased, the Tg of these molecules consistently fell, due to the lack of substituents capable of hydrogen bonding.

The mixed *meta*/*para* hexa-hydroxyphenyl benzene derivative exhibited a high Tg of over 120°C. Upon EUV irradiation, this MG produced sub-30 nm features, the first reported resist of the architectural class to do so. Through understanding the structure-property relationship of this class of MGs, it was possible to engineer a MG structure capable of pushing resolution limits further than previously possible.

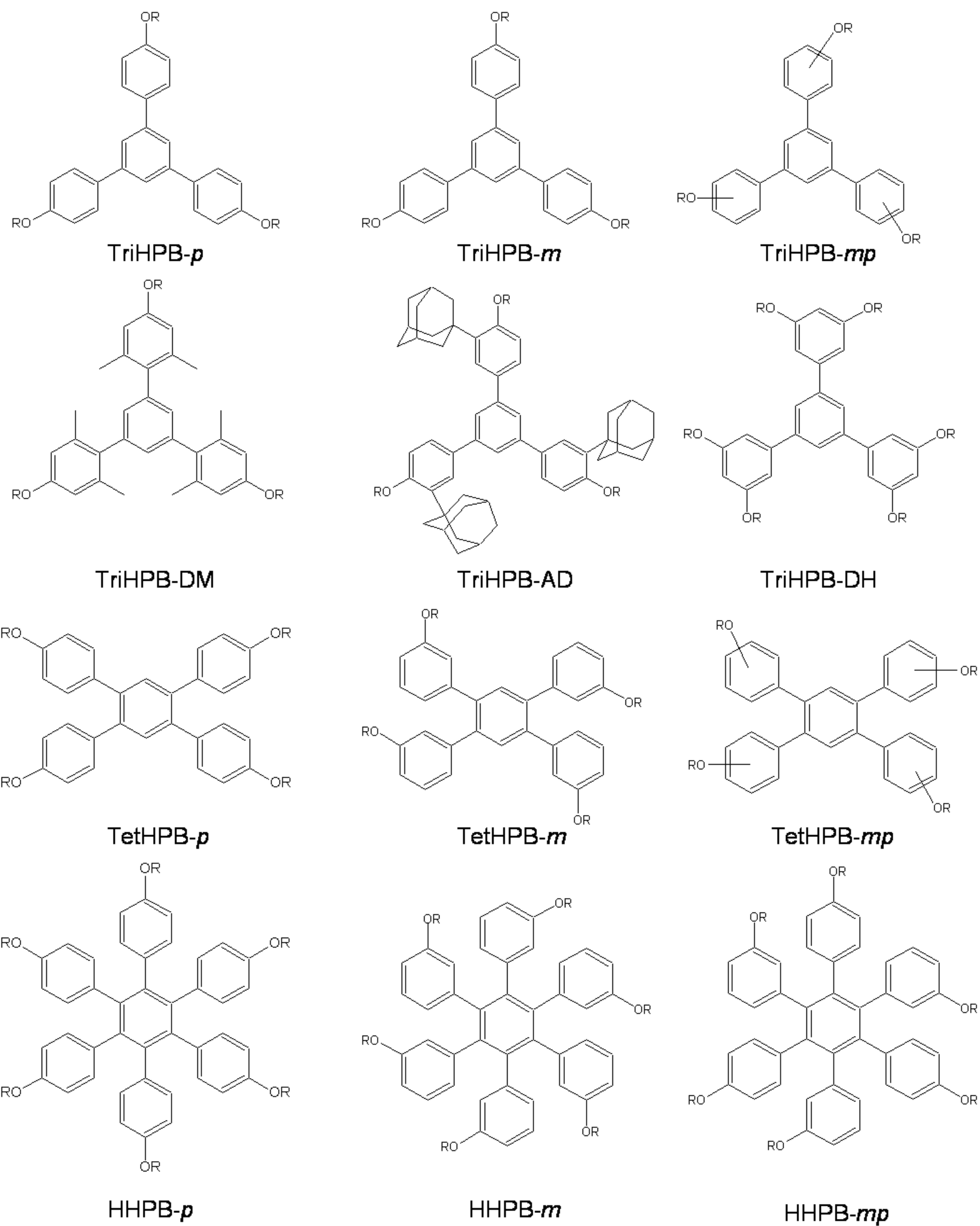

Figure 1.5 Planar MG derivatives

1.2.2 Branched MG Architectures

One of the more commonly studied MG structures is the branched architecture based on poly(4-hydroxystyrene), with short, bulky arms radiating from the core. These systems provide high etch resistance and a sufficiently high Tg. The hydroxyl groups provide base solubility and the ability to functionalize the glass with acid-labile substituents. Ober and co workers have developed a library of phenolic branched MG resists, which are shown in Figure 1.6[30]. In agreement with other MG structure studies, the Tg of the molecules increased with increasing molecular weight.

Molecule CR-15 was later used by industrial researchers to test an experimental scanning probe lithography system[31]. A heated AFM tip is used to tap the surface of the resist, which induces its evaporation in controlled amounts. The CR-15 MG was chosen because of the numerous hydrogen bonding interactions between its many hydroxyl groups. The energy barrier for thermal activation is lower for hydrogen bonds than that of covalent bonds, which allows the MG to be thermally activated without large stresses from the AFM tip. Since material removal can be done in stages, three-dimensional structures can also be patterned using this technique.

Henderson and co workers have explored branched phenolic structures functionalized with epoxide[32]. With the addition of a PAG, these negative tone MG resists undergo acid-catalyzed cationic polymerization upon UV or e-beam irradiation. Unlike chemically amplified resists, once the generated acid initiates the polymerization, it is used up and cannot participate in another reaction. The tetra-functional MG patterned with high resolution and low LER, resolving 35 nm line/space patterns, and an LER (3σ) of 2.3 nm for 70 nm dense lines. With high resolution and low LER, MGs are showing potential for use with next-generation lithography techniques.

Acid diffusion remains a critical challenge with chemically amplified resists, in both polymers and MGs. In particular, inhomogeneous distribution of acid throughout the resist matrix can lower resolution and increase LER[33]. This can be caused by poor miscibility of the PAG and resist molecules. Acid diffusion length is also a critical issue[34]. During the PEB, acid is mobilized to catalyze the deprotection reaction. With diffusion lengths measured near 45 nm for some resist matrices, this can significantly limit resolution and affect the LER of the resulting patterns.

Ober and co workers, in collaboration with the National Institute of Standards and Technology (NIST), have fundamentally studied the acid diffusion kinetics in a variety of MG structures during the PEB[35]. It was discovered that the ring structures have a higher diffusion coefficient than planar or branched structures, though reactivity and trapping of acids did not systematically vary between different architectures. This study provides vital information that can help predict the lithographic properties of various MG architectures.

Recently, Henderson and co workers have developed MG photoresists with PAGs covalently bonded to the MG core. These structures employ both ionic and non-ionic PAGs and are based on branched and twin core structures, with the MG core attached to both the acid anion and the cation[36, 37]. The single component resists provide film homogeneity as there are no blended components in the resist matrix and have the potential to control acid diffusion. They also allow for high PAG loading, which has been shown to improve sensitivity[38]. The system with PAG bound to the cation suffered from resolution limitation because of uncontrollable acid diffusion. The non-ionic PAG bound MG was able to produce patterns with 40 nm resolution with e-beam lithography, with 3.9 nm LER. These molecules are a step to improve homogeneity in the film and control the acid diffusion length.

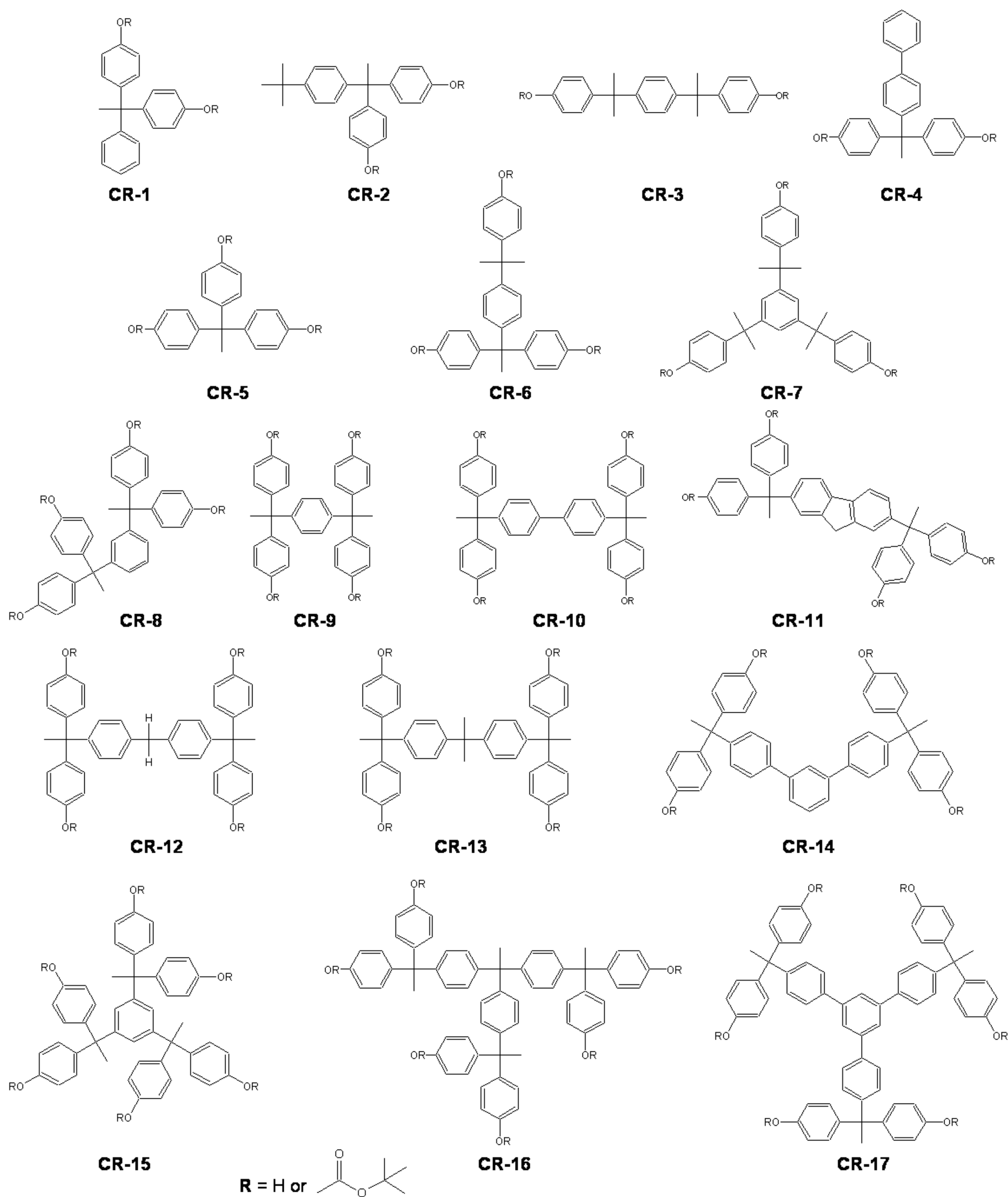

Figure 1.6 Branched MG structures

1.2.3 Ring MG Architectures

Ring structures are an excellent candidate for MG resist cores. The rigidity of the ring can promote amorphous behavior with relatively small molecules with a modest molecular weight. One of the first MG ring systems was developed by Ueda and co-workers for 365 nm lithography, and was based on a calix[4]resorcinarene structure. The material produced negative tone patterns when combined with a PAG and crosslinker, and positive tone patterns when protected with t-BOC and combined with a PAG[39, 40].

Ober and coworkers have extensively studies ring-shaped MGs with a calix[4]arene core structure. Figure 1.7 depicts the structures of the resorcinarene derivatives, with the hydroxyl groups partially protected with t-BOC. The *tert*-butyl silane-substituted calixarene exhibited a Tg of 140°C when t-BOC protected, and resolved 70 nm lines when patterned with e-beam lithography. T-BOC protected C-4-hydroxyphenyl-calix[4]resorcinarene (C-HPB-4-R) has been employed as a positive tone EUV resist and has produced sub-30 nm patterns[41].

Industrial researchers have modified the C-HPB-4-R structure with hexafluoroalcohol moieties, which improved its solubility in common casting solvents[42]. E-beam exposure produced 30 nm features, though some bridging of lines was present at these dimensions. The photospeed at EUV wavelengths was very fast, 6 mJ/cm2, with the resist printing 50 nm dense lines.

Similar to calix[4]arene, the waterwheel-shaped cyclic oligomer known as "Noria" has been synthesized by Nishikubo and co workers and studied as a candidate for high resolution lithography[43-46]. Different protecting groups were tested, and Noria protected with an adamantyl ester produces sub-30 nm patters with EUV exposure. Ober and co workers have modified the

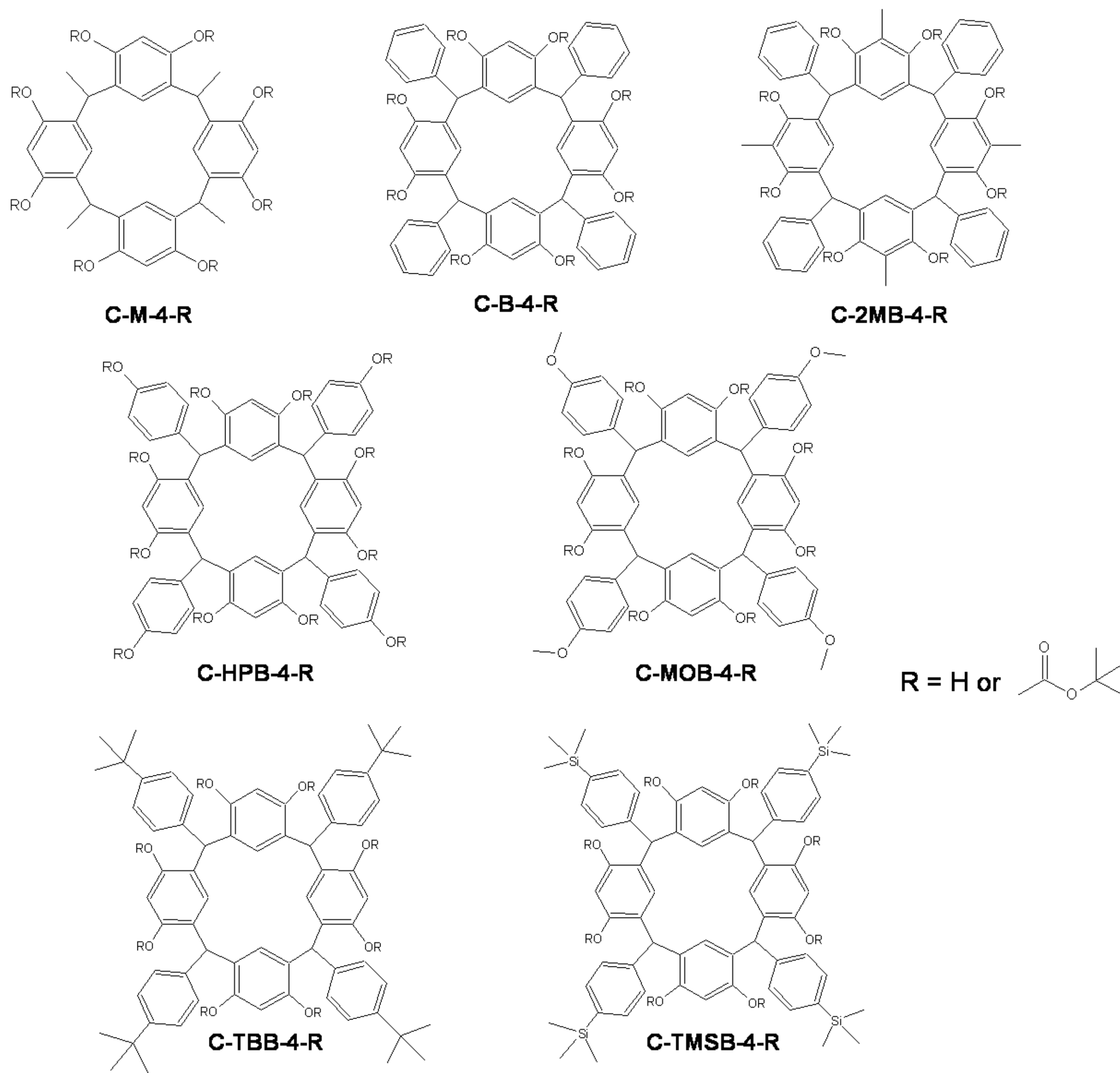

Figure 1.7 Calix[4]resorcinarene molecular glass photoresists

Noria structure with t-BOC and *tert*-butyl ester protecting groups and produced sub-100 nm patterns by using supercritical CO_2, an environmentally friendly developer[47].

1.2.4 Spiro and Fused MG Architecture

Molecular rigidity can be found in fused ring structures. The restricted rotation of this structure can raise the Tg, as well as hinder crystal formation. Ober and co workers have developed a three-component negative tone MG system consisting of a spiro-based MG, PAG and cross-linker[48]. Upon e-beam irradiation, the PAG generates acid and catalyzes cross-linking between the pendant hydroxyls of the spiro MG and the cross-linking agent. This negative tone system is capable of producing 60 nm line/space patterns with e-beam exposure.

Henderson and co workers have explored spiro cores functionalized with epoxide and oxetane functional groups[49]. The likely low Tg of these small molecule MG resists will not affect the patterning properties of this resists, since acid-catalyzed cationic polymerization occurs during the PEB step. Through PEB temperature studies, it was discovered that the epoxide group has a faster initiation and a slower propagation step than the oxetane group upon polymerization, which led to higher resolution and lower LER of the patterned epoxy-substituted MG.

Fullerene, a conjugated, 60-carbon cage, has been studied as an MG core for next-generation lithography by Robinson and co workers[50-54]. The cage has been functionalized with ester and ether linkages, and mixed with a cross-linker and PAG to produce negative-tone patterns. The fullerene derivatives are about 1 nm in diameter, and their carbon-rich structure affords them a high plasma etch resistance. When patterned with e-beam lithography, these resists have shown high resolution with 12 nm isolated lines at a dose of 11 $\mu C/cm^2$.

1.2.5 MGs for 193nm Lithography

Aromatic rings have been a common building block for 248 nm and EUV resists because of their high etch resistance and relative transparency at these wavelengths. However, these conjugated substituents absorb a significant amount of light at 193 nm, the current workhorse of the semiconductor industry, and therefore cannot be used in 193 nm resists. MGs for 193 nm lithography employ the same ring or branched architectures as EUV resists, but instead use saturated aliphatics as substituents.

Sooriyakumaran and co workers have developed a MG with a polyhedral oligomeric silesquioxane (POSS) core[55]. The core itself is a cage-like hybrid molecule comprised of silicon and oxygen with a low melting point. However, when functionalized with bulky substituents and acid labile groups, the Tg of the POSS derivative reached 80°C.The molecule utilized low activation energy (Ea) protecting groups to keep the processing temperatures down below the Tg. The resist resolved patterns with dry and immersion 193 nm lithography, and resolved 30 nm line/space patterns with e-beam lithography. Kim and co workers have developed a photobleachable POSS-based MG[56]. This non-chemically amplified resist undergoes a Wolff rearrangement upon UV exposure to generate a carboxylic acid, thereby rendering the PASS derivative soluble in aqueous base. While acid diffusion was not a problem because of the absence of a photoacid generator, the resist suffered from low sensitivity and resolution.

Cholic acid is a well-known molecule in 193 nm resists because of its bulky, rigid structure and ease of functionality with pendant hydroxyl groups. Shiono and co-workers have synthesized MGs using two cholic acid molecules as side groups attached to an ether or cyclohexyl core[57]. These materials have Tgs around 85°C, the low Tg due to the long, flexible side group linkages, and have shown 120 nm line/space patterns with e-beam lithography. Ober

and co workers have expanded on this concept by using cholic acid side arms attached to a rigid adamantane core[58]. These higher Tg materials were able to produce sub-100 nm line/space patterns with e-beam lithography(same ref). Ober and co workers have synthesized a series of adamantane-based MGs with a tripodal structure and acetal or ester protecting groups[59]. Some of these molecules exhibited Tgs over 120°C and showed high dry etch resistance because of the rigid adamantane core. E-beam lithography patterning resolved 200 nm features. These structures were later modified with bulkier side arms and showed sub-100 nm patterns with e-beam exposure[60, 61]. Cholic acid has also been modified by attaching acid-labile groups to its hydroxyls and carboxylic acid functionalities. When exposed with e-beam lithography and developed in supercritical carbon dioxide, the cholate derivative functions as a negative tone resist and resolves 150 nm line/space patterns[62]. Figure 1.8 illustrates cholic acid and cyclodextrin structures.

Cyclodextrin is a widely studied core for 193 nm lithography because of its high Tg and many hydroxyl groups that can be functionalized. A downfall of using cyclodextrin-based photoresists is their poor dry etch resistance. Because of their high oxygen content and low rigidity, these molecules etch very quickly. In an effort to improve etch resistance by adding rigidity to the resist, Kim and co workers introduced adamantane to the cyclodextrin core, taking advantage of its host-guest forming properties. When protected with t-BOC, these resists have shown 200 nm features with e-beam lithography[63]. Ober and co workers added carborane, a cage structure comprised of boron and carbon atoms, to the cyclodextrin core and increased its etch resistance beyond that of poly-hydroxystyrene[64], a standard resist for etch rate comparison. The resist was protected with *tert*-butyl ester acid-labile groups. These are converted to carboxylic acid upon deprotection, with has a higher pKa than the secondary hydroxyls generated with

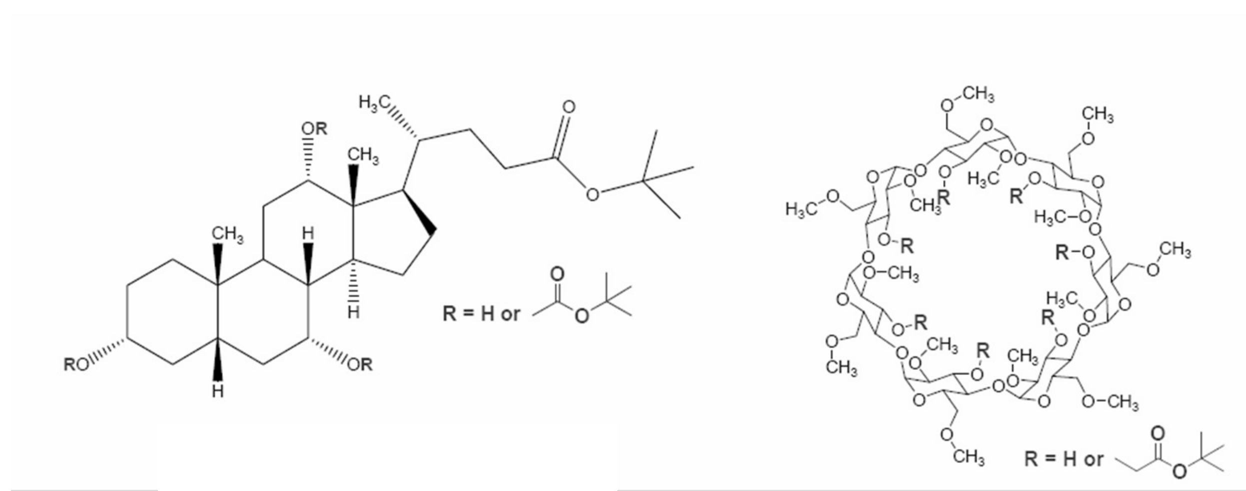

Figure 1.8 Cholic acid and cyclodextrin derivatives for 193 nm MG photoresists

deprotection of t-BOC. This enables higher contrast between the exposed and unexposed regions. Nishikubo and co workers synthesized cyclodextrin MGs with *tert*-butyl ester protecting groups, and resolved 100 nm patterns with e-beam lithography[65].

1.3 Hybrid Organic-Inorganic Small Molecule Photoresists

Molecular glass photoresists have typically been organic molecules. Ober and co-workers have explored MG resists containing a silicon core with phenolic arms radiating outward (Figure 1.9)[66]. The silicon atom provides etch resistance, as well as low absorbance at EUV wavelength. While it is necessary for the resist to absorb some EUV photons to enable the necessary chemical transformation, resist films that absorb too much radiation will prevent light from reaching the bottom of the film, resulting in t-topping or sloped resist sidewalls. The addition of silicon to these MG resists increased both the etch resistance and sensitivity at EUV wavelengths[66]. These MGs broaden the scope of materials to be considered as suitable photoresists candidates for next generation lithography.

Recently, a new resist design has garnered much attention in the lithographic community. The architecture is similar to a MG, with a core decorated with functional groups that undergo a chemical transformation upon exposure. However, instead of an organic or single atom inorganic core, the core consists of a dense metal oxide nanoparticle cluster. The two architectures are compared in Figure 1.10. Ober and co workers have synthesized hafnium oxide nanoparticles stabilized with an organic ligand, (S)-(+)-Tetrahydrofurfuryl-O-O0-diacetyl-(2R,3R)-hydrogentartrate (TDHT), to create photoresist-miscible nanoparticles[67]. The particles are less that 5 nm in diameter and are readily soluble in propylene glycol methyl ether acetate (PGMEA), a common spinning solvent with up to 50% wt/wt loading. The unusually high solubility of these metal oxide particles can be attributed to the similarity of the organic ligands with the casting

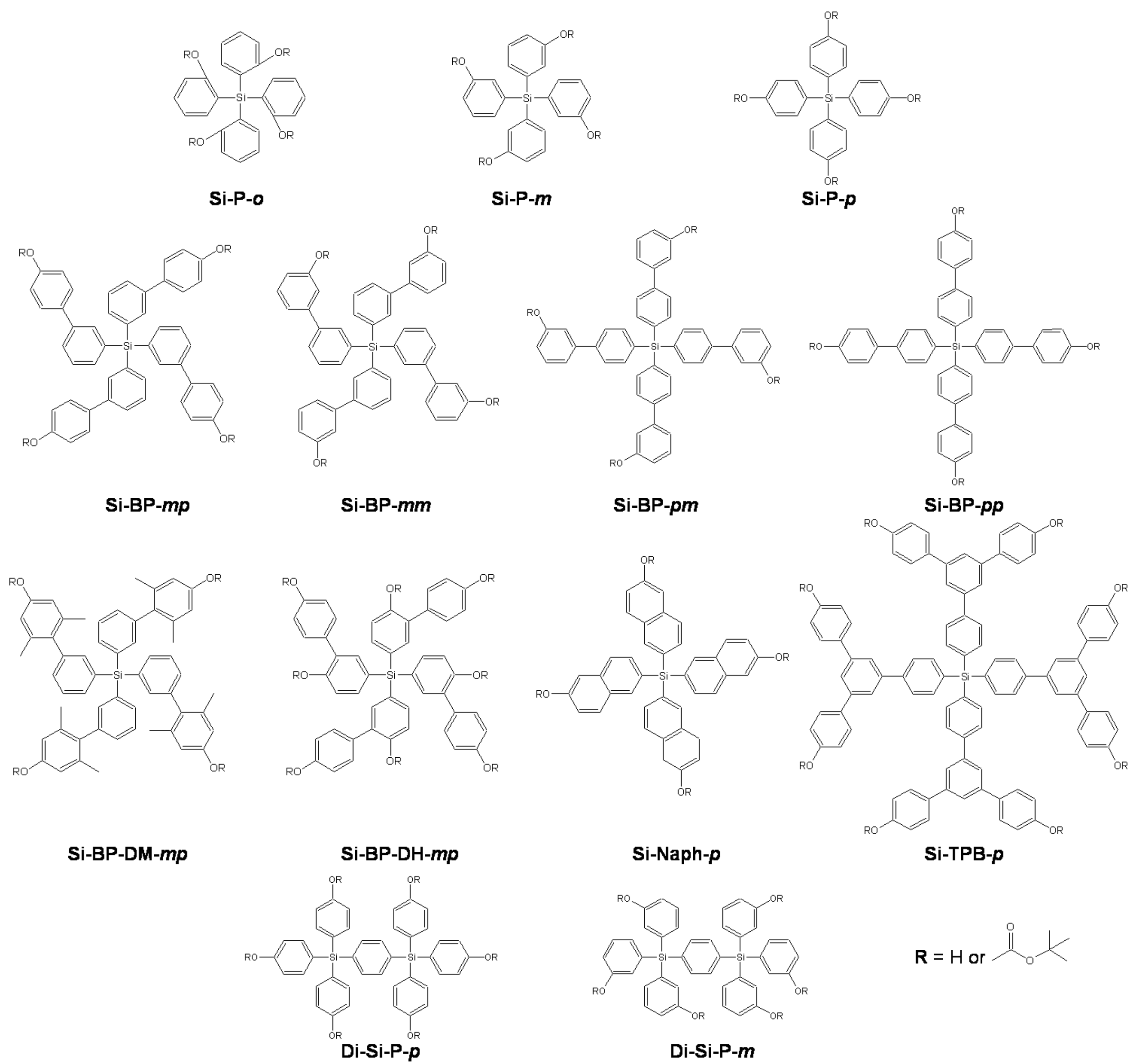

Figure 1.9 Silane MG derivatives

solvent. The particles were blended at 8 wt. % with poly(methyladamantane methacrylate-co-a-methacryloxy-g-butyrolactone) (PMAdMA-co-GBLMA) photoresist and resolved 200 nm line/space patterns with e-beam lithography.

Ober and co workers have discovered that by attaching photo-switchable ligands directly to the metal oxide core, the nanocomposites themselves can be used as a photoresist[68-70]. The structure of the resist is remarkably similar to that of a MG. Each contain a small etch resistant core decorated with photo-switchable components. With a particle diameter of around 2-3 nm, the size of the nanoparticle resist is on par with that of a MG, which is typically around 5 nm. The narrow size distribution of the nanoparticles is a testament to the monodispersity of the resist. Though a Tg of the nanoparticles has not been confirmed, they form a homogeneous, amorphous film when spin-coated onto a silicon wafer.

Methacrylic acid has been attached to a hafnium oxide core and a zirconium oxide core, and when mixed with a photo-radical initiator, can be patterned with DUV and e-beam lithography. The resist shows dual-tone patterning capability when altering the PEB and developing conditions. EUV exposure has produced 26 nm line/space patterns with an exceptionally high sensitivity of 4.2 mJ/cm^2[2,71]. The high etch resistance of the resist material enables a 40 nm thin film to be used, reducing the aspect ratio of the patterns, thereby improving resolution.

Keszler and co workers have developed a photopatternable inorganic hardmask which is also based on metal oxides[72-74]. The peroxo-modified hafnium oxide sulfate and zirconium oxide sulfate will cross-link when irradiated with UV or e-beam and produce negative tone images. High resolution patterns of 12 nm half-pitch lines have been cleanly resolved with e-beam lithography, though a high dose of 244 $\mu C/cm^2$ is required to do so. With EUV exposure, 15 nm

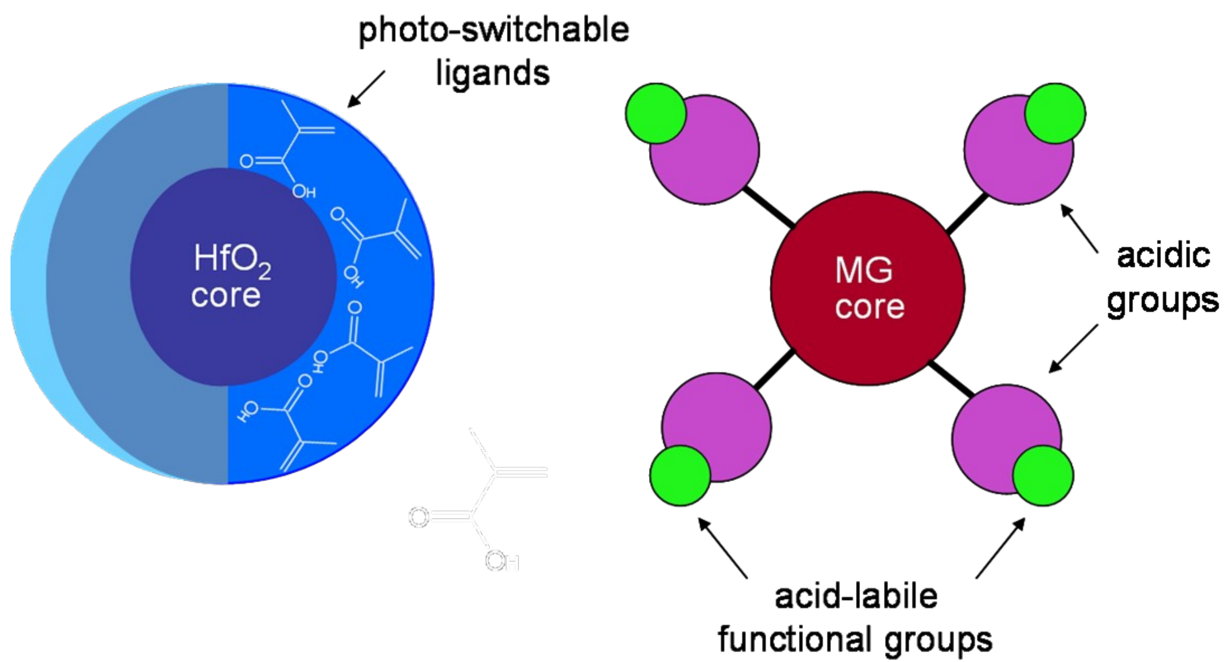

Figure 1.10 Nanoparticle and MG photoresist structures

half-pitch lines have been resolved. The metal oxide core is exceptionally etch resistant, enabling a film thickness of 20 nm, thereby reducing the aspect ratio and the threat of pattern collapse at such small dimensions.

Much research is still required to fully understand and optimize these systems. The radical new metal-oxide resist design has the potential to drive resolution limits even further, as these initial studies have resist properties that have surpassed the leading organic resist candidates.

1.4. Alternative Lithographic Processing Steps

While engineering resist materials has proved to improve resolution limits, it is necessary to consider each step of the lithography process as potential for improving the final product.

1.4.1 Vapor Deposition

Spin-coating is a common method of film deposition currently used in industry. However, several problems still exist with this method. Casting solvents must be completely dust free and without impurities. These solvents must possess a suitable vapor pressure and the ability to form a uniform thin film to be considered for use, therefore solvent choice is limited. Spin-coating is a wasteful procedure and excess solvent must be disposed of. Photoresists must be soluble in these choice solvents, narrowing the scope of usable materials. Physical vapor deposition (PVD) is a solvent free, industry standard method of deposition where materials are evaporated onto a substrate under vacuum at elevated temperatures. Small molecule resists are required for this technique, since the molecule must sublime under vacuum at a temperature lower than the decomposition temperature of the material. Defect/pinhole free films can be readily produced in a conformal manner. PVD enables compositional gradients, in depth and in plane, not possible with today’s spin coated resists.

1.4.1.1 MGs for Vapor Deposition

There are certain materials requirements that must be met in order to implement PVD in the lithography process. The substance must sublime at a temperature lower than the temperature at which the material will start to decompose. As the molecular weight of polymeric resist is too high to allow sublimation before decomposition, MG resists became the focus of PVD material research.

Schmidt and co workers have developed a vapor deposition tool capable of co-depositing up to three different substances at once, as well as enable the formation of thickness and composition gradients across a singe wafer. They have developed vapor depositable MGs based on a coumarin ester as potential next-generation lithography material candidates[75]. Coumarin derivatives can undergo a [2+2] cycloaddition upon UV exposure to yield a dimer, which eliminates the need for a photo-initiator. The coumarin derivative was co-evaporated with a sensitizer to improving the resist sensitivity by about ten times. The molecular weight change upon exposure can be exploited in the development step as well. When placed under vacuum and heated, the unexposed molecules will evaporate from the substrate, yielding negative-tone patterns on the substrate. Figure 1.11 illustrated the deposition and development processes. This all-dry lithography system eliminates the need for solvent in every step of the process.

In collaboration with Ober and co-workers, Schmidt and co workers have developed other phenolic MGs suitable for vapor deposition, developable in water and aqueous base[76, 77]. These negative-tone glasses were co-evaporated with a PAG and cross-linker. Composition and thickness gradients of these resists allowed full optimization of the resist system with only one or two wafers. The vapor deposition and thermal development techniques are cost effective and

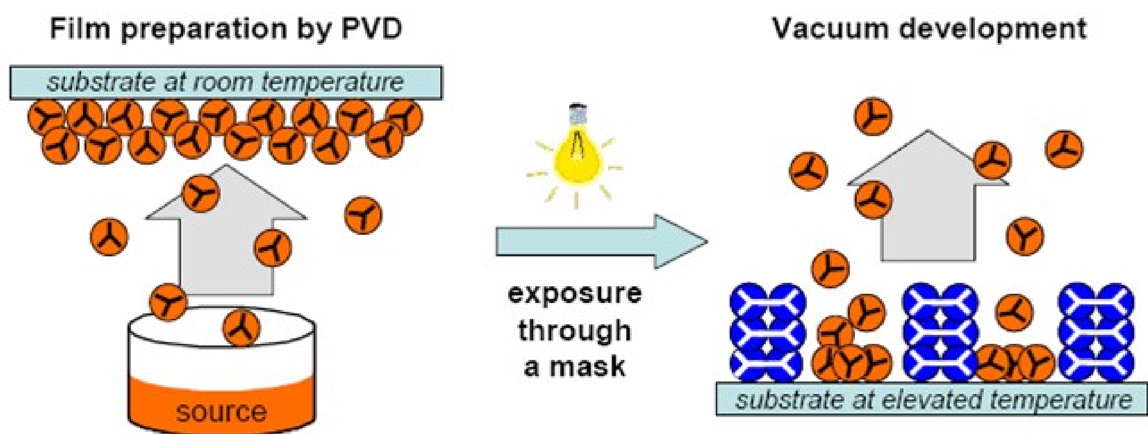

Figure 1.11 Scheme of physical vapor deposition and thermal development

environmentally friendly methods to improve the lithographic process, and the development of compatible MG resists are required to realize the full potential of the vapor deposition system.

1.4.2 Sub-millisecond Laser Post Exposure Bake

Chemically amplified resists are subject to a hardbake after exposure, which currently involves a hotplate with typical temperatures around 100°C to 150°C. At these temperatures, the bake times have been optimized in the seconds to minutes timeframe, depending on the types of materials used. The specific time and temperatures of the PEB controls both the deprotection reaction of the resist as well as the diffusion of the photogenerated acid. As previously mentioned, uncontrollable acid diffusion is considered a major factor in the LER currently seen in today's photoresists. Altering resist design to control acid diffusion has been studied at length. Recently, alternate PEB methods have been examined in order to obtain a fundamental understanding of the role of acid diffusion and resist deprotection kinetics.

Ober, Thompson and co workers have developed a CO_2 laser capable of spiking the temperature of the resist film with a high heating and cooling rate[78]. Much higher PEB temperatures can be accessed with this spike annealing system, up to 500°C. The total diffusion distance will not increase with the higher PEB temperature, since the temp. is spiked for sub-millisecond time periods. Recent studies have found that laser-PEB, or l-PEB can significantly enhance the sensitivity of a resist upon UV irradiation. Through careful molecular characterization, it was found that heating resist and PAG molecules well above their decomposition temperatures for sub-millisecond time periods will not degrade the resist components.

Much research is still needed to fully characterize and optimize this new PEB system, Preliminary studies have found that the deprotection and diffusion kinetics fundamentally change at shorter bake times and higher temperatures[79]. Ober and co workers have systematically synthesized PAG molecules with varying anion sizes to further investigate acid diffusion kinetics during l-PEB. This system has the potential to enhance sensitivity of resists while simultaneously decreasing LER, pushing resist limitations past their current limits.

1.5 Summary

The drive of the semiconductor industry to continually produce smaller chip dimensions have fueled research efforts to create resist materials capable of this. The current focus of industry is to identify key technologies for the 22 nm node and beyond. This chapter has summarized the efforts in creating alternative resist architectures to polymers to further improve resolution limits. Continued efforts on addressing critical challenges faces by the industry are explored in subsequent chapters.

Acknowledgements

The authors gratefully acknowledge the Semiconductor Research Corporation (SRC) for funding that made this review possible, as well as Intel/SRC Education Alliance for additional support. The authors thank the Cornell Nanoscale Science and Technology Facility and the Cornell Center for Materials Research use of equipment.

REFERENCES

[1] Bondyopadhyay, P. K., Moore's Law Governs the Silicon Revolution. Proceedings of the IEEE 1998, 86, (1), 78-81.

[2] Kim, J.-B.; Yun, H.-J.; Kwon, Y.-G.; Lee, B.-W., Adhesion-promoted copolymers for 193-nm photoresists without crosslinking during lithographic process. Journal of Photopolymer Science and Technology 2000, 13, (4), 629-634.

[3] Ito, H., Chemical amplification resists for microlithography. Advances in Polymer Science 2005, 172, (Microlithography, Molecular Imprinting), 37-245.

[4] Fryer, D. S.; Nealey, P. F.; de Pablo, J. J., Scaling of Tg and reaction rate with film thickness in photoresist: A thermal probe study. Journal of Vacuum Science & Technology, B: Microelectronics and Nanometer Structures 2000, 18, (6), 3376-3380.

[5] Gokan, H.; Esho, S.; Ohnishi, Y., Dry etch resistance of organic materials. Journal of the Electrochemical Society 1983, 130, (1), 143-6.

[6] Kunz, R. R.; Palmateer, S. C.; Forte, A. R.; Allen, R. D.; Wallraff, G. M.; Dipietro, R. A.; Hofer, D. C., Limits to etch resistance for 193-nm single-layer resists. Proceedings of SPIE-The International Society for Optical Engineering 1996, 2724, (Advances in Resist Technology and Processing XIII), 365-376.

[7] Bruson, H. A.; Sebrell, L. B.; Calvert, W. C., New chemical reactions of rubber hydrocarbons. Journal of Industrial and Engineering Chemistry (Washington, D. C.) 1927, 19, 1033-7.

[8] Harita, Y.; Ichikawa, M.; Harada, K.; Tsunoda, T., New photoresists of cyclized butadiene polymers.:Polymer Engineering and Science 1977, 17, (6), 372-6.

[9] Kajita, T.; Ota, T.; Nemoto, H.; Yumoto, Y.; Miura, T., Novel novolak resins using substituted phenols for high performance positive photoresist. :Proceedings of SPIE-The International Society for Optical Engineering 1991, 1466, (Adv. Resist Technol. Process. 8), 161-73.

[10] Rahman, M. D.; O. B. E., Dammel, R. R.; Sobadacha, C. J., Positive Photoresist Composition. 1993.

[11] Uetani, Y.; Hanabata, M.; Furuta, A., Observation of internal structure of a positive photoresist image using cross-sectional exposure method. Journal of Vacuum Science & Technology, B: Microelectronics and Nanometer Structures 1989, 7, (3), 569-71.

[12] Tabata, M.; Watanabe, O.; Sohma, J., Main-chain scissions of poly(methyl methacrylate) induced by chlorinated nitrosobenzenes as radical generators. Polymer Degradation and Stability 1981, 3, (6), 443-52.

[13] Ito, H.; Willson, C. G., Chemical amplification in the design of dry developing resist materials. Polymer Engineering and Science 1983, 23, (18), 1012-18.

[14] Ito, H.; Willson, C. G., Applications of photoinitiators to the design of resists for semiconductor manufacturing. ACS Symposium Series 1984, 242, (Polym. Electron.), 11-23.

[15] Breyta, G.; Hofer, D. C.; Ito, H.; Seeger, D.; Petrillo, K.; Moritz, H.; Fischer, T., The lithographic performance and contamination resistance of a new family of chemically amplified DUV photoresists. Journal of Photopolymer Science and Technology 1994, 7, (3), 449-60.

[16] Woods, R. L.; C. F. L.; Muelller, R.; Conway, J., Practical Half-Micron Lithography with a 10x KrF Excimer Laser Stepper. Proceedings of the KTI Microelectronics Seminar 1988, 341-359.

[17] Aoai, T.; Aotani, Y.; Umehara, A.; Kokubo, T., Application of silyl ether and silyl ester polymers for chemical amplification system. Journal of Photopolymer Science and Technology 1990, 3, (3), 389-400.

[18] Tsunooka, M.; Yanagi, H.; Kitayama, M.; Shirai, M., Photoinitiated acid-formation and its applications. The acid-formation mechanism of photolysis of Î²-ketosulfones in polymer matrices. Journal of Photopolymer Science and Technology 1991, 4, (2), 239-42.

[19] Crivello, J. V.; Lam, J. H. W.; Moore, J. E.; Schroeter, S. H., Triarylsulfonium salts: a new class of photoinitiators for cationic polymerization. Journal of Radiation Curing 1978, 5, (1), 2-17.

[20] Yamashita, K.; Kamimura, S.; Takahashi, H.; Nishikawa, N., A resist material study for LWR and resolution improvement in EUV lithography. Journal of Photopolymer Science and Technology 2008, 21, (3), 439-442.

[21] Yi, Y.; Ayothi, R.; Wang, Y.; Li, M.; Barclay, G.; Sierra-Alvarez, R.; Ober, C. K., Sulfonium salts of alicyclic group functionalized semifluorinated alkyl ether sulfonates as photoacid generators. Chemistry of Materials 2009, 21, (17), 4037-4046.

[22] Patsis, G. P.; Gogolides, E., Effects of model polymer chain architectures and molecular weight of conventional and chemically amplified photoresists on line-edge roughness. Stochastic simulations. Microelectronic Engineering 2006, 83, (4-9), 1078-1081.

[23] Shirota, Y.; Kageyama, H., Charge Carrier Transporting Molecular Materials and Their Applications in Devices. Chemical Reviews (Washington, DC, United States) 2007, 107, (4), 953-1010.

[24] Shirota, Y., Photo- and electroactive amorphous molecular materials-molecular design, syntheses, reactions, properties, and applications. Journal of Materials Chemistry 2005, 15,

(1), 75-93.

[25] Okumoto, K.; Wayaku, K.; Noda, T.; Kageyama, H.; Shirota, Y., Amorphous molecular materials: charge transport in the glassy state of N,N'-di(biphenylyl)-N,N'-diphenyl-[1,1'-biphenyl]-4,4'-diamines. Synthetic Metals 2000, 111-112, 473-476.

[26] Shirota, Y., Organic materials for electronic and optoelectronic devices.:Journal of Materials Chemistry 2000, 10, (1), 1-25.

[27] Drygiannakis, D.; Patsis, G. P.; Raptis, I.; Niakoula, D.; Vidali, V.; Couladouros, E.; Argitis, P.; Gogolides, E., Stochastic simulation studies of molecular resists. Microelectronic Engineering 2007, 84, (5-8), 1062-1065.

[28] Yoshiiwa, M.; Kageyama, H.; Shirota, Y.; Wakaya, F.; Gamo, K.; Takai, M., Novel class of low molecular-weight organic resists for nanometer lithography. Applied Physics Letters 1996, 69, (17), 2605-2607.

[29] De Silva, A.; Ober, C. K., Hydroxyphenylbenzene derivatives as glass forming molecules for high resolution photoresists. Journal of Materials Chemistry 2008, 18, (16), 1903-1910.

[30] De Silva, A.; Lee, J.-K.; Andre, X.; Felix, N. M.; Cao, H. B.; Deng, H.; Ober, C. K., Study of the Structure-Properties Relationship of Phenolic Molecular Glass Resists for Next Generation Photolithography. Chemistry of Materials 2008, 20, (4), 1606-1613.

[31] Pires, D.; Hedrick, J. L.; De Silva, A.; Frommer, J.; Gotsmann, B.; Wolf, H.; Despont, M.; Duerig, U.; Knoll, A. W., Nanoscale Three-Dimensional Patterning of Molecular Resists by Scanning Probes. Science (Washington, DC, United States) 328, (5979), 732-735.

[32] Lawson, R. A.; Lee, C.-T.; Wang, Y.; Tolbert, L.; Henderson, C. L., Epoxide functionalized molecular resists for high resolution electron-beam lithography. Microelectronic Engineering 2008, 85, (5-6), 959-962.

[33] Lawson, R. A.; Henderson, C. L., Mesoscale kinetic Monte Carlo simulations of molecular resists: the effect of PAG homogeneity on resolution, LER, and sensitivity. Proceedings of SPIE 2009, 7273, (Pt. 2, Advances in Resist Materials and Processing Technology XXVI), 727341/1-727341/10.

[34] Kai, T.; Nishiyama, S.; Saitou, A.; Shimokawa, T., Progress in resists development for EPL (electron beam projection lithography). Journal of Photopolymer Science and Technology 2003, 16, (3), 447-450.

[35] Sha, J.; Lee, J.-K.; Kang, S.; Prabhu, V. M.; Soles, C. L.; Bonnesen, P. V.; Ober, C. K., Architectural Effects on Acid Reaction-Diffusion Kinetics in Molecular Glass Photoresists. Chemistry of Materials 22, (10), 3093-3098.

[36] Lawson, R. A.; Lee, C.-T.; Yueh, W.; Tolbert, L.; Henderson, C. L., Single molecule chemically amplified resists based on ionic and non-ionic PAGs.:Proceedings of SPIE 2008, 6923, (Pt. 1, Advances in Resist Materials and Processing Technology XXV), 69230K/1-69230K/10.

[37] Lawson, R. A.; Tolbert, L. M.; Henderson, C. L., Single-component molecular resists containing bound photoacid generator functionality. Journal of Micro/Nanolithography, MEMS, and MOEMS 9, (1), 013015/1-013015/7.

[38] Lawson, R. A.; Henderson, C. L., Mesoscale simulation of molecular resists: The effect of PAG distribution homogeneity on LER. Microelectronic Engineering 2009, 86, (4-6), 741-744.

[39] Young-Gil, K.; Kim, J. B.; Fujigaya, T.; Shibasaki, Y.; Ueda, M., A positive-working alkaline developable photoresist based on partially tert-Boc-protected calix[4]resorcinarene and a photoacid generator. Journal of Materials Chemistry 2002, 12, (1), 53-57.

[40] Ueda, M.; Takahashi, D.; Nakayama, T.; Haba, O., Three-component negative-type photoresist based on calix[4]resorcinarene, a cross-linker, and a photoacid generator. Chemistry of Materials 1998, 10, (8), 2230-2234.

[41] Chang, S. W.; Ayothi, R.; Bratton, D.; Yang, D.; Felix, N.; Cao, H. B.; Deng, H.; Ober, C. K., Sub-50 nm feature sizes using positive tone molecular glass resists for EUV lithography. Journal of Materials Chemistry 2006, 16, (15), 1470-1474.

[42] De Silva, A.; Sundberg, L. K.; Sooriyakumaran, R.; Bozano, L.; Breyta, G.; Hinsberg, W. D.; Fujiwara, M., Hexafluoroalcohol (HFA) containing molecular resist materials for high-resolution lithographic applications. Proceedings of SPIE 7972, (Pt. 2, Advances in Resist Materials and Processing Technology XXVIII), 79721Z/1-79721Z/10.

[43] Kudo, H.; Suyama, Y.; Oizumi, H.; Itani, T.; Nishikubo, T., Novel extreme ultraviolet (EUV)-resist material based on noria (water wheel-like cyclic oligomer).:Journal of Materials Chemistry 20, (21), 4445-4450.

[44] Kudo, H.; Watanabe, D.; Nishikubo, T.; Maruyama, K.; Shimizu, D.; Kai, T.; Shimokawa, T.; Ober, C. K., A novel noria (water-wheel-like cyclic oligomer) derivative as a chemically amplified electron-beam resist material. Journal of Materials Chemistry 2008, 18, (30), 3588-3592.

[45] Seki, H.; Kato, Y.; Kudo, H.; Oizumi, H.; Itani, T.; Nishikubo, T., Negative-type extreme ultraviolet resist materials based on water-wheel-like cyclic oligomer (Noria). Japanese Journal of Applied Physics 49, (6, Pt. 2), 06GF06/1-06GF06/6.

[46] Kudo, H.; Jinguji, M.; Nishikubo, T.; Oizumi, H.; Itani, T., Extreme ultraviolet (EUV)-resist materials of noria (water wheel-like cyclic oligomer) derivatives containing acetal moieties. Journal of Photopolymer Science and Technology 23, (5), 657-664.

[47] Tanaka, M.; Rastogi, A.; Kudo, H.; Watanabe, D.; Nishikubo, T.; Ober, C. K., Environmentally friendly patterning of molecular waterwheel (Noria) in supercritical carbon dioxide. Journal of Materials Chemistry 2009, 19, (26), 4622-4626.

[48] Yang, D.; Chang, S. W.; Ober, C. K., Molecular glass photoresists for advanced lithography. Journal of Materials Chemistry 2006, 16, (18), 1693-1696.

[49] Lawson, R. A.; Noga, D. E.; Younkin, T. R.; Tolbert, L. M.; Henderson, C. L., Negative tone molecular resists using cationic polymerization: Comparison of epoxide and oxetane functional groups.:Journal of Vacuum Science & Technology, B: Microelectronics and Nanometer Structures--Processing, Measurement, and Phenomena 2009, 27, (6), 2998-3003.

[50] Ishii, T.; Nozawa, H.; Euramochi, E.; Tamamura, T., Fullerene-incorporated nanocomposite resist system for nanolithography. Materials Research Society Symposium Proceedings 2000, 584, (Materials Issues and Modeling for Device Nanofabrication), 103-115.

[51] Ishii, T.; Yokoo, A.; Murata, Y.; Shigehara, K., Fullerene nanocomposite resist for nanolithography. Materials Research Society Symposium Proceedings 2001, 636, (Nonlithographic and Lithographic Methods of Nanofabrication: From Ultralarge-Scale Integration to Photonics to Molecular Electronics), D6 4/1-D6 4/12.

[52] Gibbons, F.; Zaid, H. M.; Manickam, M.; Preece, J. A.; Palmer, R. E.; Robinson, A. P. G., A chemically amplified fullerene-derivative molecular electron-beam resist. Small 2007, 3, (12), 2076-2080.

[53] Gibbons, F. P.; Robinson, A. P. G.; Palmer, R. E.; Diegoli, S.; Manickam, M.; Preece, J. A., Fullerene resist materials for the 32 nm node and beyond. Advanced Functional Materials 2008, 18, (13), 1977-1982.

[54] Manyam, J.; Gibbons, F. P.; Diegoli, S.; Manickam, M.; Preece, J. A.; Palmer, R. E.; Robinson, A. P. G., Chemically amplified fullerene resists for e-beam lithography. Proceedings of SPIE 2008, 6923, (Pt. 1, Advances in Resist Materials and Processing Technology XXV), 69230M/1-69230M/8.

[55] Sooriyakumaran, R.; Truong, H.; Sundberg, L.; Morris, M.; Hinsberg, B.; Ito, H.; Allen, R.; Huang, W.-S.; Goldfarb, D.; Burns, S.; Pfeiffer, D., Molecular resists based on polyhedral oligomeric silsesquioxanes (POSS). Proceedings of SPIE-The International Society for Optical Engineering 2005, 5753, (Pt. 1, Advances in Resist Technology and Processing XXII), 329-337.

[56] Kim, J.-B.; Ganesan, R.; Choi, J.-H.; Yun, H.-J.; Kwon, Y.-G.; Kim, K.-S.; Oh, T.-H., Photobleachable silicon-containing molecular resist for deep-UV lithography. Journal of Materials Chemistry 2006, 16, (34), 3448-3451.

[57] Shiono, D.; Hirayama, T.; Kasai, K.; Hada, H.; Onodera, J.; Arai, T.; Yamaguchi, A.; Shiraishi, H.; Fukuda, H., Molecular resists based on cholate derivatives for electron-beam lithography. Japanese Journal of Applied Physics, Part 1: Regular Papers, Brief Communications & Review Papers 2006, 45, (6B), 5435-5439.

[58] http://www.itrs.net/Links/2007ITRS/2007_Chapters/2007_Lithography.pdf.

[59] Tanaka, S. and Ober, C., Adamantane Based Molecular Glass Resists for 193nm Lithography. Proceedings of SPIE 2006, 6153, 61532B.

[60] Tanaka, S.; Matsumoto, N.; Ohno, H.; Hatakeyama, N.; Ito, K.; Fukushima, K.; Oizumi, H.; Nishiyama, I., Adamantane-based molecular glass resist for 193-nm lithography and beyond. Proceedings of SPIE 2008, 6923, (Pt. 1, Advances in Resist Materials and Processing Technology XXV), 69231J/1-69231J/8.

[61] Tanaka, S.; Murakami, M.; Fukushima, K.; Kawano, N.; Uenoyama, Y.; Ito, K.; Ohno, H.; Matsumoto, N., Adamantane-based molecular glass resist for 193-nm lithography. Proceedings of SPIE 2009, 7273, (Pt. 2, Advances in Resist Materials and Processing Technology XXVI), 72732M/1-72732M/8.

[62] Sha, J.; Lee, J.-K.; Ober, C. K., Molecular glass resists developable in supercritical carbon dioxide for 193 nm lithography. Proceedings of SPIE 2009, 7273, (Pt. 2, Advances in Resist Materials and Processing Technology XXVI), 72732T/1-72732T/8.

[63] Kwon, Y.; Yun, H.; Ganesan, R.; Kim, J.-B.; Choi, J.-H., High performance molecular resists based on Î²-cyclodextrin. Polymer Journal (Tokyo, Japan) 2006, 38, (9), 996-998.

[64] Krysak, M.; De Silva, A.; Sha, J.; Lee, J.-K.; Ober, C. K., Molecular glass resists for next-generation lithography. Proceedings of SPIE 2009, 7273, (Pt. 2, Advances in Resist Materials and Processing Technology XXVI), 72732N/1-72732N/8.

[65] Kudo, H.; Inoue, N.; Nishimura, I.; Nishikubo, T., Novel molecular photoresists based on the cyclodextrin derivatives containing fluorine atoms and tert-butyl ester groups. Bulletin of the Chemical Society of Japan 2005, 78, (4), 731-737.

[66] Silva, A. D. Molecular Glass Photoresists for High Resolution Patterning. Cornell University, Ithaca, 2008.

[67] Bae, W. J.; Trikeriotis, M.; Sha, J.; Schwartz, E. L.; Rodriguez, R.; Zimmerman, P.; Giannelis, E. P.; Ober, C. K., High refractive index and high transparency HfO2 nanocomposites for next generation lithography. Journal of Materials Chemistry 20, (25), 5186-5189.

[68] Trikeriotis, M.; Rodriguez, R.; Zettel, M. F.; Bakandritsos, A.; Bae, W. J.; Zimmerman, P. A.; Ober, C. K.; Giannelis, E. P., High refractive index nanoparticle fluids for 193-nm

immersion lithography. Proceedings of SPIE 2009, 7273, (Pt. 1, Advances in Resist Materials and Processing Technology XXVI), 72732A/1-72732A/6.

[69] Trikeriotis, M.; Bae, W. J.; Schwartz, E.; Krysak, M.; Lafferty, N.; Xie, P.; Smith, B.; Zimmerman, P. A.; Ober, C. K.; Giannelis, E. P., Development of an inorganic photoresist for DUV, EUV, and electron beam imaging. Proceedings of SPIE 7639, (Pt. 1, Advances in Resist Materials and Processing Technology XXVII), 76390E/1-76390E/10.

[70] Krysak, M.; Trikeriotis, M.; Schwartz, E.; Lafferty, N.; Xie, P.; Smith, B.; Zimmerman, P.; Montgomery, W.; Giannelis, E.; Ober, C. K., Development of an inorganic nanoparticle photoresist for EUV, e-beam, and 193 nm lithography. Proceedings of SPIE 7972, (Pt. 1, Advances in Resist Materials and Processing Technology XXVIII), 79721C/1-79721C/6.

[71] Trikeriotis, M.; Krysak, M.; Chung, Y. S.; Ouyang, C.; Cardineau, B.; Brainard, R.; Ober, C. K.; Giannelis, E. P.; Cho, K. Y.; Nanoparticle photoresists from HfO2 and ZrO2 for EUV patterning. Journal of Photopolymer Science and Technology 2012, 25, (5), 583-586.

[72] Stowers, J.; Keszler, D. A., High resolution, high sensitivity inorganic resists. Microelectronic Engineering 2009, 86, (4-6), 730-733.

[73] Telecky, A.; Xie, P.; Stowers, J.; Grenville, A.; Smith, B.; Keszler, D. A., Photopatternable inorganic hard mask. Journal of Vacuum Science & Technology, B: Nanotechnology & Microelectronics: Materials, Processing, Measurement, & Phenomena 28, (6), C6S19-C6S22.

[74] Stowers, J. K.; A. T.; Kocsis, M.; Clark, B. L.; Keszler, D. A.; Grenville, A.; Anderson, C. N.; Nalleau, P. P., Directly patterned inorganic hardmask for EUV lithography. Proceedings of SPIE 2011, 7969, 79691-5.

[75] Pfeiffer, F.; Neuber, C.; Schmidt, H.-W., All-dry photoresist systems: physical vapor

deposition of molecular glasses. Proceedings of SPIE 2008, 6923, (Pt. 1, Advances in Resist Materials and Processing Technology XXV), 69231F/1-69231F/8.

[76] Pfeiffer, F.; Felix, N. M.; Neuber, C.; Ober, C. K.; Schmidt, H.-W., Physical vapor deposition of molecular glass photoresists: a new route to chemically amplified patterning. Advanced Functional Materials 2007, 17, (14), 2336-2342.

[77] Pfeiffer, F.; Felix, N. M.; Neuber, C.; Ober, C. K.; Schmidt, H.-W., Towards environmentally friendly, dry deposited, water developable molecular glass photoresists. Physical Chemistry Chemical Physics 2008, 10, (9), 1257-1262.

[78] Sha, J.; Jung, B.; Thompson, M. O.; Ober, C. K.; Chandhok, M.; Younkin, T. R., Submillisecond post-exposure bake of chemically amplified resists by CO2 laser spike annealing. Journal of Vacuum Science & Technology, B: Microelectronics and Nanometer Structures--Processing, Measurement, and Phenomena 2009, 27, (6), 3020-3024.

[79] Krysak, M.; Jung, B.; Thompson, M. O.; Ober, C. K.; Investigation of acid diffusion during laser spike annealing with systematically designed photoacid generators. Proceedings of SPIE 2012, 8322, 83220U-83220U-6.

CHAPTER 2

SYNTHESIS AND CHARATERIZATION OF MOLECULAR GLASS PHOTOACID GENERATORS

Abstract

This paper reports a fundamental study of the photophysical characteristics of molecular glass (MG) photoacid generators (PAGs). A library of MG PAG compounds were systematically designed and synthesized. The anion architecture includes bulky aromatic substituents which can limit diffusion of a generated acid and control miscibility when added to host materials. The effect of molecular size, molecular weight and number of substituents on thermal stability, optical properties, photoacid generation efficiency, and acid diffusion behavior has been examined. These PAGs were observed to reduce photo-generated acid diffusion conditions, and have shown low toxicity in environmental compatibility tests. This study has helped identify a PAG structure with a high quantum yield of 0.042, a reduced acid diffusion length and a widened processing window.

2.1 Introduction

When exposed to UV radiation, photoacidgenerators (PAGs) undergo a photochemical rearrangement to generate acid. This acid can act as a catalyst for subsequent reactions of the resin in which it is dispersed, which can include cationic polymerization, cross-linking, and decomposition of acid-labile protecting groups. Photoacid generators (PAGs) have a broad range

of applications, such as a curing agent in adhesives[1], coatings[2], drug delivery agents[3], and inks[4], and most extensively, as a catalyst in chemically amplified photoresist systems[5,6].

The structure of a PAG typically consists of an acid generating group, and an acid diffusion inhibiting group, separated by a spacer chain. Sulfonates that produce sulfonic acid derivatives upon UV irradiation are common acidic units, since sulfonic acid is one of the strongest known organic acids. The use of a fluorosulfonic acid can provide higher acidity because of its high electronegativity and poor polarizability, as well as promote solubility of the PAG compounds[7]. Along with its primary function, the acid diffusion inhibitor can be chosen to promote PAG miscibility within the resin in which it is dispersed.

Perfluorooctane sulfonate (PFOS) based PAGs have shown excellent performance in photopatterning applications, but it has recently been discovered that these compounds are toxic and non-biodegradable[8]. PFOS accumulation has been reported in several areas of the world and has even been found in human blood samples in trace quantities through environmental exposure[9]. There has been an effort to design PFOS-free PAGs based on naturally occurring cores[10,11] which have shown low toxicity as well as biodegradability.

One of the main drawbacks of state of the art PAGs is uncontrollable acid diffusion. Most PAG applications require a thermal treatment after photoexposure to initiate the acid catalyzed reaction. Some mobility of the photo-generated acid is necessary for the reaction to take place, but excess diffusion into unexposed areas of the film can have a negative effect. Acid diffusion in chemically amplified photoresists is thought to be the cause of critical dimension variation and line edge roughness in high resolution patterns[12,13]. Miscibility of the PAG with the other components of the resin is also an issue. PAGs can aggregate in solution, causing

inhomogeneous distribution throughout the resulting film. This can lead to reduced sensitivity and poor pattern quality[14].

Efforts have been made to reduce excess diffusion and inhomogeneous distribution of acid in photolithography by covalently attaching the PAG to the polymeric resist. PAG monomers have been attached to a resist polymer backbone in order to improve film homogeneity and reduce acid mobility[15-17]. These PAG-bound compounds have improved pattern roughness, but their use is restricted to photoresist applications. Henderson and co-workers have attached a PAG substituent to small molecule photoresists, or molecular glasses (MGs)[18,19]. MGs are characterized by their small, bulky structures which enable thin film formation of these molecules, as well as a high glass transition temperature, which is necessary to withstand high bake temperatures in the lithography process. They combine the positive characteristics of polymers with the benefits of small molecules, such as high purity and uniform size distribution. MG resists have been extensively studied[20-24], and are capable of producing high resolution patterns[25].

In this paper, we report the synthesis, and in-depth characterization of molecular glass PAGs. The effects of the anion structure on a variety of properties were studied to gain insight on an optimal PAG anion structure.

2.2 Experimental

2.2.1 Materials

Most starting materials were purchased from Sigma Aldrich and used without further purification. 1,2-dibromotetrafluoroethane was purchased from SynQuest Laboratories. Triphenylsulfonium chloride was purchased from Alfa Aesar. Solvents used were anhydrous or

HPLC grade unless otherwise noted. All reactions were run under an inert atmosphere unless indicated otherwise.

2.2.2 Characterization

^{1}H and ^{19}F NMR were recorded on a Varian Inova-400 NMR spectrometer at room temperature. Chemical shifts reported are quoted in parts per million (ppm) and relative to $CHCl_3$ (δ 7.26 ppm), DMSO (δ 2.50 ppm) or, in case of ^{19}F NMR, CH_3COOH as an external standard. The decomposition temperatures were measured using a TA Instruments Q500 Thermogravimetric Analyzer (TGA), and the glass transition temperatures were measured using a TA Instruments Q1000 Modulated Differential Scanning Calorimeter (MDSC). UV absorbance was recorded by spin-coating the materials onto quartz wafers and measuring absorbance with a Shimadzu-UV3101PC-UV-Vis-NIR Spectrometer, and a Varian Cary 5000 spectrophotometer was used to measure fluorescence.

2.2.3 Synthesis

The photoacid generators were synthesized using a similar procedure found in the literature[11]. A representative procedure for 3P2A is described below.

Potassium 4-[1-(4-phenoxide)-1-phenylethyl]phenoxide

To a round bottomed flask containing 3.5 g (12.1 mmol) 4,4'-(1-phenylethylidene) biphenol was added 24 mL of a 1.0 M solution of potassium hydroxide in methanol. The resulting solution was stirred for 45 minutes at room temperature. The methanol was removed

under reduced pressure, and the product was dried at 95°C under vacuum overnight. The resulting product was used in the subsequent reaction without further purification.

1-(2-bromo-1,1,2,2-tetrafluoroethoxy)-4-{1-[4-(2-bromo-1,1,2,2-tetrafluoroethoxy)phenyl]-1-phenylethyl}benzene

5.68 g (21.9 mmol) of 1,2-dibromotetrafluoroethane was added to a round bottomed flask equipped with a dropping funnel and condenser. Potassium 4-[1-(4-phenoxide)-1-phenylethyl]phenoxide, dissolved in 10 mL DMSO, was added slowly via a dropping funnel. The solution was stirred for 6 hours at 60 °C. After completion of the reaction, cold water was added, and the aqueous layer extracted with dichloromethane. The organic layers were combined, dried over Na_2SO_4 and concentrated in vacuo to give a light orange oil used subsequently in the next reaction.

Sodium 1,1,2,2-tetrafluoro-2-(4-{1-phenyl-1-[4-(1,1,2,2-tetrafluoro-2-sulfinoethoxy)phenyl]ethyl}phenoxy)ethane-1-sulfinate

5.6 g of 1-(2-bromo-1,1,2,2-tetrafluoroethoxy)-4-{1-[4-(2-bromo-1,1,2,2-tetrafluoroethoxy)phenyl]-1-phenylethyl}benzene, dissolved in acetonitrile, was added dropwise to a three-necked round bottomed flask containing a deoxygenated aqueous acetonitrile solution consisting of 30 mL H_2O, 10 mL acetonitrile, 3.21 g (38.2 mmol) $NaHCO_3$, and 6.02 g (34.6 mmol) $Na_2S_2O_4$. The mixture was stirred at 60°C for 2 hrs and then at 70°C for 5 hrs. The solution was then cooled to room temp and allowed to separate into two phases. Ethyl acetate was added, and the layers were separated. The aqueous layer was then washed several times with ethyl acetate. The organic layers were combines, dried over Na_2SO_4 and concentrated in vacuo.

The resulting low-melting solid was washed several times with hexane to produce a light yellow solid. Further purification of the material was achieved by dissolving the product in isopropanol and precipitating in hexanes for 3-5 cycles, until NMR showed no evidence of starting material. Yield = 3.64g (59%) ^{1}H NMR (400 MHz, DMSO-d6) δ 6.67-7.14 (m, 13H), 2.08 (s, 3H). ^{19}F NMR (376 MHz, DMSO-d6) δ -81.41 (t), -132.15 (t).

Sodium 1,1,2,2-tetrafluoro-2-(4-{1-phenyl-1-[4-(1,1,2,2-tetrafluoro-2-sulfinoethoxy)phenyl]ethyl}phenoxy)ethane-1-sulfonate

To a round-bottomed flask was added 1.81 g (5.50 mmol) sodium tungstate dihydrate, 0.78 g (5.50 mmol) sodium hydrogen phosphate, and 3.64 (5.50 mmol) sodium 1,1,2,2-tetrafluoro-2-(4-{1-phenyl-1-[4-(1,1,2,2-tetrafluoro-2-sulfinoethoxy)phenyl]ethyl}phenoxy) ethane-1-sulfinate in 12.6 mL H_2O and 21 mL acetonitrile. 1.5 mL H_2O_2 solution was then added dropwise while stirring at room temperature. After the addition was complete, the resulting mixture was heated to 60°C for 24 hours. Upon completion, the reaction was cooled to room temperature, and the solvents removed under reduced pressure. The resulting low-melting solid was extracted three times with isopropanol. The organic layers were combined and concentrated in vacuo. Further purification was achieved by several washings with hexanes. Yield = 0.95g (40%).^{1}H NMR (400 MHz, DMSO-d6) δ 6.68-7.14 (m, 13H), 2.08 (s, 3H). ^{19}F NMR (376 MHz, DMSO-d6) δ -81.03 (t), -116.86 (t).

Triphenylsulfonium 1,1,2,2-tetrafluoro-2-(4-{1-phenyl-1-[4-(1,1,2,2-tetrafluoro-2-sulfinoethoxy)phenyl]ethyl}phenoxy)ethane-1-sulfonate

To an aqueous solution of triphenylsulfonium bromide (50 wt. %) (0.94 g, 2.74 mmol) was added 0.95 g (1.37mmol) sodium 1,1,2,2-tetrafluoro-2-(4-{1-phenyl-1-[4-(1,1,2,2-tetrafluoro-2-sulfinoethoxy)phenyl]ethyl}phenoxy) ethane-1-sulfonate. Acetonitrile was added dropwise until the starting material was completely dissolved. The solution was stirred in atmospheric conditions at room temperature overnight. The acetonitrile was removed under reduced pressure, and the resulting mixture was extracted with dichloromethane. The organic layers were then combined, washed with brine, dried over Na_2SO_4, and concentrated in vacuo. The pure compound was obtained by precipitation in a CH_2Cl_2/ether mixture. Yield = 1.49g (93%) ^{1}H NMR (400 MHz, DMSO-d6) δ 7.83 – 7.75 (m, 15H), 7.74 – 7.58 (m, 4H), 7.28 – 7.12 (m, 6H), 7.09 – 6.95 (m, 1H), 2.12 (s, 3H). ^{19}F NMR (376 MHz, DMSO-d6) δ -81.66 (t), -116.98 (t).

1P1A

*Sodium 2-(4-*tert*-butylphenoxy)-1,1,2,2-tetrafluoroethanesulfinate*

Yield = 65%

^{1}H NMR (400 MHz, DMSO-d6) δ 7.44 (d, *J* = 8.9 Hz, 2H), 7.15 – 7.08 (d, 2H), 1.28 (s, 9H) ^{19}F NMR (376 MHz, DMSO-d6) δ -81.17 (t), -132.06 (t, *J* = 3.3 Hz).

*Sodium 2-(4-*tert*-butylphenoxy)-1,1,2,2-tetrafluoroethanesulfonate*

Yield = 70%

^{1}H NMR (400 MHz, DMSO-d6) δ 7.50 – 7.41 (m, 2H), 7.18 – 7.09 (m, 2H), 1.75 (s, 9H). ^{19}F NMR (376 MHz, DMSO-d6) δ -80.83(t), -116.72 (t, *J* = 2.7 Hz).

*Triphenylsulfonium 2-(4-*tert*-butylphenoxy)-1,1,2,2-tetrafluoroethanesulfonate* (1P1A)

Yield = 90%

^{1}H NMR (400 MHz, Chloroform-d) δ 7.82 – 7.62 (m, 15H), 7.35 – 7.24 (m, 2H), 7.21 – 7.12 (m, 2H), 1.29 (d, J = 1.5 Hz, 9H). ^{19}F NMR (376 MHz, Chloroform-d) δ -81.54 (t, J = 2.9 Hz), -116.83 (t).

2P2A

Sodium 2,2'-[propane-2,2-diylbis(benzene-4,1-diyloxy)]bis(tetrafluoroethanesulfinate)

Yield = 62%.

^{1}H NMR (400 MHz, DMSO-d6) δ 7.32 – 7.19 (m, 4H), 7.16 – 7.07 (m, 4H), 1.64 (s, 6H). ^{19}F NMR (376 MHz, DMSO-d6) δ -81.35 (t, J = 3.4 Hz), -132.15 (t, J = 3.2 Hz).

Sodium 2,2'-[propane-2,2-diylbis(benzene-4,1-diyloxy)]bis(tetrafluoroethanesulfonate)

Yield = 68%

^{1}H NMR (400 MHz, DMSO-d6) δ 7.31 – 7.23 (d, 4H), 7.12 (d, J = 8.7 Hz, 4H), 1.56 (s, 6H). ^{19}F NMR (376 MHz, DMSO-d6) δ -80.96 (t), -116.77 (t, J = 2.5 Hz).

Triphenylsulfonium 2,2'-[propane-2,2-diylbis(benzene-4,1 diyloxy)] bis(tetrafluoroethanesulfonate) (2P2A)

Yield = 92%

^{1}H NMR (400 MHz, Chloroform-d) δ 7.79 – 7.54 (m, 30H), 7.19 – 6.60 (m, 8H), 1.60 (s, 6H). ^{19}F NMR (376 MHz, Chloroform-d) δ -81.65 (t, J = 3.1 Hz), -117.00 (t, J = 3.4 Hz).

3P3A

Sodium 2-(4-{1,1-bis[4-(1,1,2,2-tetrafluoro-2-sulfinoethoxy)phenyl]ethyl}phenoxy)-1,1,2,2-tetrafluoroethane-1-sulfinate

Yield = 52%

^{1}H NMR (400 MHz, DMSO-d6) δ 7.24 – 7.01 (m, 12H), 2.12 (s, 3H). ^{19}F NMR (376 MHz, DMSO-d6) δ -81.42 (t, *J* = 3.0 Hz), -132.16 (t, *J* = 3.2 Hz).

Sodium 2-(4-{1,1-bis[4-(1,1,2,2-tetrafluoro-2-sulfinoethoxy)phenyl]ethyl}phenoxy)-1,1,2,2-tetrafluoroethane-1-sulfonate

Yield = 67%

^{1}H NMR (400 MHz, DMSO-d6) δ 7.26 – 7.05 (m, 12H), 1.75 (s, 3H). ^{19}F NMR (376 MHz, DMSO-d6) δ -81.04 (t, *J* = 3.0 Hz), -116.84 (t, *J* = 3.1 Hz).

Triphenylsulfonium 2-(4-{1,1-bis[4-(1,1,2,2-tetrafluoro-2-sulfinoethoxy)phenyl]ethyl}phenoxy)-1,1,2,2-tetrafluoroethane-1-sulfonate (3P3A)

Yield = 90%

^{1}H NMR (400 MHz, Chloroform-d) δ 7.86 – 7.59 (m, 45H), 7.51-7.27 (m, 12H), 2.12 (m, 3H). ^{19}F NMR (376 MHz, DMSO-d6) δ -81.32(t) , -121.79 (t, *J* = 3.0 Hz).

4P3A

Sodium 1,1,2,2-tetrafluoro-2-(4-{1-[4-(1,1,2,2-tetrafluoro-2-sulfinoethoxy)phenyl]-1-(4-{2-[4-(1,1,2,2-tetrafluoro-2-sulfinoethoxy)phenyl]propan-2-yl}phenyl)ethyl}phenoxy)ethane-1-sulfinate

Yield = 48%

^{1}H NMR (400 MHz, DMSO-d6) δ 7.27 – 6.39 (m, 16H), 1.94 (s, 3H), 1.57 (s, 6H). ^{19}F NMR (376 MHz, DMSO-d6) δ -81.39 (t), -132.10 (t).

Sodium 1,1,2,2-tetrafluoro-2-(4-{1-[4-(1,1,2,2-tetrafluoro-2-sulfinoethoxy)phenyl]-1-(4-{2-[4-(1,1,2,2-tetrafluoro-2-sulfinoethoxy)phenyl]propan-2-yl}phenyl)ethyl}phenoxy)ethane-1-sulfonate

Yield = 63%

^{1}H NMR (400 MHz, DMSO-d6) δ 7.30-6.49 (m, 16H), 1.84 (s, 3H), 1.52 (s, 6H). ^{19}F NMR (376 MHz, DMSO-d6) δ -81.00 (t), -116.78 (t).

Triphenylsulfonium 1,1,2,2-tetrafluoro-2-(4-{1-[4-(1,1,2,2-tetrafluoro-2-sulfinoethoxy)phenyl]-1-(4-{2-[4-(1,1,2,2-tetrafluoro-2-sulfinoethoxy)phenyl]propan-2-yl}phenyl)ethyl}phenoxy) ethane-1-sulfonate (4P3A)

Yield = 88%

^{1}H NMR (300 MHz, DMSO-d6) δ 7.91 – 7.71 (m, 45H), 7.35 – 6.55 (m, 16H), 2.04 (s, 3H), 1.59 (s, 6H). ^{19}F NMR (376 MHz, DMSO-d6) δ -81.32 (t), -116.85 (t).

2.2.4 Lithographic Characterization of Photoacid Generators

The PAGs were mixed with a molecular glass resist at 5 wt % with respect to the resist and dissolved in 2-butanone to make a 5 wt % solution. The resist was filtered with a 0.2 µm membrane filter, then spin-coated onto a hexamethyldisilazane (HMDS) primed wafer at 2000 rpm for 1 minute. The film was baked at 110°C for 1 minute, and exposed with either UV

radiation with an ABM contact aligner (254nm) or electron beam radiation with a JEOL JBX-9300FS Electron Beam Lithography system operating at 100 keV. A post-exposure bake (PEB) of 90°C for 1 minute was performed after exposure, followed by development in AZ 726-MIF developer (0.26N TMAH) for 1 minute. Scanning electron Micrographs (SEMs) of patterned images were taken using a Zeiss Ultra 55 scanning electron microscope.

2.2.5 Constructing Bilayers to Measure Acid Diffusion

The characterization of the acid diffusion front was measured using a bilayer method[12]. The photoresist and 5 wt % of the appropriate PAG were dissolved in PGMEA and spin-coated onto an HMDS primed wafer at 2000 rpm for 1 minute, and baked at 130°C for 1 minute. The film thickness of this bottom layer was measured with a Woollamm ellipsometer, and then the film set aside. A flexible stamp was made by cross-linking poly-dimethylsilane (PDMS) on top of a silicon wafer to ensure a smooth surface. The cross-linked stamp was then used as a substrate onto which the same photoresist and PAG mixture was spin-coated, using the same procedure was described above. The film was then exposed to UV radiation with an array of doses. The two films were heated at various temperatures for 1 minute, then the PDMS stamp peeled off. The bilayer was then developed, and the thicknesses of the remaining film at various exposure doses were measured.

2.3 Results and Discussion

2.3.1 Synthesis and Design Strategy of Molecular Glass Photoacid Generators

The photoacid generators were synthesized in a five step process, starting with phenolic cores of varying sizes. A deprotonation of the phenol is followed by a Williamson ether synthesis

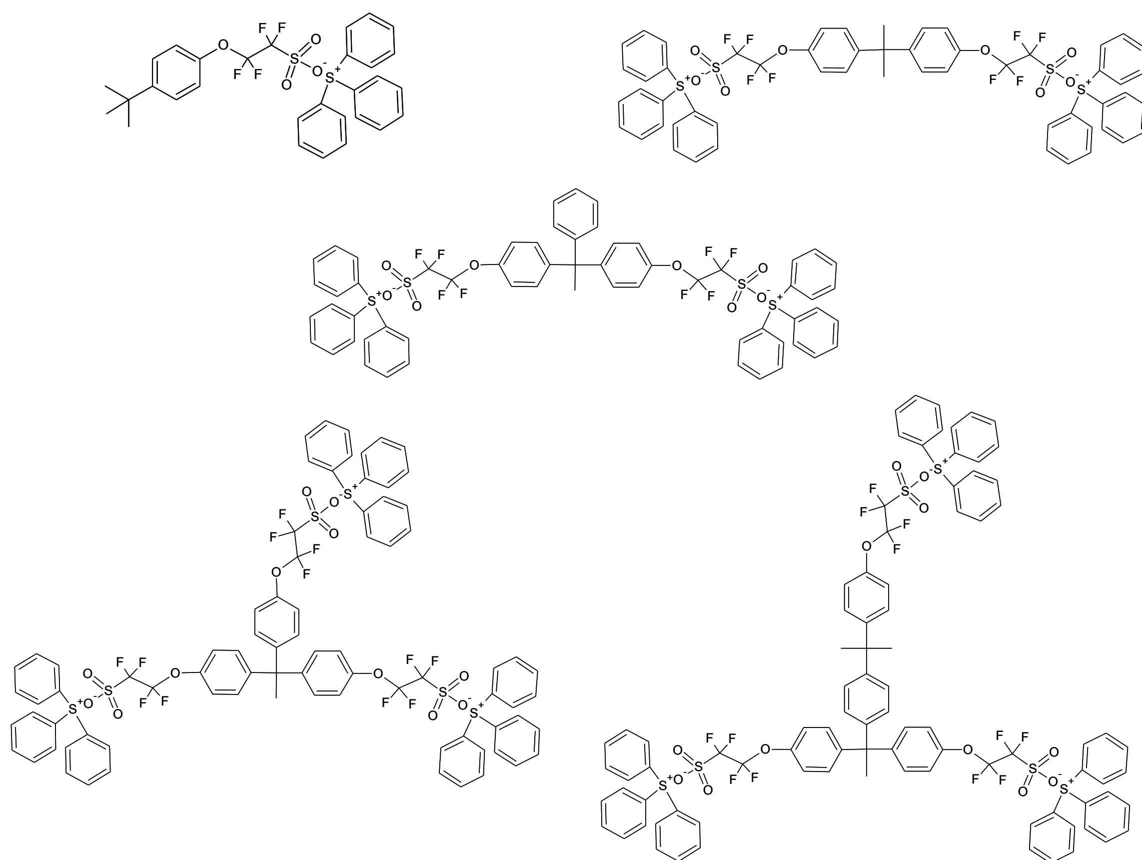

Figure 2.1 Molecular glass PAG structures

to attach the brominated fluorine chain. The pendent bromine is sulfinated, and then oxidized to produce sodium sulfonate. The final reaction exchanges the sodium ion for a triphenylsulfonium ion. Careful synthesis and purification produces full substitution of mono-, di- and tri-substituted PAGs. The anion structures have varying numbers of phenyl rings (P) and acid generating substituents (A), and these numbers are reflected in the short-hand names given to each molecule.

The bulky, rigid anion structures of these new molecules are designed to reduce acid diffusion by anchoring the molecule into the film. These PAGs can be blended into other systems, and can form a thin film because of their amorphous nature. Their thermal, optical and patterning properties have been studied to form an understanding of optimal anion architecture.

2.3.2 Thermal Properties

All of the PAGs do not show any weight loss until heated to temperatures above 200°C, which ensures that no thermal decomposition occurs during the bake steps. (Table 2.1). As a general trend, increased PAG size leads to reduced decomposition temperature. The chemical bonds of the larger molecules in this study have less restricted movement, which could account for the reduced decomposition temperature. The 3P2A and 3P3A PAGs share the same core structure, but vary only by the number of photoacid-generating substituents. The number of photoacid-generating substituents is found to have little or no effect on the decomposition temperature of the PAGs.

The glass transition temperature (Tg) generally increases with a larger molecular size. However, the flexibility of the fluorinated chains can suppress the Tg. This is supported by the observation of the Tg trends in molecules with the same core and different numbers of PAG

Table 2.1 Thermal characterization of MG PAGs

PAG	MW (g·mol^{-1})	Decomposition Temperature (°C)	Tg(°C)
1P1A	592.47	300°C	25°C
2P2A	1112.8	250°C	55°C
3P2A	1174.7	210°C	76°C
3P3A	1632.8	210°C	65°C
4P3A	1868.3	205°C	81°C

substituents, namely 3P2A and 3P3A. The presence of an additional photoacid-generating functionality on the 3P3A molecule lowers the Tg from that of the 3P2A molecule. The Tg then increased for the 4P3A molecule, which has the same number of PAG sites, but a larger anion core.

2.3.3 Optical Properties

The UV absorption spectra of the PAGs is shown in Figure 2.2. As a PAG must absorb a photon to produce acid, it is imperative to observe the absorbance behavior of the new compounds. The maximum absorbance peak for all PAGs occurs around 190 nm, due to the aromatic rings in the anion. A shoulder peak appears around 240 nm, and shows a trend of higher intensity with an increasing number of acid generating substituents. The PAGs show no significant absorbance at longer wavelengths up to 600 nm. Based on this data, the PAGs will be most efficient when exposed to wavelengths around 240 nm, as the sulfonate group absorbs in this region.

The quantum yield of a PAG can measure the efficiency of acid generation, or how much acid is produced as a function of absorbed photons. The quantum yields of the new PAGs were measured by a method described by Scaiano[26], using rhodamine B base as an indicator of the amount of acid produced (Figure 2.3). As acid is introduced to the rhodamine solution, the lactone ring in the base structure is converted to a carboxylic acid, thereby changing the fluorescence properties. The intensity of the new acid peak is plotted as a function of UV exposure dose, and the slope of this line is used to calculate the quantum yield. Triphenylsulfonium triflate PAG was used as the actinometer, as the quantum yield has been previously reported[27].

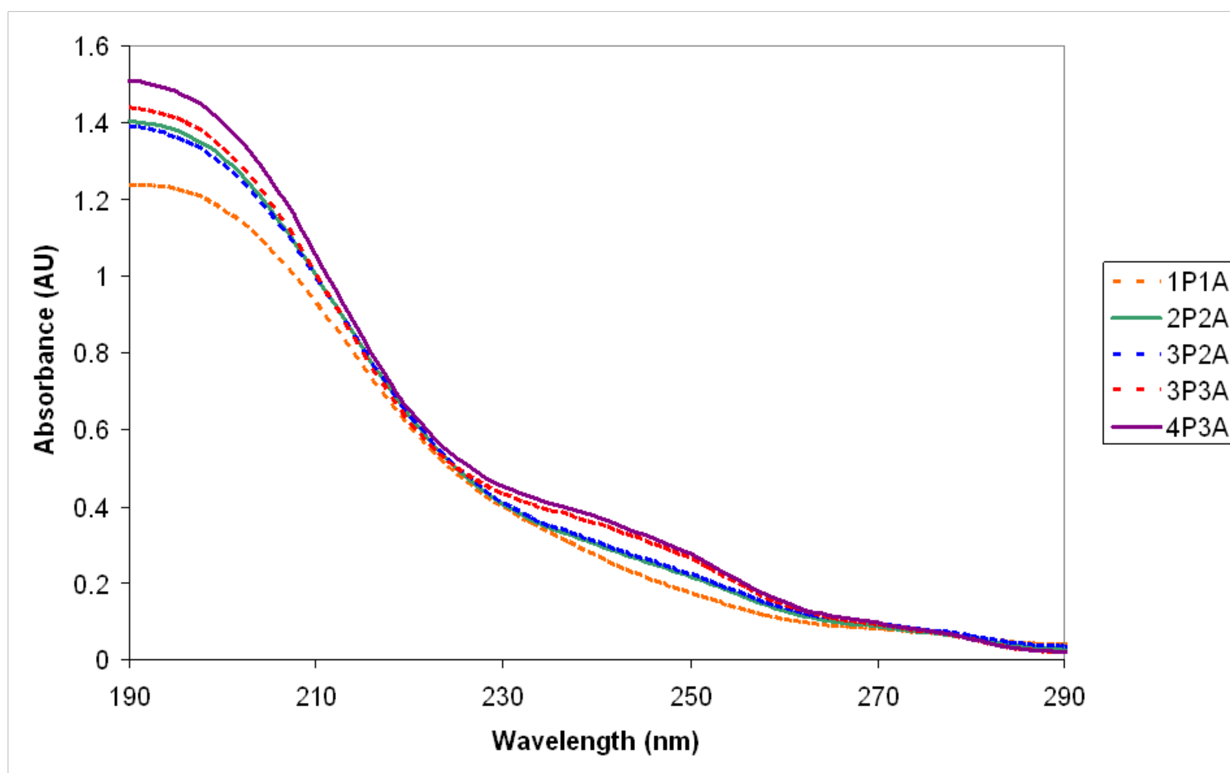

Figure 2.2 UV absorbance spectra for each MG PAG

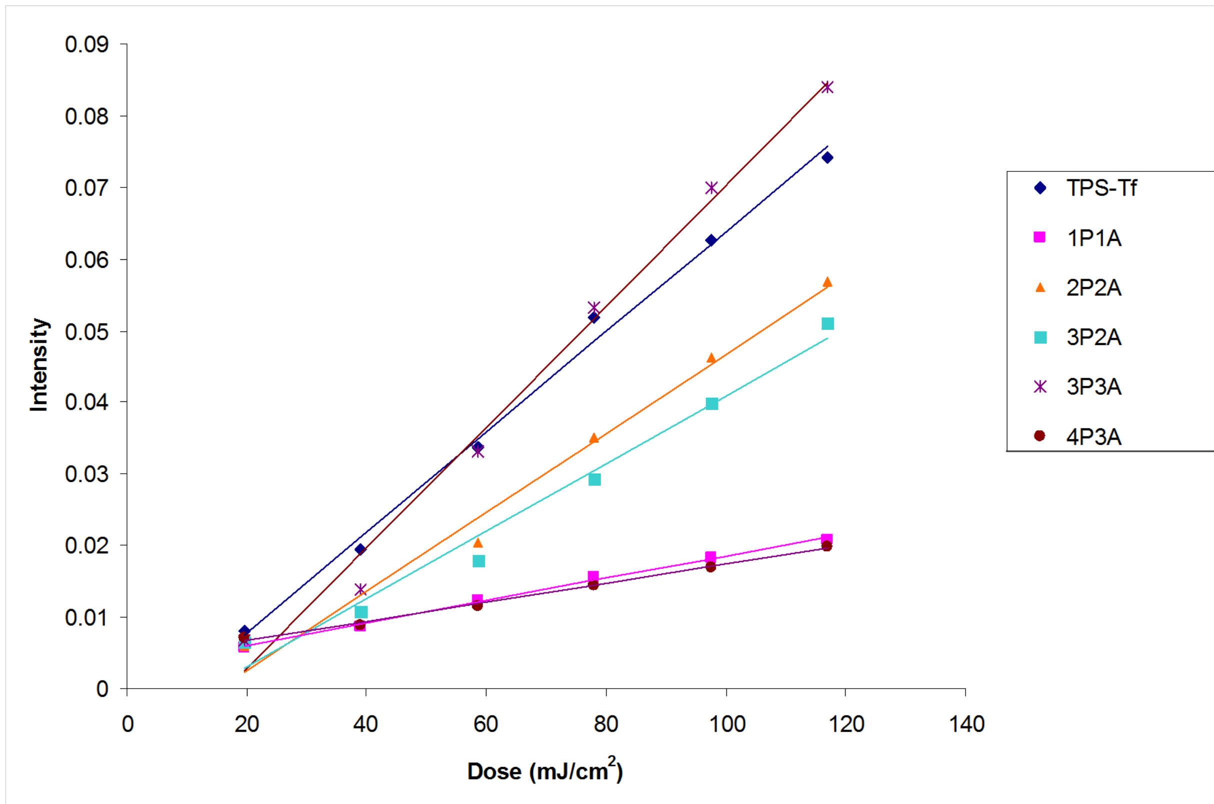

PAG	Quantum Yield[a] ϕ_{MGPAG}
1P1A	0.010
2P2A	0.032
3P2A	0.026
3P3A	0.042
4P3A	0.005

[a] quantum yield was calculated by the following equation: $\phi_{MGPAG} = \phi_{act} \frac{S_{MGPAG}}{S_{act}}$

Figure 2.3 Plot of intensity at the maximum absorbance as a function of UV dose and the calculated quantum yields

The 2P2A PAG showed a significantly higher quantum yield than the 1P1A molecule, most likely due to the extra acid generating substituent on the 2P2A PAG. The 3P2A molecule has a slightly lower quantum yield than the 2P2A molecule. The extra phenyl ring on the 3P2A PAG can account for this change, as it can absorb photons without producing acid. The 4P3A quantum yield is substantially lower, suggesting that its four phenyl rings are absorbing a significant amount of the photons. The 3P3A molecule has the highest quantum yield of all, likely due to the three PAG substituents on the anion core. The efficiency of this PAG is higher than that of triphenylsulfonium triflate, the commercial PAG used as the control in this study.

2.3.4 Lithographic Characterization

The solubility of the PAG molecules in common spinning solvents is crucial for further analysis and characterization. The molecules were insoluble in propylene glycol methyl ether acetate (PGMEA), due to the hydrophobic nature of the anions. 2-butanone, which is more hydrophobic, was used as a spinning solvent.

To determine the effect of PAG loading on the sensitivity of the resist matrix, contrast curves of a mixture of a single resist and photoacid generator were measured using resist mixtures with varying PAG concentrations (Figure 4.4). The amorphous nature of the PAGs allowed high concentrations of PAG to be tested, even up to a film of PAG only. It has been previously shown that as PAG concentration increases, the sensitivity of the film will also increase, because the overall quantum yield of the film will be higher. More photons can be absorbed during exposure, which translates to more acid in the film, and therefore an increase in the amount of deprotection for a given exposure dose[18].

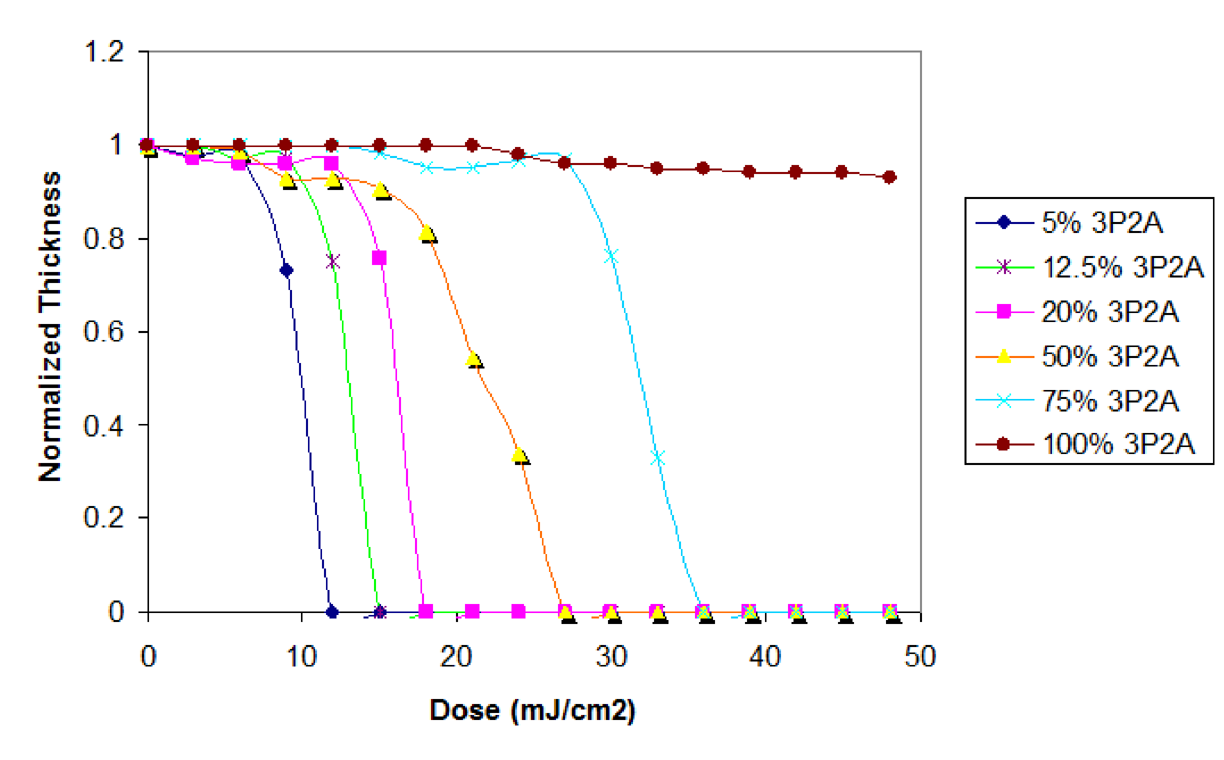

Figure 2.4 The effect of PAG concentration on the sensitivity of the MG resist- MG PAG system

Chemically amplified resists require a solubility change to render the exposed portion soluble in the developer. This is achieved by the generated photoacid catalyzing the deprotection reaction, which decomposes the *tert*-butoxycarbonyl (t-BOC) to reveal a hydroxyl group. As this reaction produces acid, one acid molecule can deprotect many t-BOC groups, which is the reason chemically amplified resists have increased sensitivity. As the amount of PAG in the film increases, it plays a larger role in the overall hydrophilicity of the film. As the PAG requires one photon per even of acid generation, the sensitivity of the film will decrease as more PAG is added. This is supported by the data shown in Figure 2.3, in which the sensitivity of the MG resist- MG PAG system decreases as the PAG concentration increases.

2.3.5 Acid Diffusion Analysis

The PAGs were mixed with poly(gammabutyrolactone-*co* methyl adamantanemethacrylate) at 5 wt %, and were used to construct bilayers as described above. It is important to note that the acid diffusion lengths reported are relative to the different PAG molecules in this study, as factors other than acid diffusion can cause a film thickness change. However, the process can give an insight on the relative diffusion behaviors of the different PAG systems.

The bar graph in Figure 2.5 shows the relative acid diffusion lengths of the different PAG systems at different PEB temperatures. The 1P1A PAG showed the largest diffusion length, due to its small size and low molecular weight. By adding a second aromatic group and PAG substituent to the anion core, the length of diffusion was greatly reduced. By increasing the size of the PAGs beyond that of the 2P2A PAG, there is little gain in the reduction of diffusion.

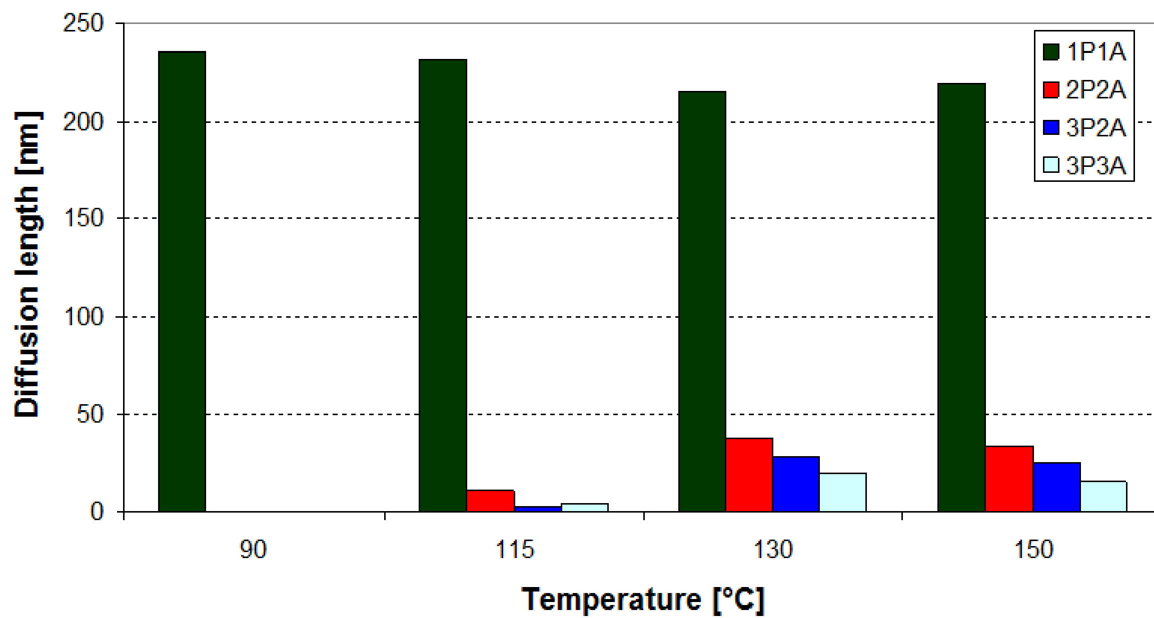

Figure 2.5 Comparison of acid diffusion behavior of the MG PAGs

The 3P2A and 3P3A PAGs have the same core structure, and vary only by the number of PAG substituents. The 3P3A PAG shows less diffusion than the 3P2A molecule, indicating that molecular size has a greater effect on diffusion length than the number of PAG substituents. The additional PAG substituent on 3P3A can restrict movement through its molecular weight and bulky size, thereby reducing diffusion.

The mobility of the photo-generated acid can also affect the range of exposure doses at which the material can produce acceptable features. With doses that are too low, the critical dimension of patterns generated will be lower than the desired feature size. Conversely, overdosing the material will results in patterns that are larger than intended. The process window for a dose range that produces features of the correct size should be maximized for ease of use in other processes. The 3P3A PAG was tested against a commercially available PAG, Triphenylsulfonium perfluoro-1-butanesulfonate (TPS-nonaflate), with 70 % t-BOC protected CR-15 MG resist[25]. Each resist mixture was patterned with an ASML 300C DUV Stepper at various doses, and the features were measured at each dose. The measured feature sizes plotted vs. exposure dose (Figure 2.6). The commercially available PAG showed a steep increase in feature size with increasing dose. However, the 3P3A PAG has a much slower feature size increase as a function of dose, indicating that the process window for the MG PAG is much larger than that of TPS-nonaflate. With restricted acid diffusion, more energy is required for the MG PAG to migrate from the exposed to unexposed portion of the film, which will limit the size increase of the patterns produced. The MG PAGs show promise for use in a resin with a large process window.

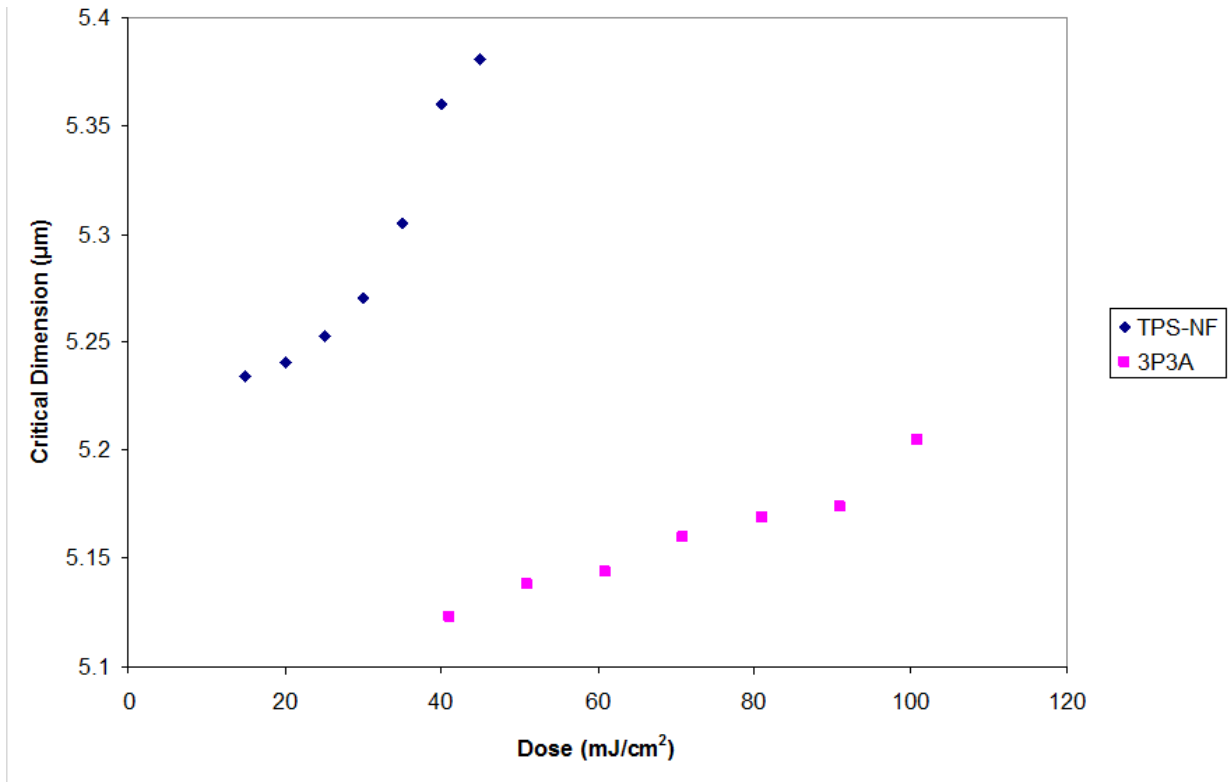

Figure 2.6 Actual feature size as a function of exposure dose for TPS-Nonaflate (TPS-NF) and 3P3A MG PAG with a MG resist

2.3.6 Patterninng by E-beam Lithography

E-beam lithography was used to achieve high resolution patterning of these materials. Figure 2.7 shows a SEM image of the patterns obtained after exposure and development of a 70% t-BOC protected CR-15[25] molecular glass photoresist with 5 wt% 3P3A PAG. The 100 nm line/space patterns were analyzed using SumMIT software, and exhibit 3.0 nm line edge roughness (LER), which is the length of deviation from a straight sidewall. The MG PAGs are capable of producing higher resolution patterns with low LER.

2.3.7 Environmental Compatibility Evaluation

As mentioned above, PFOS-containing PAGs pose a threat to the safety of the environment and the heath of both animals and humans. The MG PAG compounds were specifically designed with a shortened fluorinated chain, which has been shown to reduce toxicity from PFOS-containing structures[11].

The aerobic- and anaerobic biodegradability of the 3P3A PAG compound was investigated in bioassays. After more than 6 months of incubations, no biodegradation was observed in any case. The results (data not shown) demonstrated that the 3P3A PAG is very recalcitrant to microbial degradation in conventional wastewater treatment system. The non-degradability is attributed to the chemically stable structure of the PAG. Although it is non-biodegradable, in the cytotoxicity assays (Table 2.2), 3P3A showed very low toxicity to anaerobic microorganisms in wastewater treatment sludge. The results indicated that 3P3A did not cause significant inhibition to the biological wastewater treatment processes at relatively high concentrations (hundreds of milligrams per liter). In addition, the PAG also showed low to moderate toxicity towards the luminescent bacterium utilized in the Microtox assay (*V.*

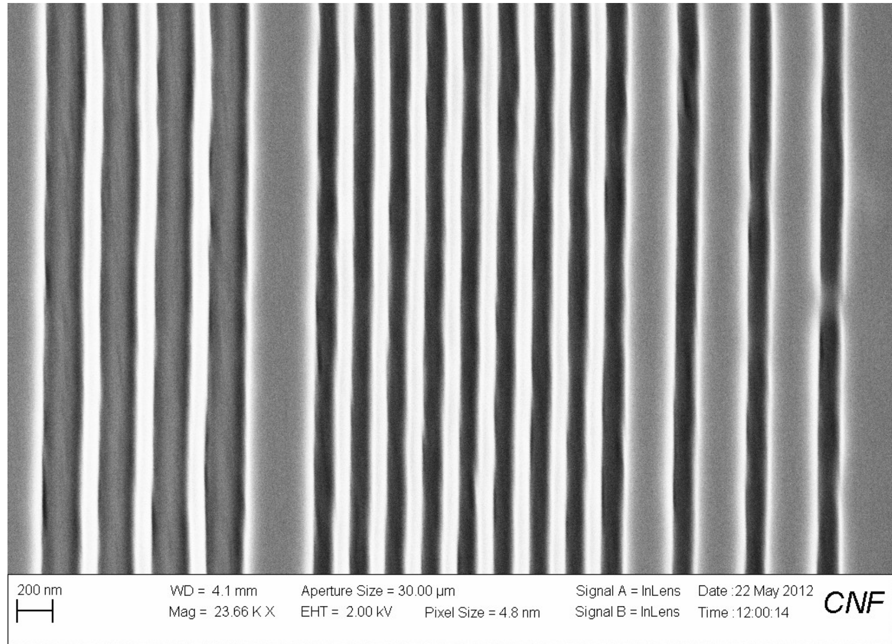

Figure 2.7 SEM image of 100 nm line/space patterns with low LER obtained by patterning with e-beam lithography

Table 2.2 Summary of inhibitory concentrations determined for the molecular glass in different toxicity assays

Toxicity Assay	**IC_{20} (mg·L^{-1})**	**IC_{20} (mg·L^{-1})**	**Max. Concentration Tested (mg·L^{-1})**
Microtox[a]	35.2	113.0	1000
Methanogenic[b]	1000	GMC*	1000
Xcelligence	GMC	GMC	400

*GMC= Greater than maximum concentration tested.

[a]Based on the results after exposure time of 30 min.

[b]Based on results of two experiments with hydrogen and acetate as electron donor, respectively.

fischeri) and human lung epithelial 16HBE14o- cells. This study provides insight that 3P3A will be an environmental friendly compound in lithography, posing low toxic effects to the environment and ecological systems.

2.4 Conclusions

In this chapter, we report a fundamental study on molecular glass photoacid generators through synthesis and characterization of various anion sizes and number of PAG-functionalized sites. The effect of these variations on thermal stability, optical properties, patternability and diffusion of the photoacid has been examined, and the effects of structural properties of these compounds have been evaluated. The quantum yield of these compounds has been shown to improve with additional acid generating substituents. The MG PAGs were observed to reduce acid diffusion by increasing the size of the anion. The 3P3A molecule has been identified by this study to be an efficient PAG with a quantum yield of 0.042, and has shown an increased process window over the commercially available PAG. 3P3A has demonstrated high resolution patterning ability, and showed a very low toxicity to anaerobic microorganisms in cyctotoxicity arrays.

Acknowledgements

This work was funded by the Semiconductor Research Corporation (SRC), as well as Globalfoundries. Dr. Wenjie (Alex) Sun and Prof. Reyes Sierra at the University of Arizona are thanked for their collaboration on environmental compatibility studies. The Cornell Nanoscale Science and Technology Facility (CNF), the Cornell Center for Materials Research (CCMR) and

SuMMIT Technologies are thanked for use of facilities and software. Intel and the SRC Education Alliance is gratefully acknowledged for granting a fellowship to support this research.

REFERENCES

[1] Inui, T.; Sato, E.; Matsumoto, A., Pressure-Sensitive Adhesion System Using Acrylate Block Copolymers in Response to Photoirradiation and Postbaking as the Dual External Stimuli for On-Demand Dismantling. *ACS Applied Materials & Interfaces* **2012,** 4, (4), 2124-2131.

[2] Shih, J. C.; Cheng, J. H.; Owe-Yang, D. C.; Chang, C. Y., A Si device making method by using PAG contained TARC to enhance DOF of lithography process. *Journal of Photopolymer Science and Technology* (2005), 18(3), 415-418.

[3] Koo, H. Y.; Lee, H. J.; Kim, J. K.; Choi, W. S., UV-triggered encapsulation and release from polyelectrolyte microcapsules decorated with photoacid generators. *Journal of Materials Chemistry* **2010,** 20, 3932-3937.

[4] Liu, T. H.; Chemng, W. T.; Huang; K. T., Pigmentation of BOC-indanthrone through Photoacid-Catalysis in the Photo-polymeric Film. *Journal of Photopolymer Science and Technology* **2010,** 23, (4), 529-533.

[5] Utsumi, Y.; Seshimo, T.; Komuro, Y.; Kawaue, A.; Ishiduka, K.; Matsuzawa, K.; Hada, H.; Onodera, J., Studies of the photoacid generator material design for chemically amplified photoresists. *Japanese Journal of Applied Physics* **2009,** 48, (6), 06FC07/1-06FC07/5.

[6] Saito, Y.; Matsumoto, K.; Higashihara, T.; Ueda, M., A chemically amplified, negative-type photosensitive poly(phenylene ether ketone) (PEK) resist based on ketal-protected PEK and a photoacid generator. *Chemistry Letters* **2009,** 38, (11), 1048-1049.

[7] Houlihan, F. M.; Nalamasu, O.; Reichmanis, E, Retrospective of work at Bell Laboratories on the effect of fluorine substitution on the properties of photoacid

generators. *Journal of Fluorine Chemistry* **2003,** 122, (1), 47-55.

[8] Nakayama, S.; Harada, K.; Inoue, K.; Sasaki, K.; Seery, B.; Saito, N.; Koizumi, A., Distributions of perfluorooctanoic acid (PFOA) and perfluorooctane sulfonate (PFOS) in Japan and their toxicities. *Environmental Toxicology and Pharmacology* **2007,** 23, (1), 1-9.

[9] Zhang, T.; Sun, H.; Lin, Y.; Wang, L.; Zhang, X.; Liu, Y.; Geng, X.; Zhao, L.; Li, F.; Kannan, K.; Perfluorinated Compounds in Human Blood, Water, Edible Freshwater Fish, and Seafood in China: Daily Intake and Regional Differences in Human Exposures. *Journal of Agricultural and Food Chemistry* **2011,** 59, (20), 11168-11176.

[10] Yi, Y.; Ayothi, R.; Wang,Y.; Li, M.; Barclay, G.; Ca, H.; Ober, C. K., Sulfonium Salts of Alicyclic Group Functionalized Semifluorinated Alkyl Ether Sulfonates As Photoacid Generators. *Chemistry of Materials* **2009,** 21, (17), 4037-4046.

[11] Ayothi, R.; Yi, Y.; Cao, H.; Wang, Y.; Putna, S.; Ober, C. K., Arylonium photoacid generators containing environmentally compatible aryloxyperfluoroalkanesulfonate groups. *Chemistry of Materials* **2007,** 19, (6), 1434-1444.

[12] Vogt, B. D.; Kang, S.; Prabhu, V. M.; Lin, E. K.; Satija, S. K.; Turnquest, K.; Wu, W., Measurements of the Reaction Diffusion Front of Model Chemically Amplified Photoresists with Varying Photoacid Size. *Macromolecules* **2006**, 39, (24), 8311-8317.

[13] Rodriguez-Canto, P. J.; Nickel, U.; Abargues, R., Understanding Acid Reaction and Diffusion in Chemically Amplified Photoresists: An Approach at the Molecular Level. *Journal of Physical Chemistry C* **2011,** 115, (42), 20367-20374.

[14] Lawson, R. A.; Henderson, C. L., Mesoscale kinetic Monte Carlo simulations of molecular resists: effects of photoacid homogeneity on resolution, line-edge roughness, and sensitivity. *Journal of Micro/Nanolithography, MEMS, and MOEMS* **2010,** 9, (1), 013016/1-

013016/8.

[15] Wang, M.; Gonsalves, K. E.; Rabinovich, M.; Yueh, W.; Roberts, J. M., Novel anionic photoacid generators (PAGs) and corresponding PAG bound polymers for sub-50 nm EUV lithography. *Journal of Materials Chemistry* **2007,** 17, 1699-1706.

[16] Wang, M.; Jarnagin, N. D.; Lee, C. T.; Henerson, C. L.; Yueh, W.; Roberts, J.; Gonsalves, K. E., Novel polymeric anionic photoacid generators (PAGs) and corresponding polymers for 193 nm lithography. *Journal of Materials Chemistry* **2006,** 16, 3701-3707.

[17] Wu, Hengpeng; Gonsalves, K. E., Preparation of a photoacid generating monomer and its application in lithography. *Advanced Functional Materials* **2001,** 11, (4), 271-276.

[18] Lawson, R. A.; Lee, C. H.; Yueh, W.; Tolbert, L.; Henderson, C. L., Single Molecule Chemically Amplified Resists Based On Ionic and Non-ionic PAGs. *Proceedings of SPIE* **2008,** 6923, 69230K-1-10.

[19] Lawson, R. A.; Lee, C. H.; Whetsell, R.; Yueh, W.; Roberts, J.; Tolbert, L.; Henderson, C. L., Molecular Glass Photoresists Containing Photoacid Generator Functionality: A Route to a Single Molecule Photoresist. *Proceeding of SPIE* **2007,** 6519, 65191N-1-10.

[20] Sha, J.; Lee, J. K.; Kang, S.; Prabhu, V. M.; Soles, C. L., Bonnesen, P. V.; Ober, C. K., Architectural Effects on Acid Reaction-Diffusion Kinetics in Molecular Glass Photoresists. *Chemistry of Materials* **2010,** 22, (10), 3093-3098.

[21] De Silva, A.; Ober, C. K.; Hydroxyphenylbenzene derivatives as glass forming molecules for high resolution photoresists. *Journal of Materials Chemistry* **2008,** 18, 1903-1910

[22] Felix, N. M.; De Silva, A.; Ober, C. K., Calix[4]resorcinarene Derivatives as High Resolution Resist Materials for Supercritical CO2 Processing. *Advanced Materials* **2008,** 20, (7), 1303-1309.

[23] Yang, D.; Chang, S. W.; Ober, C. K., Molecular glass photoresists for advanced lithography. *Journal of Materials Chemistry* **2006,** 16, 1693-1696.

[24] Pfeiffer, F.; Felix, N. M.; Neuber, C.; Ober, C. K.; Schmidt, H. W., Physical Vapor Deposition of Molecualr Glass Photoresists: A New Route to Chemically Amplified Patterning. *Advanced Functional Materials* **2007,** 17, (14), 2336-2342.

[25] De Silva, A.; Lee, J. K.; Andre, X.; Felix, N. M.; Cao, H. B.; Deng, H.; Ober, C. K., Study of the Structure-Properties Relationship of Phenolic Molecular Glass Resists for Next Generation Photolithography. *Chemistry of Materials* **2008,** 20, (4), 1606-1613.

[26] Pohlers, G.; Scaiano, J. C., A Novel Photometric Method for the Determination of Photoacid Generation Efficiencies Using Benzothiazole and Xanthene Dyes as Acid Sensors. *Chemistry of Materials* **1997,** 9, 3222-3230.

[27] Naito, T.; Asakawa, K.; Shida, N.; Ushirogouchi, T.; Nakase, M., Highly Transparent Chemically Amplified ArF Excimer Laser Resists by Absorption Band Shift for 193 nm Wavelength. *Japanese Journal of Applied Physics* **1994,** 33, 7028-7032.

CHAPTER 3

INORGANIC-ORGANIC HYBRID NANOPARTICLE PHOTORESISTS FOR NEXT GENERATION LITHOGRAPHY

Abstract

While organic-based chemically amplified photoresists have provided the sensitivity and resolution necessary for high-throughput fabrication of semiconductor devices, there are still issues that need to be addressed to continue to follow Moore's Law beyond the 22 nm node. A system of inorganic-organic photoresists with a completely new patterning mechanism has been developed to address these issues. Hafnium oxide and zirconium oxide nanoparticles functionalized on the surface with various carboxylic acid-based ligands have been synthesized. The particles have an average size of 1-3 nm, with a narrow size distribution. The metal oxide core provides significantly higher etch resistance than even the most robust polymeric resist, enabling thin films to be used, eliminating pattern collapse due to high aspect ratio patterns. Compared to PHOST, the resists have shown over 25 times better etch resistance. This material has shown superior resolution when imaged with EUV lithography, producing 25 nm features with a sensitivity of 4.2 mJ/cm^2, the highest EUV sensitivity reported to date. Complete removal of organic material was achieved through a UV ozone/heat treatment to produce patterned metal oxides. These new hybrid systems have structural versatility, and have paved the way for an onset of new resist architectures to surpass the limitations of the state of the art material capabilities.

3.1 Introduction

Extreme Ultraviolet (EUV) Lithography has gained momentum as a leading candidate to extend to the sub-30 nm nodes[1,2], and has created a push to develop resist materials to take full advantage of its resolution capabilities. Because of the low power output of the current EUV source, resist sensitivity and the diffusion limitations of chemically amplified photoresists are central concerns of resist developers[3]. In order to meet the sensitivity and resolution demands, radical new resist designs must be considered.

Polymer systems are the current resist structures used in nanofabrication processes. However, the polydispersity and large molecular dimensions of polymers can limit the size of features that can be lithographically patterned[4,5]. Reducing the size of a resist molecule is believed to be an improvement to consistently yield high resolution patterns. Line edge roughness (LER) has been theoretically shown to decrease with reduced molecular weight of photoresists[6]. LER has been directly linked to the radius of gyration of a polymer resist. A smaller radius of gyration will consistently produce patterns with lower LER[6,7]. Low molecular weight organic compounds known as molecular glasses have been studied as an alternative to polymeric resists. Ober and co-workers have studied the effect of MG architecture on glass transition temperature (Tg) and resist performance, and have developed MG resists capable of producing sub-30 nm patterns with EUV lithography[8,9].

Traditionally, photoresists have been comprised of mainly organic materials because of the ease of synthesis, and their ability to be covalently functionalized. They can be modified to possess desirable photoresist properties such as thermal stability and an amorphous nature. Etch resistance is a key property to consider when choosing a successful photoresist structure. Previously, aromatic rings and rigid aliphatics have provided sufficient resistance to plasma etch

processes[10,11]. However, etch resistance limits are being challenged by the need for smaller features. As size requirements are driven to the sub-30 nm regime, aspect ratio becomes an increasingly large concern[12]. With a constant film thickness, smaller lines will produce high aspect ratio patterns. They become susceptible to pattern collapse during development by the capillary force created by the surface tension of the developer. In order to prevent pattern distortion, thinner, more robust films are needed.

Resists comprised solely of inorganic material have recently been studied[13-15]. Upon exposure to UV light, $Ge_2Sb_{1.5}Bi_{0.5}Te_5$ undergoes a phase change, which changes solubility of the material. While the etch resistance is exceptional, resolution is limited to around 250 nm. Recently, Stowers and co-workers have developed an inorganic resist based on hafnium oxide, which cross-links upon UV irradiation[16,18]. The resist can form high resolution features, but it is limited by its low sensitivity. Because these resists are all comprised of mostly inorganic material, they are not soluble in common organic spinning solvents. Deposition can be achieved by sputtering with a high vacuum system, or spin casting from an aqueous solvent. Each of these methods would require re-optimization of the well-established industrial lithographic process.

Organic-inorganic hybrid systems combine the favorable aspects of both materials. The structures are analogous to MG architectures, comprised of etch resistant cores and arms containing acid- or photo-labile substituents. The robust inorganic core provides thermal stability and resistance to plasma etching, while the organic portion enables solubility in organic solvents and ease of functionality. Functionalized inorganic-organic hybrid nanocomposites have been blended into resist materials[19]. The particles are less that 5 nm in diameter and are readily soluble in propylene glycol methyl ether acetate (PGMEA), a common spinning solvent with up to 50% wt/wt loading. The unusually high solubility of these metal oxide particles can be attributed to

the similarity of the organic ligands with the casting solvent. The particles were blended at 8 wt. % with poly(methyladamantane methacrylate-co-α-methacryloxy-γ-butyrolactone) (PMAdMA-co-GBLMA) photoresist and resolved 200 nm line/space patterns with e-beam lithography. These promising results helped pave the way for resists structures based on nanoparticles. Titanium oxide functionalized with methyl methacrylate has been patterned with nanoimprint lithography to produce 20 nm feature sizes[20]. Titanium and zirconium oxide nanoparticles decorated with methacrylic acid ligands have produced 250 nm features when exposed to DUV radiation[21]. Hafnium oxide nanoparticles have been previously studied by Ober and co-workers for 193 nm lithography and e-beam lithography, showing around 35 nm feature sizes with very high sensitivity for both exposure methods[22-25].

This paper discusses the preparation and characterization of hafnium and zirconium oxide nanoparticles containing carboxylic-acid based ligands. The versatile, one-pot synthesis can be used to prepare various metal oxide nanoparticles functionalized with a variety of carboxylic-acid based ligands. The new materials have the capability to produce high resolution features with extremely low EUV radiation doses by a completely new patterning mechanism. By radically redesigning the molecular architecture, these materials can surpass the limitations seen with previously studied photo-reaction pathways.

3.2 Experimental

3.2.1 Materials

All materials were purchased form Sigma Aldrich and were used as received.

3.2.2 Nanoparticle Synthesis

A similar synthesis of inorganic-organic nanoparticles has been described in a previous publication[21]. 5 g (12 mmol) of either hafnium or zirconium isopropoxide was added to 25 mL of the appropriate carboxylic acid to a three-necked round-bottomed flask fitted with a condenser. The mixture was heated to 65°C while stirring, and then allowed to equilibrate for 15 minutes. In a separate flask, 9 mL acid was added to 1 mL deionized (DI) water, and stirred to form a homogeneous solution. The resulting solution was added slowly to the reaction flask via a syringe, over the course of one minute. Complete dissolution of the starting material occurred during this addition. The solution was stirred at 65°C for 18 hours, at which time another homogeneous solution of 9 mL acid and 1 mL DI water was added. After an additional 2 hours, the reaction was cooled and the nanoparticles precipitated by adding DI water in a 2:1 volume ratio. The nanoparticles were then centrifuged at 8000 rpm for 8 minutes to separate them from the reaction solvent, which was decanted after this process. Unbound acid was removed from the nanoparticles by dissolving them in acetone, precipitating in DI water, and separating the solids and liquids via centrifuge. This process was repeated 4 times to ensure the complete removal of any free acid. The resulting white solid was placed under vacuum at room temperature for 24 hours to form 3.1 g of a dry white powder. The yield of this reaction is around 70%.

3.2.3 Negative Tone Processing

The nanoparticles were dissolved in PGMEA to make a 3 wt % solution. The photoactive compound was added at 5 wt% with respect to the nanoparticles. The solution was filtered twice with a 0.2 μm filter and then spin-coated onto a bare silicon wafer at 2000 rpm for 1 minute. The film was subject to a post apply bake (PAB) of 110°C for 1 minute to remove residual casting

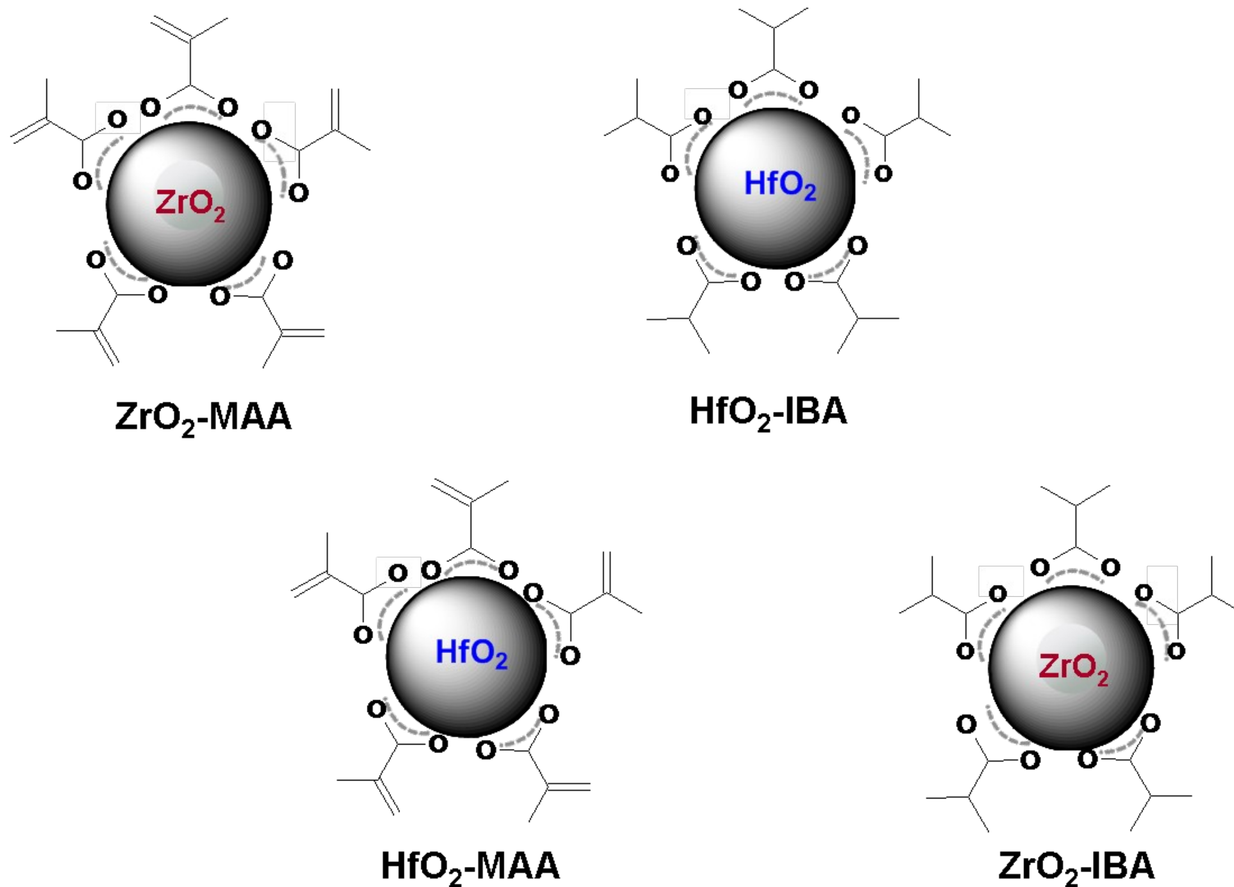

Figure 3.1 Structures of the inorganic-organic hybrid nanoparticles

solvent, then exposed with DUV, EUV or e-beam radiation. The film was then developed in a mixture of 4-methyl-2-pentanol and PGMEA.

3.2.4 Positive Tone Processing

The positive tone process follows the same procedure stated above until after the exposure step. The film is subject to a post exposure bake (PEB) of 130°C for 3 minutes, and then developed in a tetramethylammonium hydroxide solution (0.1 to 1.0 N).

3.2.5 Characterization

^{1}H NMR spectra were recorded on a Varian Inova-400 (400 MHz) spectrometer at room temperature. The chemical shift of a residual protic solvent ($CHCl_3$ at δ 7.26 ppm or DMSO at δ 2.50 ppm) was used as an internal reference. FT-IR spectra were recorded on a Mattson Instruments Galaxy 2020 FT-IR spectrometer. A TA Instruments Q500 Thermogravimetric Analyzer (TGA) was used measure the thermal decomposition of the hybrid materials. A Malvern Zetasizer Nano-ZS was used to measure the size of the nanoparticles with Dynamic Light Scattering. Materials were exposed using an ABM contact aligner for DUV exposure, the SEMATECH 0.3-NA extreme ultraviolet (EUV) microlithography tool for EUV exposure, or a JEOL JBX-9300FS Electron Beam Lithography System. Etch studies were done using a PlasmaTherm PT-72 reactive ion etcher using O_2, CF_4 or SF_6/O_2 plasma with various powers a flow rates.

3.3 Results and Discussion

3.3.1 Synthesis

A traditional hydrolysis condensation reaction is employed to synthesize the hybrid materials. The metal isopropoxide precursor is first dispersed in a large molar excess of a carboxylic acid derivative. Upon addition of water, the cloudy mixture becomes clear, indicating the onset of the hydrolysis condensation reaction to form a metal-oxide-metal network. The carboxylic acid plays a multi-functional role in the synthesis, acting both as a catalyst for the metal-oxide core formation, as well as participating in an esterification reaction to coat the surface of the inorganic core with organic ligands.

3.3.2 Structural Characterization

Several methods of characterization were used to ensure both nanoparticle formation and ligand attachment. Dynamic light scattering has been employed to determine the average size of the synthesized particles. All of the various nanoparticle systems have an average size between 1-3 nm and have a narrow size distribution (Figure 3.2). The ZrO_2 containing particles are consistently smaller than the HfO_2 particles, most likely due to the smaller atomic radius of zirconium. By optimizing the hydrolysis condensation reaction, it is possible to control the size of the nanoparticles. The 18 hour reaction run at the mild temperature of 65°C consistently produces nanoparticles of not only a small size, but a narrow size distribution as well.

FT-IR spectra of HfO_2-MAA and HfO_2-IBA were taken using thin films spin-coated on IR transparent double-sided polished silicon wafers (Figure 3.3). The strong peaks at 1427 and 1576 cm^{-1} correspond to the C-O stretch vibrations of the carboxylic acid. As expected, these peaks are shifted to a lower wavenumber than free methacrylic acid because bound ligands will

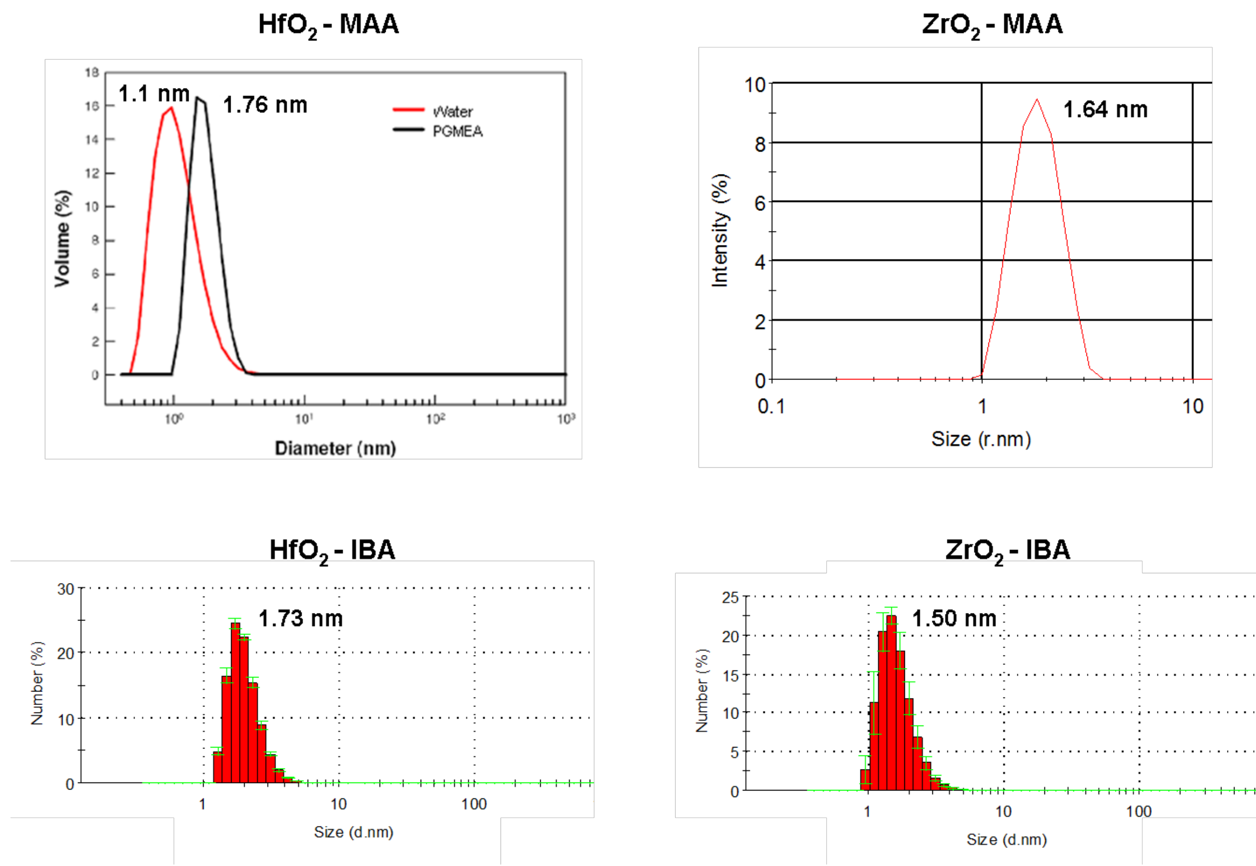

Figure 3.2 Size distribution plots of nanoparticle systems via dynamic light scattering

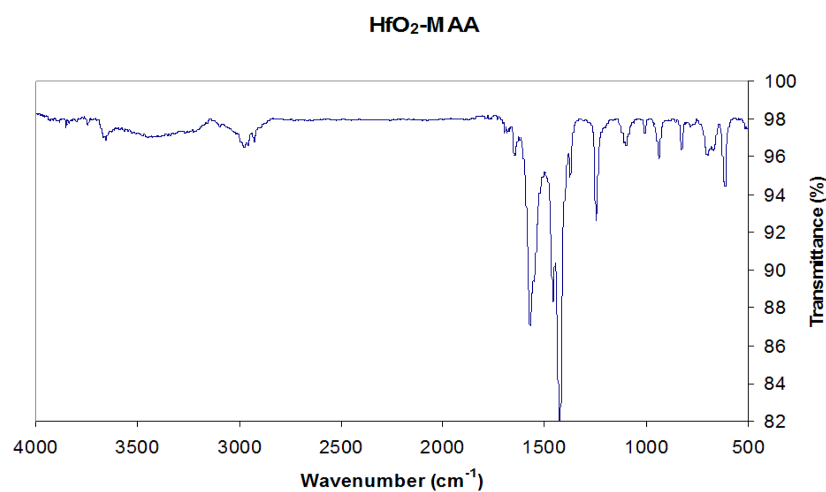

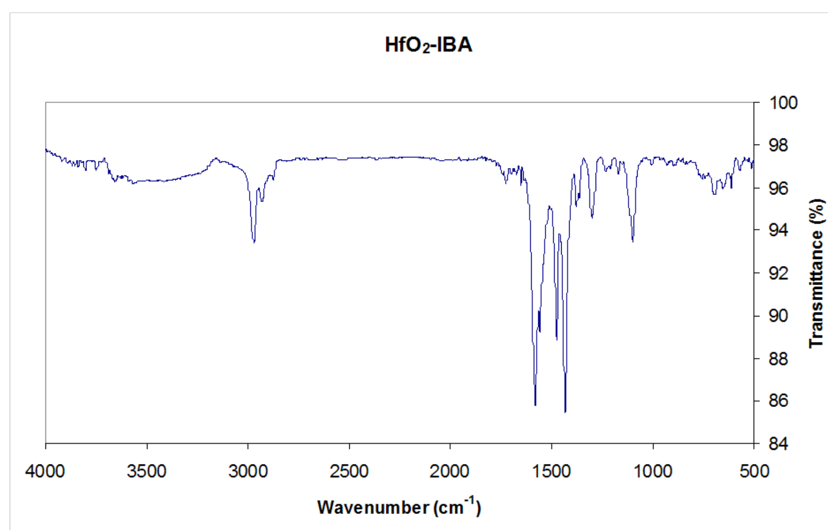

Figure 3.3 In-film FT-IR spectra of HfO_2-MAA and HfO_2-IBA

vibrate at a lower frequency. Each of the spectra show a peak of medium intensity around 1100 cm^{-1}, which corresponds to the C-O-C stretch of PGMEA, the spinning solvent used during the spin-coating process. The characteristic peak at 1650 cm^{-1} in the HfO_2-MAA spectrum corresponds to free double bond present in methacrylic acid. This peak is notably absent in the HfO_2-IBA spectrum, as there are no vinyl substituents in the structure.

^{1}H NMR was used to characterize the organic portion of the materials (Figure 3.4). The NMR spectra for both free methacrylic acid and isobutyric acid contain narrow peaks, as well as a characteristic peak at 12.5 ppm, corresponding to the hydroxyl proton of the carboxylic acid. The broadened peaks observed in the proton NMR spectra of the nanoparticles, as well as the absence of peaks around 12.5 ppm, indicate the organic ligands are bound to the metal oxide core[26], and that little or no free acid remains.

Thermogravimetric analysis was used to determine both the decomposition temperature of the resists, as well as the amount of organic present (Figure 3.5). The ZrO_2 nanoparticles show around 10 wt % more organics than the HfO_2 counterparts. Because of the smaller size of the Zr atom, there will most likely be more surface area on the metal oxide core on which to attach organic ligands, leading to a higher organic content in the ZrO_2 nanoparticles.

3.3.3 Effect of Ligand on Nanoparticle Solubility

Solubility in a suitable spinning solvent is a requirement for materials to be considered as photoresists. The organic ligand enables solubility of the nanoparticles in organic solvents for an otherwise insoluble metal oxide. To examine the effect of ligand structure on solubility, a variety of ligands were attached via a ligand exchange reaction with HfO_2-acetic acid nanoparticles[22]. The solubility of the resulting samples were tested in propylene glycol methyl ether acetate

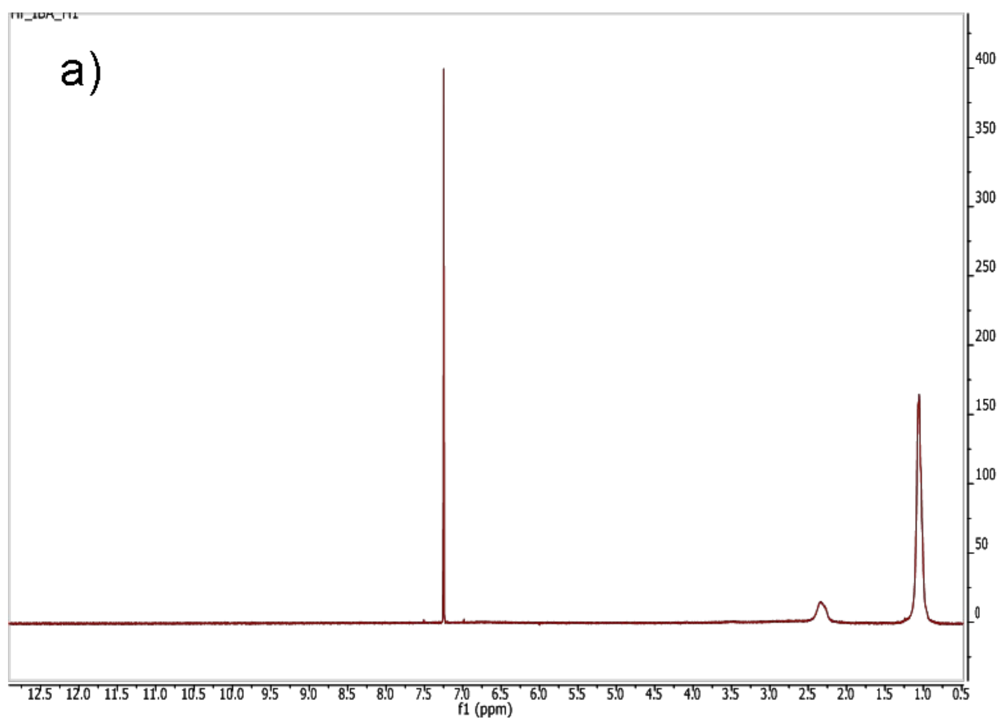

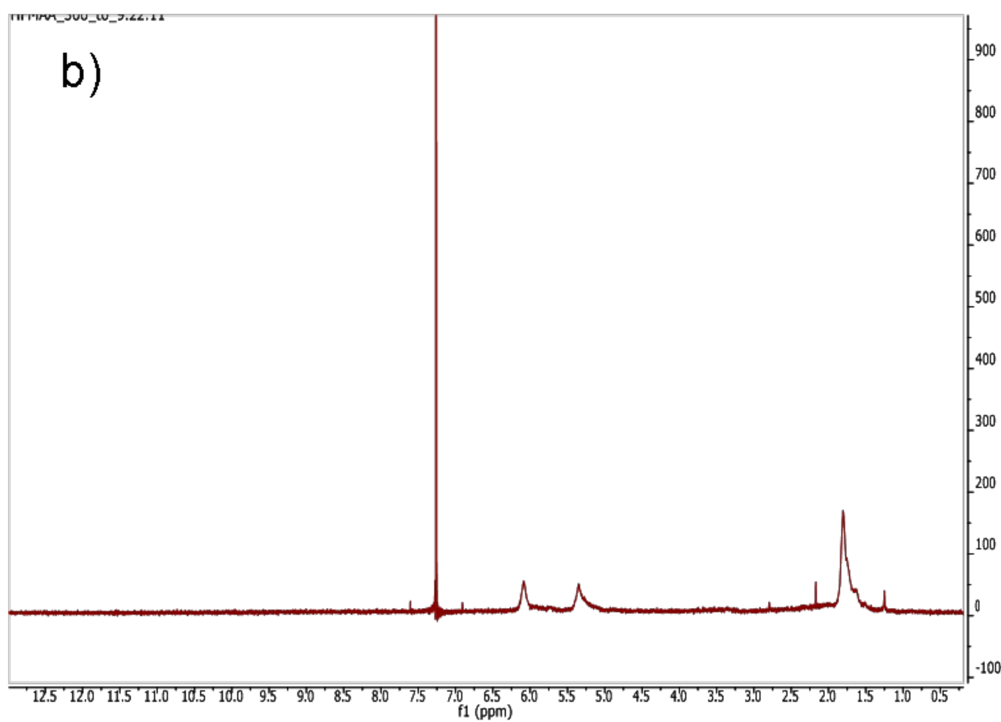

Figure 3.4 1H NMR spectra for a) HfO_2-IBA and b) HfO_2-MAA

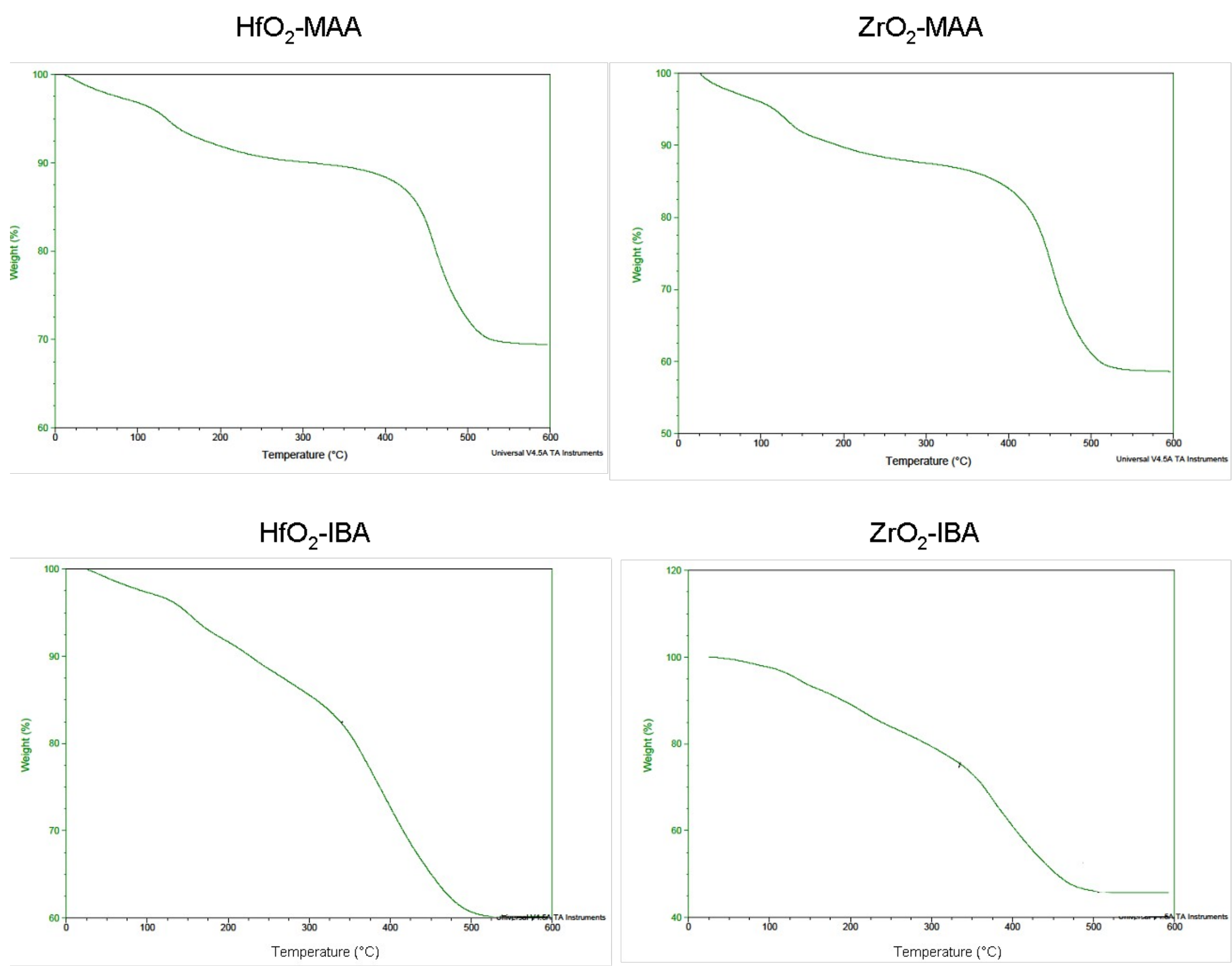

Figure 3.5 TGA curves of the hybrid nanoparticle systems

(PGMEA) (Figure 3.6). The mixtures were sonicated for 30 minutes to disperse the aggregated particles. The citric acid and phosphonopropionic acid nanoparticle mixtures were both turbid even after sonication. Citric acid is soluble in water, and insoluble in PGMEA, due to the three polar carboxylic acid substituents. When water soluble ligands, such as those substituted with sulfonic acid, are bound to a nanoparticle core, the system remains soluble in water[23], indicating that the citric acid nanoparticles will be water soluble, and continue to have poor solubility in PGMEA.

Methacrylic acid and acetic acid are both mono-functional carboxylic acid derivatives with a balance of hydrophobic methyl and vinyl groups and a hydrophilic carboxylic acid. The resulting functionalized nanoparticles were soluble in PGMEA. By covering the surface of the metal oxide with organic ligands, aggregation in solution is inhibited, which results in the formation of a clear, stable solution in organic solvents. Other mono-functional ligands such as the aforementioned isobutyric acid and propionic acid can form stable solutions in PGMEA when attached to a HfO_2 core.

3.3.4 Patternability

The solubility of the nanoparticles in a common spinning solvent enables lithographic processing of the materials with the well-established procedure. Before depositing onto a substrate, either a photoacid generator or photo-radical initiator is added to the solution at 5 wt % with respect to the nanoparticles. Free acid ligand is added to each mixture in very small amounts to keep the inorganic to organic content ratio the same for each resist batch. The amorphous materials create a homogeneous film when spin-coated onto a silicon substrate. The

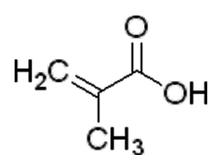

Methacrylic acid (MA)

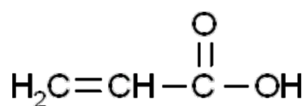

acrylic acid (AA)

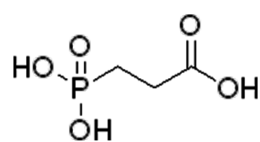

Phosphonopropionic acid (PA)

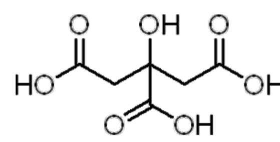

Citric acid (CA)

HfO$_2$-acetic acid
in PGMEA

Ligand addition and sonication

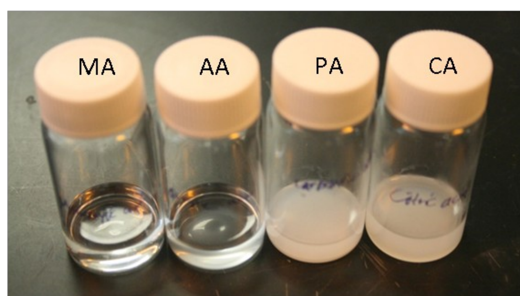

Figure 3.6 Solubility testing of HfO2 nanoparticles functionalized with various ligands

particles were exposed to DUV (254 nm) to establish usability as a photoresist. When initially designed, the expected patterning mechanism for the HfO_2-MAA and ZrO_2-MAA nanoparticles was the photo-radical induced cross-linking of the free double bonds, which would create negative-tone patterns. If this theory were correct, the HfO_2-IBA particles would not produce patterns. However, Figure 3.7 shows optical images of both positive and negative tone patterns produced with HfO_2-IBA particles with both a photo-radical initiator and a photo-acid generator. Because cross-linked material is insoluble in just about any solvent, the positive tone patterns suggest that cross-linking is not taking place during exposure. As HfO_2-IBA particles contain no double bonds, the reaction mechanism likely involves the detachment of the organic ligands from the nanoparticle surface. Further discussion of the patterning mechanism as well as a full mechanistic theory will be presented in the next chapter.

The ability to pattern not only the HfO_2-MAA but the HfO_2-IBA particles as well is a testament to the versatility of this new system. With the lithographic capabilities of the new systems established for DUV wavelengths, higher resolution lithographic techniques are needed to study the full capabilities of the nanoparticle systems.

3.3.5 EUV Lithography

3.3.5.1 Absorbance at EUV wavelength

In the range of DUV wavelengths, the absorbing behavior is dependent on the types of chemical bonds present. Isolated double bonds absorb in the range of 162 – 190 nm, while conjugated structures absorb at wavelengths of 210 nm and above. Therefore, designing a successful photoresist for a given wavelength required the presence or absence of certain chemical structures. For example, compounds designed for use with 193nm exposure contained

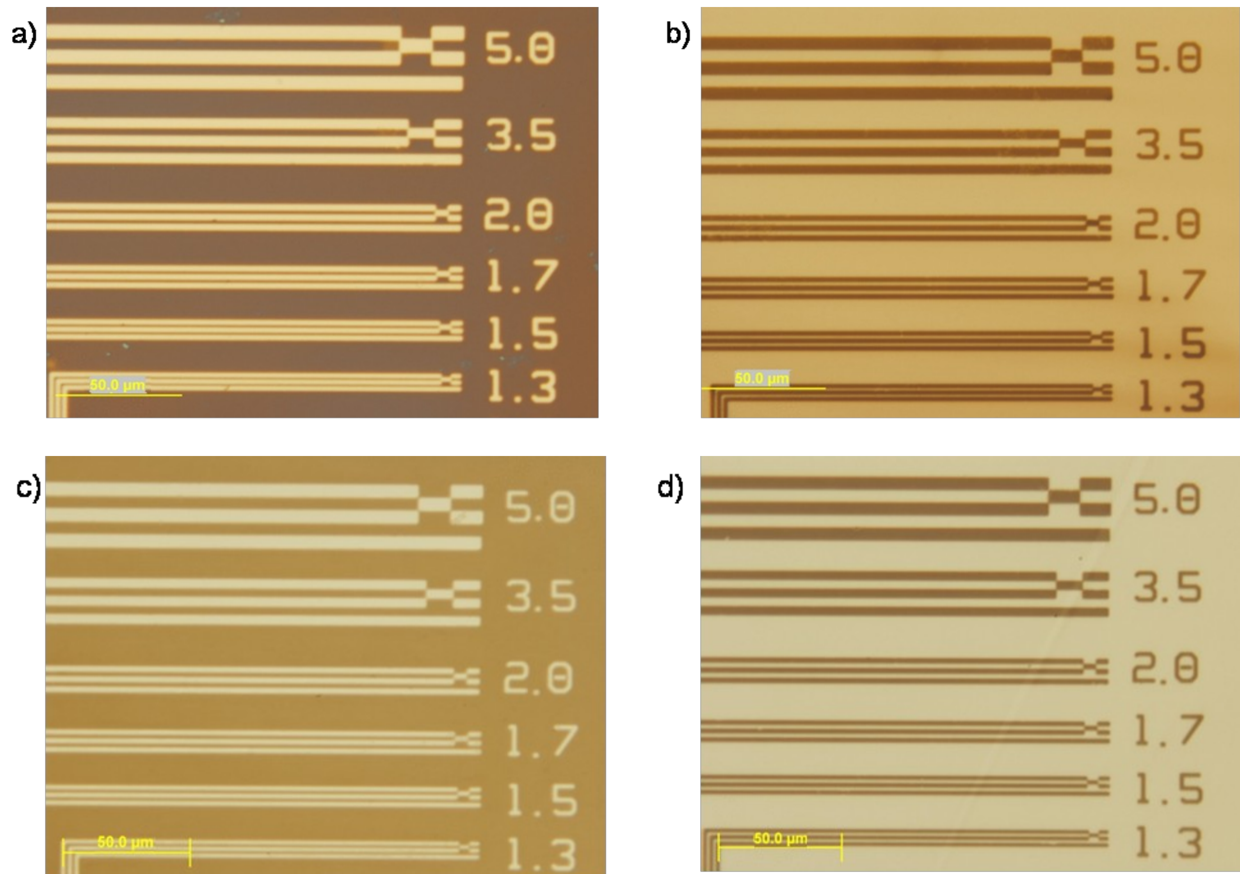

Figure 3.7 a) Positive and b) negative-tone patterns with HfO_2-IBA nanoparticle resist mixed with a photo-radical initiator (DPAP) c) positive and b) negative-tone patterns with HfO_2-IBA nanoparticle resist mixed with a photoacid generator

rigid aliphatic structures, as aromatics and double bonds absorbed too strongly in that region. At 13.5 nm, the absorbance characteristics of compounds drastically change. The amount of radiation that a material will absorb is based on its atomic composition and density. Figure 3.8 shows the relative photo-absorption cross-section of atoms at 13.5 nm.

When considering a material for use at EUV wavelength, it is necessary to strike a delicate balance of the amount of absorbed radiation. A material with too low absorbance will not absorb enough energy to induce the photochemistries required to produce a change in solubility. If the compounds absorb too much radiation, the light will not reach the bottom of the film. This has been known to cause distorted material profiles[27], if patterns are produced at all. The atoms found in the nanoparticle materials are highlighted in Figure 3.8. Hydrogen, carbon and zirconium are all absorb at relatively low amounts. Hafnium is more strongly absorbing, as is oxygen, which is found in all resist compositions. The presence of these atoms can increase the absorption of the materials, making them suitable candidates for EUV lithography. Absorption is also related to density, as shown in Equation 1. The higher the density of the material, the more absorbing the material will be. Both HfO_2 and ZrO_2 have a much higher density than typical organic compounds used in photoresists, which will lead to a higher absorbance, helping achieve optimum absorbance for high sensitivity and optimal resist profiles.

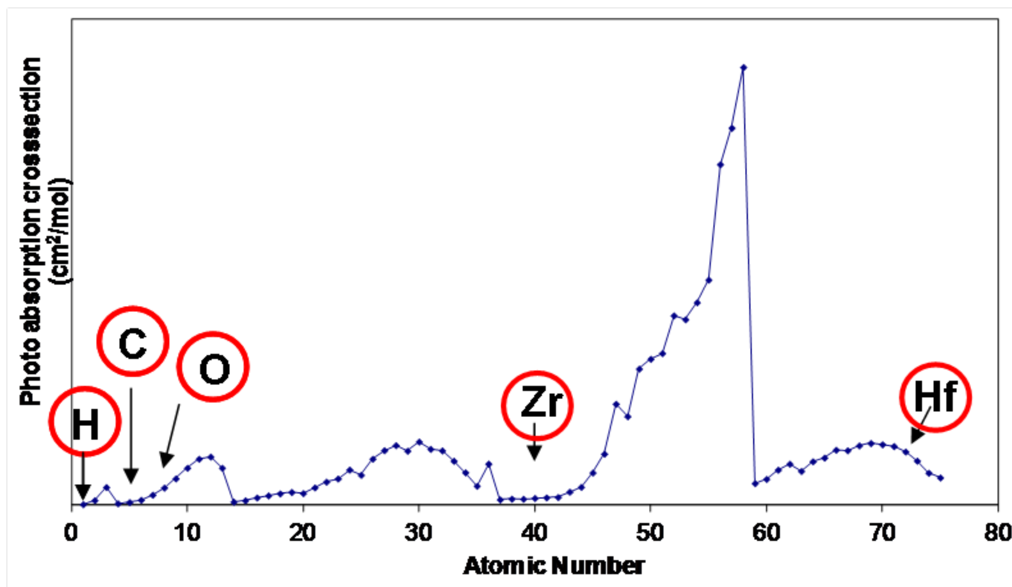

Figure 3.8 Relative photo-absorption cross section of atoms at EUV wavelengths

Equation 1 – Theoretical calculation of absorbance at 13.5 nm

$$\mu = \frac{N_A \rho}{MW} \sum_i x_i \sigma_{\alpha i}$$

where μ is the linear absorption coefficient of the given compound, ρ is the density, $\sigma_{\alpha i}$ is the atomic photo-absorption cross section, $MW = \sum_i x_i A_i$, where x_i is the number fraction of component i and A_i is the atomic weight of component i.

3.3.5.2 Additive Concentration

In order to understand the full potential of these materials for use with EUV lithography, it is necessary to examine the role of additives on the quality of the produced patterns. As a point of reference, 40 nm line/space patterns were imaged with the negative tone process with EUV lithography for each of the different resist compositions to compare the effects of varying the additive concentrations (Figure 3.9). With 3 wt % PAG added to the resist mixture, bridging between adjacent lines and inconsistent line widths is evident. By increasing the PAG concentration to 5 wt %, no bridging is observed, and with 7 % of the photoactive compound, very little line width variation is observed. As discussed previously, the theory of the patterning mechanism involves a displacement of the ligands by photo-generated acid. By increasing the amount of acid, the number of detached ligands in the exposed area increases. This will provide a larger solubility contrast between exposed and unexposed regions, which can produce smoother patterns.

The ratio of inorganic to organic components is an important factor in the ability to create high resolution patterns. The amount of free methacrylic acid added to the resist solution has been varied, and the effect on the resulting patterns was studied. The organic content shown in

Figure 3.9 corresponds to the total weight percentage of organics in the resist system. In samples with higher than 55 wt % organics, rougher lines are evident. With too much free acid in the resist mixture, the solubility contrast is less sharp between the exposed and unexposed regions, which can cause the boundaries to be blurred, increasing the roughness of the observed patterns.

3.3.5.3 Patterning with EUV Lithography

After optimization of the resist formula, an array of features with different exposure doses was created to gain insight on sensitivity of the material to EUV irradiation. The best results in terms of pattern quality are shown with a scanning electron micrograph in Figure 3.10. Extremely high resolution patterns with line widths of 25 nm were achieved with 3.8 nm line edge roughness, or amount of deviation from a perfectly straight line edge. The most notable aspect of this resist is the incredibly high sensitivity of 4.2 mJ/cm^2, or amount of UV radiation required to cause a photochemically-induced solubility switch. The resist industry currently relies on chemically amplified resist systems to achieve high sensitivity. The concept of chemical amplification involves the generation of acid catalyst upon UV irradiation that is regenerated after reacting with the acid-labile portion of the resist. Therefore, one acid molecule is responsible for a cascading set of reactions, so very little acid is needed to effectively cause a solubility change. While chemically amplifies systems have desirable exposure doses, uncontrolled diffusion of the photo-generated acid has plagues the industry, causing line broadening, image blur and increased pattern roughness[28, 29]. Though the nanoparticle resists require the addition of a photoacid generator or photo-radical initiator, it is important to note that this is a non-chemically amplified resist system. Therefore, high sensitivity is possible without the disadvantages of chemically amplified systems. The low levels of radiation needed to produce a solubility change of the material can be attributed to the strength of the bond between

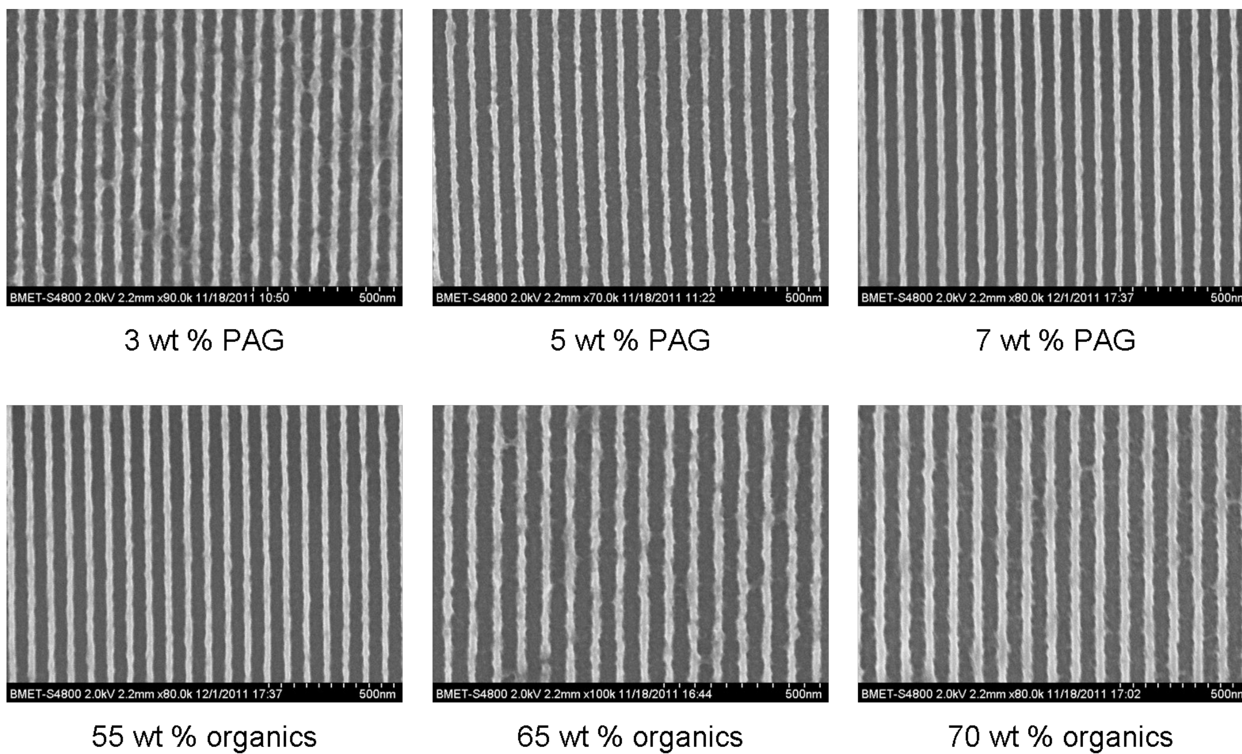

Figure 3.9 SEM images of HfO_2-MAA (negative tone) containing varied concentrations of PAG and free methacrylic acid

the organic and inorganic component. The bond is strong enough to produce stable nanoparticles capable of withstanding the harsh conditions of the lithographic process, yet delicate enough to break with minimal amounts of generated acid. Details on the new patterning mechanism of the nanoparticle resists will be discussed in a later chapter.

3.3.6 Etch Resistance

As discussed earlier, in order to fabricate smaller features, it is necessary to work with thinner films in order to prevent pattern collapse. Because of this requirement, etch resistance is a key factor for high resolution patterning. The metal oxide nanoparticle core is inert to oxygen plasma, and provides a strong resistance to fluorinated plasma gases. In order to maximize the etch resistance of the nanoparticle resists, various pre-etch treatments were used to remove the organic components, leaving the robust metal oxide core.

A post-development bake, or hard bake, was applied to decompose the organic portion of the photoresist. The patterned films were baked for 2 minutes at 200 °C, which will decompose the organic portion as indicated by TGA data. The resulting wafer was then examined to observe the effects of the thermal treatment on pattern quality. The resist patterns were cleaved, and the line edges were examined using a SEM, which revealed the formation of debris after heating (Figure 3.11). While 200°C is a high enough temperature to decompose the organics, the byproducts of decomposition are most likely not volatile, and can re-deposit onto the sample.

The method of using oxygen plasma to remove the organics was a more attractive method than a heat treatment because the process takes place under vacuum, which can prevent the re-deposition of the decomposed organics. The patterns were subjected to O_2 plasma operating at 150W, 60 mtorr, 50 sccm O_2 for 30 seconds. Figure 3.12 shows the etch rate of O_2 plasma

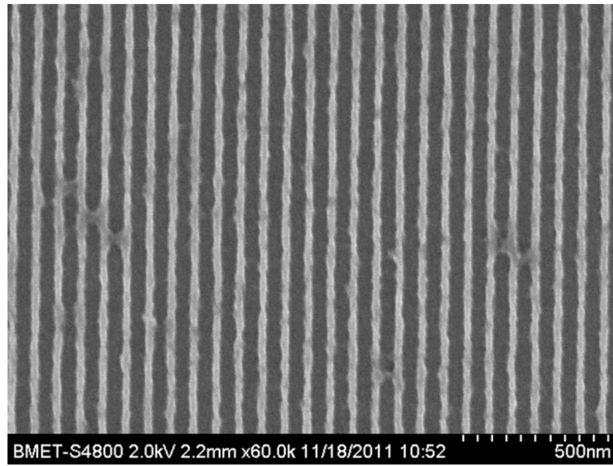

Figure 3.10 SEM image of 25 nm line-space patterns with ZrO_2-MAA (negative tone) obtained with EUV lithography with a dose of 4.2 mJ/cm^2

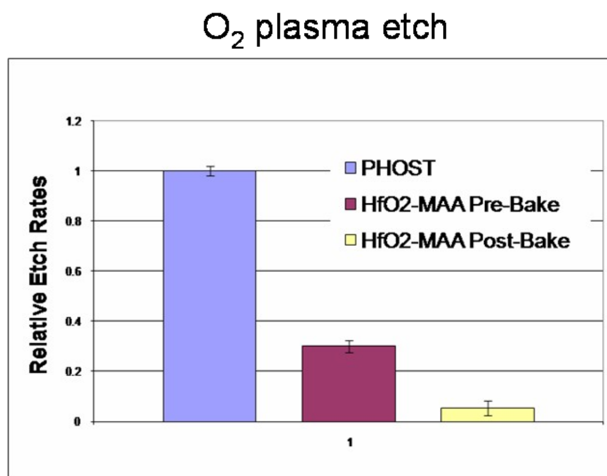

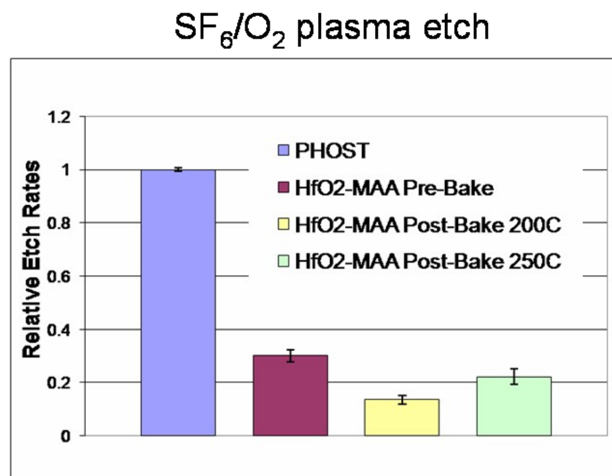

a) **b)**

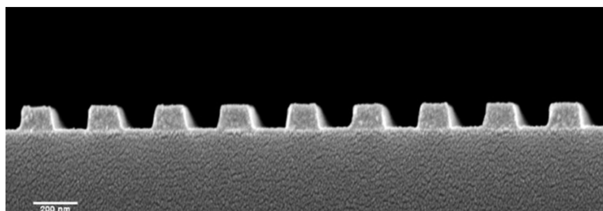

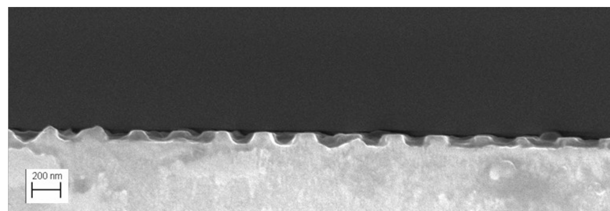

Figure 3.11 Top: Relative etch rates of HfO_2-MAA with and without a post-development bake compared to PHOST. Bottom: SEM image of resist profiles a) before and b) after the post-development bake

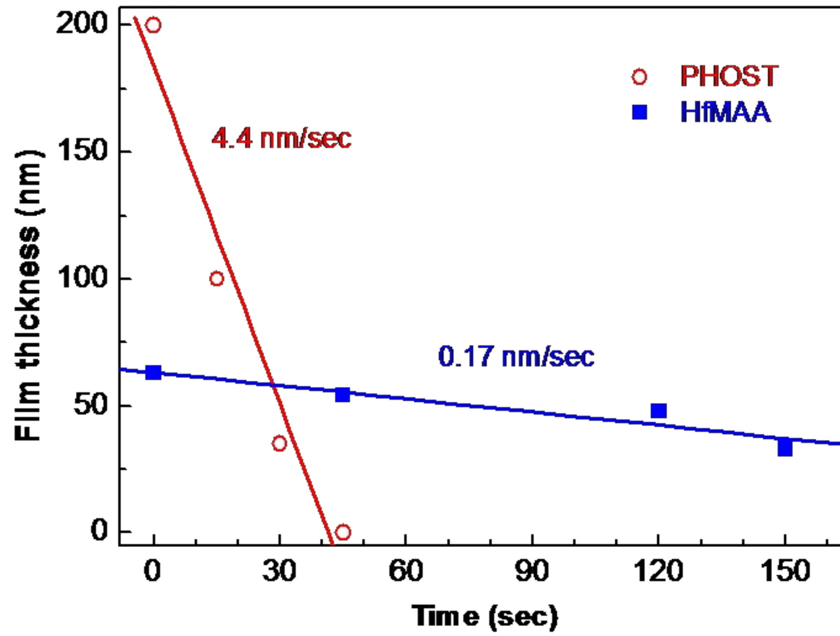

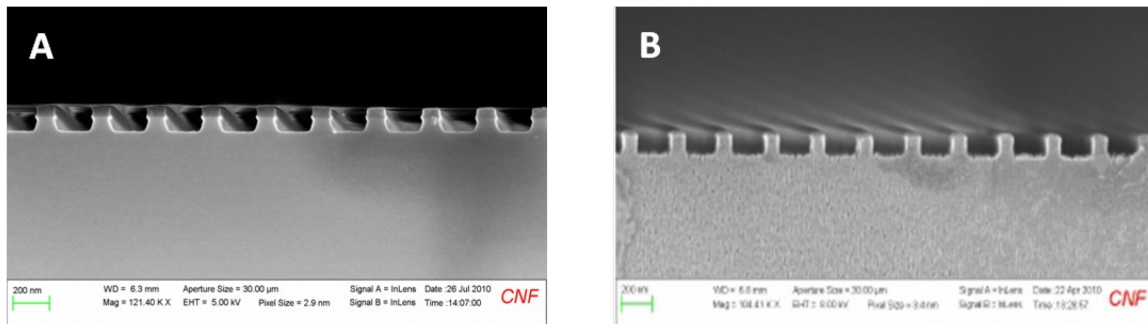

Figure 3.12 Top: Bottom: SEM images of A) Side view of 1:1 line/space patterns transferred by etching with SF_6/O_2 plasma, B) Side view of 1:1 line/space patterns transferred by etching with CF_4 plasma.

treated HfO_2-MAA to be over 25 times slower than that of poly(hydroxystyrene) with SF_6/O_2 plasma etch gas. Side views of the etched patterns reveal not only that the O_2 plasma treatment has no detrimental effect on the pattern shape, but that both SF_6/O_2 and CF_4 etch gases can effectively transfer the resist pattern to the underlying substrate without shape distortion.

By combining thermal and O_2 plasma treatment, it is possible to completely remove the organic components, leaving pure metal oxide patterns. Patterned HfO_2-MAA was subject to a UV Ozone clean process at 300°C for various time periods, and the film thickness was measured after each cycle to monitor the removal of organic material. The initial film thickness was measured to be 82 nm, and after 15 minutes of heated ozone treatment, the remaining film thickness was measured to be 22 nm. Treatments for longer times did not produce thinner films, indicating the complete removal of all organic material from the film. AFM studies were done on the resulting patterns to observe the film quality after treatment (Figure 3.13). The image reveals that there is no remaining debris on the patterns or substrate, and that the patterns retain the original shape. Because of the high resolution capabilities of this material, it can be used to pattern pure metal oxides with high resolution feature sizes, opening the door for a variety of applications.

3.4 Conclusions

This chapter presents the preparation and characterization of various metal oxide nanoparticles functionalized with carboxylic acid-functionalized ligands. The particles have a narrow size distribution between 1-3 nm, and can be purified to remove traces of unbound

a)

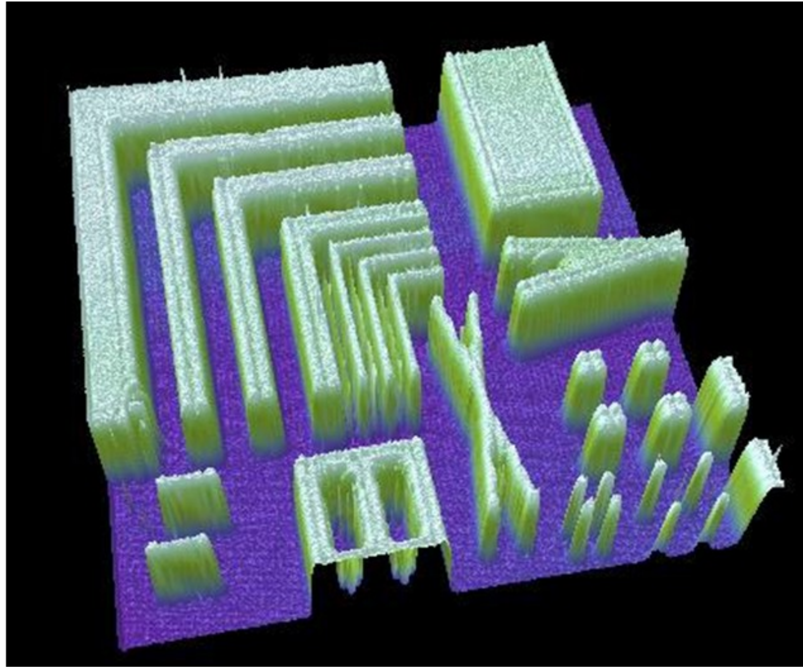

b)

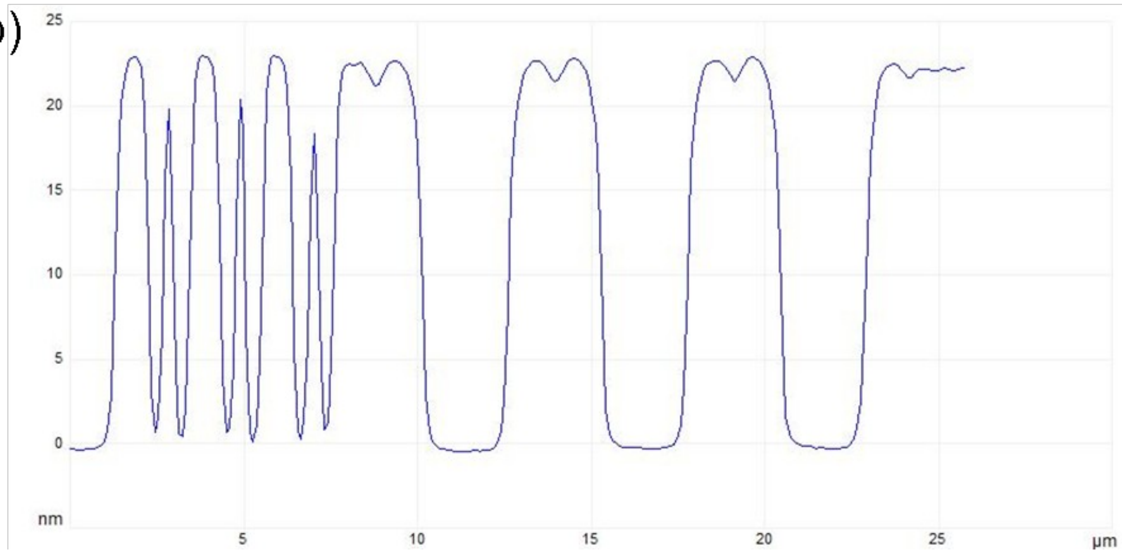

Figure 3.13 a) AFM image showing pattern surface after O_2 plasma treatment and b) height measurement of remaining patterns

ligands. The effect of multi-functional ligands on solubility of the particles was studied, and the nanoparticles were characterized with EUV lithography. Feature sizes of 25 nm with 3.8 nm LER were obtained, with the unprecedented high sensitivity of 4.2 mJ/cm^2, the highest EUV sensitivity reported to date. The etch resistance was studied while using multiple post-development treatments. Oxygen plasma was found to increase the etch resistance of HfO_2-MAA to over 25 times that of PHOST without degrading the features. A UV Ozoze/heat treatment was used to completely remove the organic material from the patterns, leaving pure metal oxide features. This material has shown the ability to function as a high resolution resist, and can be used for a variety of other applications as a patternable metal oxide material.

Acknowledgements

SEMATECH is gratefully acknowledged for funding. The Cornell Nanoscale Science and Technology Facility (CNF) and the Cornell Center for Materials Research (CCMR) are thanked for the use of their facilities. The Lawrence Berkeley National Lab, especially Patrick Nalleau, Chris Anderson and Lorie Mae Baclea-an, are thanked for the use of the Berkeley microfield exposure tool as well as valuable discussions. Prof. Paul McEuen and Josh Kevek are thanked for the use of the UV/Ozone cleaning tool, as well as assistance with AFM measurements. Intel and the Semiconductor Research Corporation Education Alliance (SRCEA) are gratefully acknowledged for a fellowship to support this research.

REFERENCES

[1] Cao, H. B.; Yueh, W.; Rice, B. J.; Roberts, J.; Bacuita, T.; Chandhok, M., Sources of Line-Width Roughness for EUV Resists. *Proceedings of SPIE* **2004,** 5376, 757-764.

[2] LaFontaine, B., et. al., The use of EUV lithography to produce demonstration devices. *Proceedings of SPIE* **2008,** 6921, 69210P/1-69210P/10.

[3] Bakshi, V., et. al., Status report on EUV source development and EUV source applications in EUVL. *Proceedings of SPIE* **2007**, 6533, 653315/1-653315/11.

[4] Yoshimura, T.; Shiraishi, H.; Yamamoto, J.; Okazaki, S., Nano edge roughness in polymer resist patterns. *Applied Physics Letters* **1993,** 63, (6), 764-766.

[5] Shiraishi, H.; Yoshimura, T.; Sakamizu, T.; Ueno, T.; Okazaki, S.; Nanometer-scale imaging characteristics of novolak resin-based chemical amplification negative resist systems and molecular weight distribution effects of the resin matrix. *Journal of Vacuum Science & Technology B: Microelectronics Processing and Phenomena* **1994,** 12, (6), 3895-3899

[6] Patsis, G. P.; Constantoudis, V.; Gogolides, E., Effects of photoresist polymer molecular weight on line-edge roughness and its metrology probed with Monte Carlo simulations. *Microelectronic Engineering* **2004,** 75, (3), 297-308.

[7] Patsis, G. P.; Gogolides, E., Effects of model polymer chain architectures and molecular weight of conventional and chemically amplified photoresists on line-edge roughness. Stochastic simulations. *Microelectronic Engineering* **2006,** 83, (4-9), 1078-1081.

[8] De Silva, A.; Ober, C. K., Hydroxyphenylbenzene derivatives as glass forming molecules for high resolution photoresists. *Journal of Materials Chemistry* **2008,** 18, 1903-1910.

[9] De Silva, A.; Lee, J. K.; Andre, X.; Felix, N. M.; Cao, H. B.; Deng, H.; Ober, C. K., Study

of the Structure-Properties Relationship of Phenolic Molecular Glass Resists for Next Generation Photolithography. *Chemistry of Materials* **2008,** 20, (4), 1606-1613.

[10] Huang, W. – S.; Kwong, R. W.; Moreau, W. M.; Lang, R.; Robinson, C. F.; Medeiros, D. R.; Petrillo, K. E.; Aviram, A.; Mahorowala, A. P.; Angelopoulos, M.; et al, A High Performance E-beam Resist Coupling Excellent Dry Etch Resistance and Sub 100nm Resolution for Advanced Mask and Device Making. *Proceedings of SPIE-The International Society for Optical Engineering* **2001,** 4343, 268-277.

[11] Abe, N.; Takechi, S.; Kaimoto, Y.; Takahashi, M.; Nozaki, K., Study of ArF resist material in terms of transparency and dry etch resistance. *Journal of Photopolymer Science and Technology* **1995,** 8, (4), 637-42.

[12] Chang, W.; Kim, E. – J.; Kang, Y. - M.; Park, S. - W.; Lim, C. – M.; Won, K. – T. ; Kim, J. - S.; Oh, H. –K., Characteristics and prevention of pattern collapse in EUV lithography. *Proceedings of SPIE-The International Society for Optical Engineering* **2007,** 6517, 65172S/1-65172S/7.

[13] Hongzhu Xi, H.; Liu,Q.; Tian, Y.; Wang, Y.; Guo, S.; Chu, M., $Ge_2Sb_{1.5}Bi_{0.5}Te_5$ thin film as inorganic photoresist. *Optical Materials Express* **2012,** 2, (4), 461-468.

[14] Lyubin, V.; Arsh, A.; Klebanov, M.; Dror, R.; Sfez, B., Nonlinear photoresists for maskless photolithography on the basis of Ag-doped As_2S_3 glassy films. *Applied Physics Letters* **2012,** 92, 011118-1-3.

[15] Indutnyy, I. Z.; Popescu, M.; Lorinczi, A.; Sava, F.; Min'ko, V. I.; Shepeliavyi, P. E., Interference lithography using chalcogenide inorganic photoresist. *Journal of Optoelectronics and Advanced Materials* **2008,** 10, (12), 3188-3192.

[16] Stowers, J.; Keszler, D. A., High resolution, high sensitivity inorganic resists.

Microelectronic Engineering **2009,** 86, (4-6), 730-733.

[17] Telecky, A.; Xie, P.; Stowers, J.; Grenville, A.; Smith, B.; Keszler, D. A., Photopatternable inorganic hard mask. *Journal of Vacuum Science & Technology, B: Nanotechnology & Microelectronics: Materials, Processing, Measurement, & Phenomena* 28, (6), C6S19-C6S22.

[18] Stowers, J. K.; A. T., Kocsis, M.; Clark, B. L.; Keszler, D. A.; Grenville, A.; Anderson, C. N.; Nalleau, P., Directly patterned inorganic hardmask for EUV lithography. *Proceedings of SPIE* **2011,** 7969, 79691-5.

[19] Bae, W. J.; Trikeriotis, M.; Sha, J.; Schwartz, E. L.; Rodriguez, R.; Zimmerman, P. A.; Giannelis, E. P.; Ober, C. K., High refractive index and high transparency HfO_2 nanocomposites for next generation lithography. *Journal of Materials Chemistry* **2010,** 20, 5186-5189.

[20] Lim, Su Hui; Saifullah, M. S. M.; Hussain, Hazrat; Loh, Wei Wei; Low, Hong Yee, Direct imprinting of high resolution TiO_2 nanostructures. *Nanotechnology* **2010,** 21, (28), 285303/1-285303/6.

[21] Ridaoui, H.; Weider, F.; Ponche; A.; Soppera, O., Direct ArF laser photopatterning of metal oxide nanostructures prepared by the sol-gel route. Nanotechnology **2010**, 21, (6), 065303/1-065303/10.

[22] Trikeriotis, M.; Rodriguez, R.; Zettel, M. F.; Bakandritsos, A.; Bae, W. J.; Zimmerman, P. A.; Ober, C. K.; Giannelis, E. P., High refractive index nanoparticle fluids for 193-nm immersion lithography. *Proceedings of SPIE* **2009,** 7273, (Pt. 1, Advances in Resist Materials and Processing Technology XXVI), 72732A/1-72732A/6.

[23] Cardineau, B.; Krysak, M.; Trikeriotis, M.; Giannelis, E.; Ober, C. K.; Cho, K. Y.;

Brainard, R., Tightly-Bound Ligands for Hafnium Nanoparticle EUV Resists. *Proceedings of SPIE* **2012,** 8322, 83220V-83220V-10.

[24] Trikeriotis, M.; Bae, W. J.; Schwartz, E.; Krysak, M.; Lafferty, N.; Xie, P.; Smith, B.; Zimmerman, P. A.; Ober, C. K.; Giannelis, E. P., Development of an inorganic photoresist for DUV, EUV, and electron beam imaging. *Proceedings of SPIE* **2010**, 7639, (Pt. 1, Advances in Resist Materials and Processing Technology XXVII), 76390E/1-76390E/10.

[25] Krysak, M.; Trikeriotis, M.; Schwartz, E.; Lafferty, N.; Xie, P.; Smith, B.; Zimmerman, P.; Montgomery, W.; Giannelis, E.; Ober, C. K., Development of an inorganic nanoparticle photoresist for EUV, e-beam, and 193 nm lithography. *Proceedings of SPIE* **2011**, 7972, (Pt.1, Advances in Resist Materials and Processing Technology XXVIII), 79721C/1-79721C/6.

[26] Owen, J. S.; Park, J.; Trudeau, P. – E.; Alivisatos, P., Reaction chemistry and ligand exchange at cadmium selenide nanocrystal surfaces. *Journal of the American Chemical Society* **2008,** 130, (37), 12279-12281.

[27] McIntyre, G.; Sanders, D.; Sooriyakumaran, R.; Truong, H.; Allen, R., The limitations of high index resists for 193nm hyper-NA lithography. *Proceedings of SPIE* **2008,** 6923, 692304/1-692304/12.

[28] Vogt, B. D.; Kang, S.; Prabhu, V. M.; Lin, E. K.; Satija, S. K.; Turnquest, K.; Wu, W., Measurements of the Reaction Diffusion Front of Model Chemically Amplified Photoresists with Varying Photoacid Size. *Macromolecules* **2006**, 39, (24), 8311-8317.

[29] Rodriguez-Canto, P. J.; Nickel, U.; Abargues, R., Understanding Acid Reaction and Diffusion in Chemically Amplified Photoresists: An Approach at the Molecular Level. *Journal of Physical Chemistry C* **2011**, 115, (42), 20367-20374.

CHAPTER 4

INVESTIGATION OF THE PATTERNING MECHANISM OF ORGANIC/INORGANIC HYBRID NANOPARTICLE PHOTORESISTS

Abstract

As Moore's Law continues to drive down size requirements for transistors, photoresist materials need to advance to pattern the required feature sizes. Extreme Ultraviolet Lithography (EUV-L) has emerged as a leading candidate to extent the resolution capabilities of current materials. However, due to the current low power source used with this tool, resist sensitivity is a central concern to resist manufacturers. Inorganic-organic nanoparticle photoresists have been introduced as a new photoresist material that has the capability to pattern high-resolution features with a dose of 4.2 mJ/cm^2, the highest EUV sensitivity reported to date. This material has also shown superior etch capabilities, with an etch resistance over 25 times better than that of poly(hydroxystyrene). While this system has exceptional lithographic characteristics, the mechanism by which it patterns was not fully understood. This paper provides in-depth analysis and characterization of the chemical and physical changes that occur during the lithographic process, and presents a complete mechanistic theory. A ligand exchange occurs during the exposure process, followed by a loss of organic ligands during the post exposure bake. This new understanding will enable the resist to be modified and engineered to produce lithographic results beyond its current capabilities.

4.1 Introduction

Nanoparticle systems have gained much attention in the scientific community because of their unique properties and extensive range of applications, including drug delivery[1,2], coatings[3,4], fuel cells[5,6], and biosensors[7]. The addition of an organic shell around the inorganic core can combine the properties of both components to create a compound with a unique set of physical and chemical properties[8]. The inorganic core can provide thermal stability, while the organic ligands can stabilize the particle, as well as promote solubility in organic solvents.

The organic ligands can also improve the miscibility of the particles in organic media. By dispersing inorganic-organic hybrid materials in polymer matrices, it is possible to enhance the system properties. A variety of properties can be altered by the addition of nanoparticles, including mechanical strengthening[9,10] and changing the refractive index[11-13]. Polymer nanocomposites have been used to control the viscosity of polymers[14], as well as reduce volume shrinkage, which have applications as OLED materials[15,16]. Nanocomposites have even been shown to control the flammability of vinyl polymers[17]. In addition to increasing the refractive index, the addition of an inorganic material into an organic polymer matrix can improve the robustness of the material when exposed to reactive ion etch plasma. Because of the great potential, functionalized hafnium oxide nanoparticles have been synthesized and used as additives with polymer photoresist to increase its refractive index to yield high resolution patterns with DUV lithography[18].

The small size of nanoparticles makes them an attractive candidate to function as the resist structure. Their structure is analogous to a molecular glass (MG), a low molecular weight amorphous material. MGs have been studied as alternatives to polymer resists[19-23] because it has been shown that reducing the size of a resist molecule can have a favorable effect on the

consistency of the line edge and line width of the resulting lithographic patterns[24,25]. While MGs mainly consist of organic materials, a strong effort has been made to incorporate inorganic materials into the structures. Recently, metal-oxide containing materials have been investigated for use as high-resolution photoresists. Keszler and co workers have developed a cross-linkable resist based on hafnium dioxide capable of 18 nm half-pitch line patterns with electron-beam lithography[26-28]. These materials show promise as next-generation photoresists, though low sensitivity is still a concern. As the metal oxides are comprised of mostly inorganic material, they are not soluble in common organic spinning solvents, requiring special processing during spin-coating. Inorganic-organic hybrid resists containing titanium oxide have been patterned with optical and nano-imprint lithography[29,30].

Ober and co-workers developed a photoresist system comprised of a hafnium- or zirconium-oxide core with a functionalized outer layer of organic ligands[31-33]. Hafnium dioxide is an intriguing material with a high refractive index and a high dielectric constant. With a melting point of 2758°C, it provides excellent thermal stability. The metal oxide is an exceptionally robust material in terms of chemical stability. The organic ligands coating the metal oxide surface enable solubility in common organic spinning solvents, which allow this material to be processed with current lithographic tools. The hybrid resist has shown extremely high etch resistance to oxygen plasma as well as various fluorinated etch gases. The most exciting aspect of this resist is the unprecedented sensitivity to extreme ultraviolet (EUV) radiation. High resolution patterns of 25 nm half-pitch lines have been resolved with a dose of 4.2 mJ/cm^2, the highest EUV sensitivity reported to date.

When mixed with a photoacid generator, this unique resist system is capable of dual-tone patterning by simply changing the post-exposure condition, and has shown amazing performance

with EUV lithography. One of the most intriguing aspects of this system is the mechanism by which the patterning proceeds. It was originally thought that free-radical cross-linking was causing the solubility change, but upon further investigation, it became evident that another mechanism was responsible. Though a photoacid generator is used, the system is non-chemically amplified, since there is no reaction occurring to regenerate the catalyst. Similar molecules have been studied as patternable materials[29,30], though no investigations into the patterning mechanism have been reported to our knowledge.

This paper reports an extensive, in-depth analysis of the positive and negative-tone patterning mechanism. A broad range of spectroscopic and other characterization techniques have been employed to probe the physical and chemical changes that occur to alter the solubility of the resist material. This study presents corroborative data and offers a theory of both the positive and negative tone patterning process. By fully understanding this new photochemistry, it is possible to use this knowledge to further engineer the material to push the sensitivity and resolution to unprecedented levels.

4.2 Experimental

4.2.1 Materials

All synthetic materials and photoresist additives were purchased from Sigma Aldrich and used without further purification.

4.2.2 Synthesis

A similar synthesis of hafnia nanoparticles has been described in a previous publication[30]. 5 g (12 mmol) of either hafnium or zirconium isopropoxide was added to 25 mL of the

appropriate carboxylic acid to a three-necked round-bottomed flask fitted with a condenser. The mixture was heated to 65°C while stirring, and then allowed to equilibrate for 15 minutes. In a separate flask, 9 mL acid was added to 1 mL deionized (DI) water, and stirred to form a homogeneous solution. The resulting solution was added slowly to the reaction flask via a syringe, over the course of one minute. Complete dissolution of the starting material occurred during this addition. The solution was stirred at 65°C for 18 hours, at which time another homogeneous solution of 9 mL acid and 1 mL DI water was added. After an additional 2 hours, the reaction was cooled and the nanoparticles precipitated by adding DI water in a 2:1 volume ratio. The nanoparticles were then centrifuged at 8000 rpm for 8 minutes to separate them from the reaction solvent, which was decanted after this process. Unbound acid was removed from the nanoparticles by dissolving them in acetone, precipitating in DI water, and separating the solids and liquids via centrifuge. This process was repeated 4 times to ensure the complete removal of any free acid. The resulting white solid was placed under vacuum at room temperature for 24 hours to form 3.1 g of a dry white powder. The yield of this reaction is around 70%.

4.2.2 Negative Tone Processing

The nanoparticles were dissolved in PGMEA to make a 3 wt % solution. The photoactive compound was added at 5 wt% with respect to the nanoparticles. The solution was filtered twice with a 0.2 μm filter and then spin-coated onto a bare silicon wafer at 2000 rpm for 1 minute. The film was subject to a post apply bake (PAB) of 110°C for 1 minute to remove residual casting solvent, then exposed with DUV, EUV or e-beam radiation. The film was then developed in a mixture of 4-methyl-2-pentanol and PGMEA.

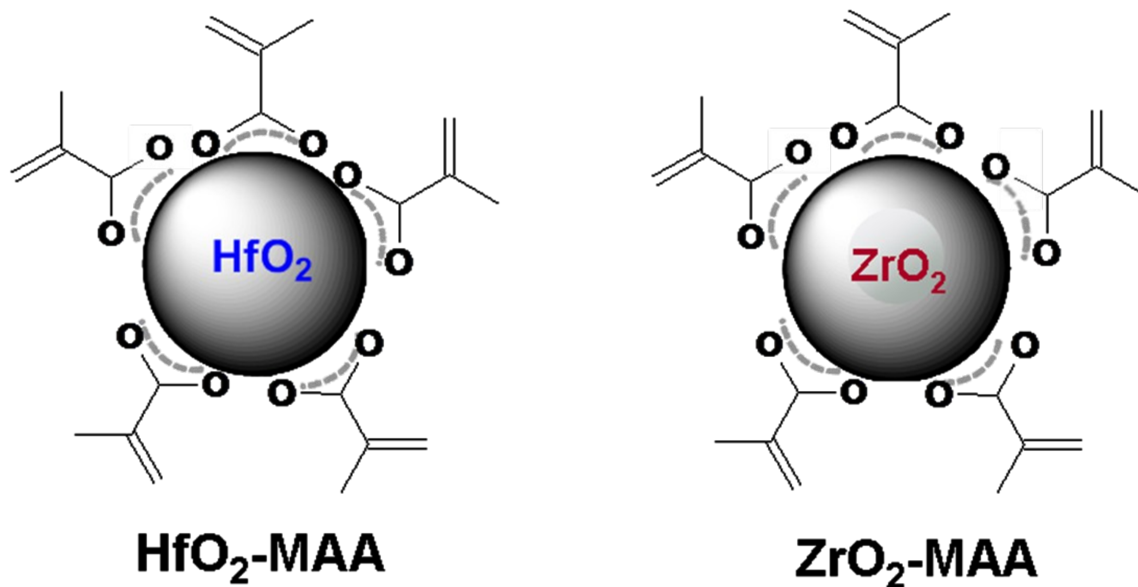

Figure 4.1 Nanoparticle resist structures

4.2.3 Positive Tone Processing

The positive tone process follows the same procedure stated above until after the exposure step. The film is subject to a post exposure bake (PEB) of 130°C for 3 minutes, and then developed in a tetramethylammonium hydroxide solution (0.1 to 1.0 N).

4.2.4 Characterization

^{1}H NMR experiments were performed using a Varian Inova-400 NMR spectrometer at room temperature. Chemical shifts reported are quoted in parts per million (ppm) and relative to DMSO (δ 2.50 ppm). FT-IR spectra were recorded on a Mattson Instruments Galaxy 2020 FT-IR spectrometer. Thin films were exposed with an ABM contact aligner using a 254 nm or 220 nm mirror, or a JEOL JBX-9300FS Electron Beam Lithography System operating at 100 keV. A Malvern Zetasizer Nano-ZS was used to measure the size of the nanoparticles via Dynamic Light Scattering. UV absorbance was measured with a Shimadzu-UV3101PC-UV-Vis-NIR Spectrometer. A TA Instruments Q500 Thermogravimetric Analyzer (TGA) was used to measure the resist weight loss as a function of temperature. Transmission electron microscopy images were taken using a FEI T12 Spirit TEM STEM. Ellipsometry measurements were made on a Woollamm Spectroscopic Ellipsometer.

4.3 Results and Discussion

4.3.1 Investigation of Patterning Mechanism During UV Irradiation

4.3.1.1 Optical Absorbance

The C=C double bond can be monitored with UV absorbance because it shows a strong absorption peak around 190-210 nm. To ensure that the absorbance peak at 200 nm is due to the double bond of the methacrylic acid and not any other part of the resist structure, hafnium propionic acid nanoparticles were synthesized according to the synthetic process above, using propionic acid. This ligand is similar to methacrylic acid; the only difference between the ligands is the absence of a double bond in propionic acid. The UV absorbance of these particles, as well as HfO_2-MAA particles were measured (Figure 4.2). The HfO_2-MAA particles show a strong absorption peak at 200 nm, while the hafnium propionic acid nanoparticles show very little absorbance in this region. This signifies that the double bond of the methacrylic acid is responsible for the absorption peak.

To determine if the double bond concentration is decreasing upon exposure, the resist formulation was spin-coated onto quartz wafers. The films were exposed to UV light at various doses, from completely unexposed to 600 mJ/m^2. The UV absorbance of each film was measured, and the results plotted in Figure 4.3. The optimum patterning dose of this resist formulation has been previously determined to be 150 mJ/cm^2. In doses of up to 200 mJ/cm^2, very little change was observed in film absorbance, indicating little to no loss of double bonds upon UV exposure.

4.3.1.2 Nuclear Magnetic Resonance Analysis

To corroborate the UV absorbance data, the presence of the double bonds was also monitored during UV irradiation with proton NMR spectroscopy. In-film conditions were simulated while performing NMR experiments. Resist solutions were spin-coated onto a silicon wafer and baked. One of the wafers was exposed to UV light at a dose of 150 mJ/cm^2, while the

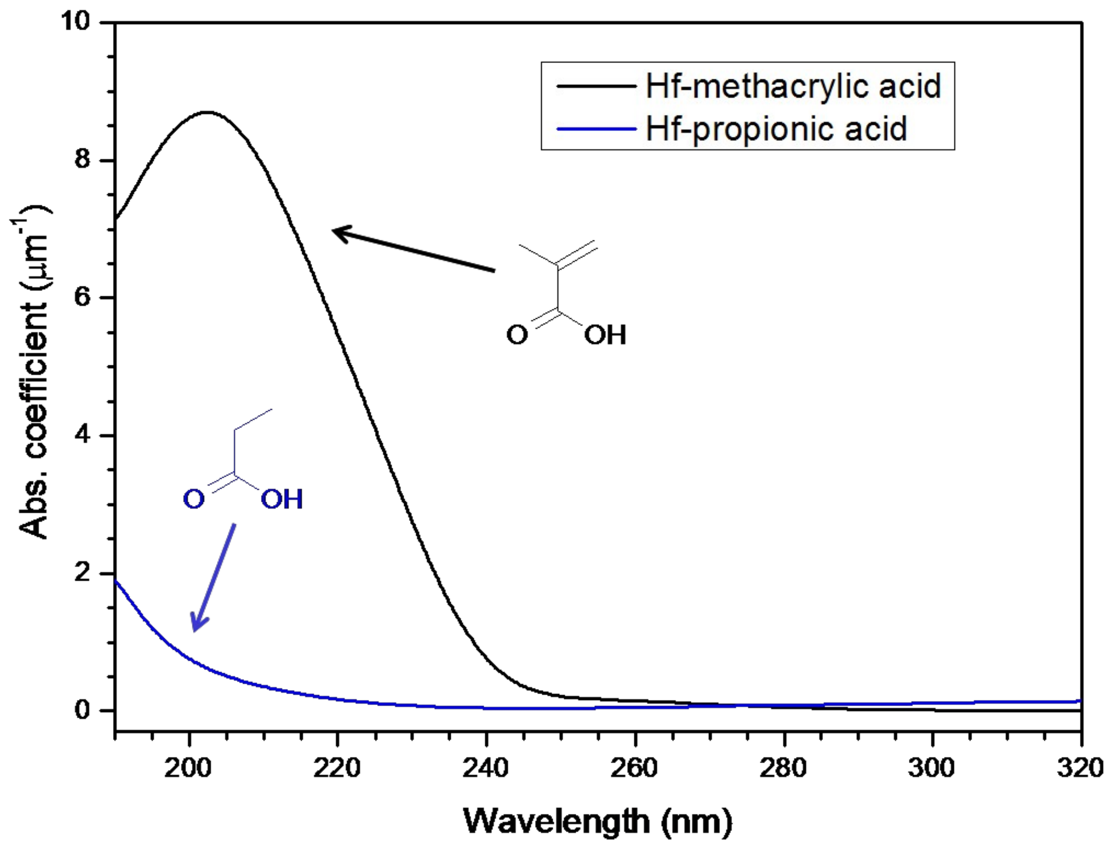

Figure 4.2 UV absorbance of HF-MAA and HF-propionic acid nanoparticles

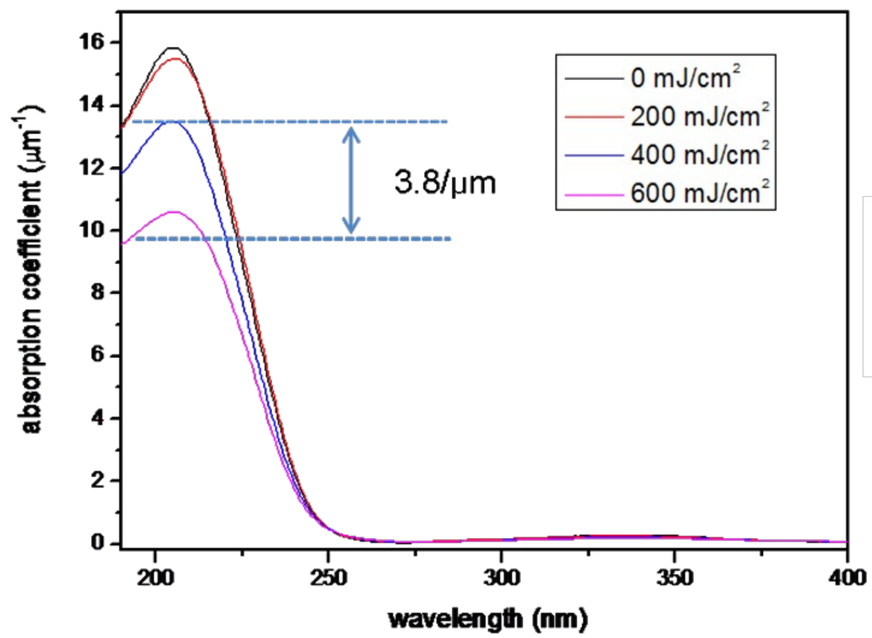

Figure 4.3 UV Absorbance of nanoparticles with different exposure doses

other film was left unexposed. The films were then scraped off, and the resulting powder was dissolved in deuterated DMSO solvent. The resulting NMR spectra are shown in Figure 4.4. The peaks at 5.30 and 5.95 ppm each correspond to one proton of the CH_2 at the end of the double bond of the methacrylic acid. The peak at 1.73 ppm represents the 3 protons of the methyl group. As this substituent is not reactive with UV irradiation, the ratios of double bond protons to methyl protons were measured before and after UV exposure to follow the vinyl group concentration. As expected, there was very little loss of vinyl protons, indicating that the double bonds are not cross-linking.

A final indication that free radical cross-linking is not responsible for the patterning mechanism has been shown in a previous chapter. Isobutyric acid ligands were attached to hafnium oxide particles and these resists were subject to the same patterning conditions as HfO_2-MAA. Isobutyric acid has the same chemical structure as methacrylic acid, except the vinyl group of methacrylic acid is replaced by a methyl group in isobutyric acid. The resist produced both positive and negative tone images without the presence of a vinyl group. Because of the overwhelming evidence against free-radical cross-linking at UV exposure doses used for patterning, other possible chemical and physical changes were explored.

4.3.1.3 Scanning Transmission Electron Microscopy (TEM) Analysis

To investigate the possibility of a metal-oxide network formation upon exposure, the particles were imaged using TEM after various steps in the lithographic process. As a control, the nanoparticle resist solution was spun on a bare Si wafer and subsequently baked at 110°C. The film was scraped off the surface using a razor blade, which resulted in about 1 mg of white powder. Care was taken to ensure the nanoparticles, whether in solution or film state, were never

exposed to UV radiation. The resulting powder was dissolved in dimethyl sulfoxide (DMSO), which resulted in a completely clear solution. The solution was filtered to remove aggregates, using a 0.2 μm filter. This filter will exclude any particles with a size of 200 nm and above, and since the resist has repeatedly produced lithographic patterns with 20-30 nm dimensions, it is not likely that the filter will remove any metal-oxide structures formed during UV exposure. These filtered solutions were then drop-cast onto a carbon-coated copper TEM grid. After the solvent dried, a thin layer of nanoparticles remained, which were imaged with TEM (Figure 4.5). Image a) shows the unexposed resist, and image b) depicts the resist after UV exposure. Both images show particles with an average size of less than 2 nm, which is consistent with the dynamic light scattering data shown in the previous chapter. This indicates that the metal-oxide core does not change size during the spin coating or thermal processes, and therefore is not a contributor to the solubility switch seen upon exposure.

To verify the TEM images, dynamic light scattering (DLS) was employed to investigate the size of the nanoparticle cores before and after exposure. While TEM is an effective method to visually confirm inorganic particle size, the images only represent a small portion of the film. DLS is measured in solution, and therefore can take a statistical average particle size of the entire resist film, providing a more accurate measurement. HfO_2-MAA was mixed with 5 wt % PAG, and half of the powder mixture was exposed to 254 nm UV light with a dose of 150 mJ/cm^2, while the other half remained unexposed. The two samples were dissolved in PGMEA and filtered using a 0.2 μm filter to remove dust particles and aggregates, and then measured using DLS. Figure 4.6 shows the size distribution of both the unexposed and exposed resist. The data is in agreement with the TEM images, and confirms that the metal oxide core is not changing in size.

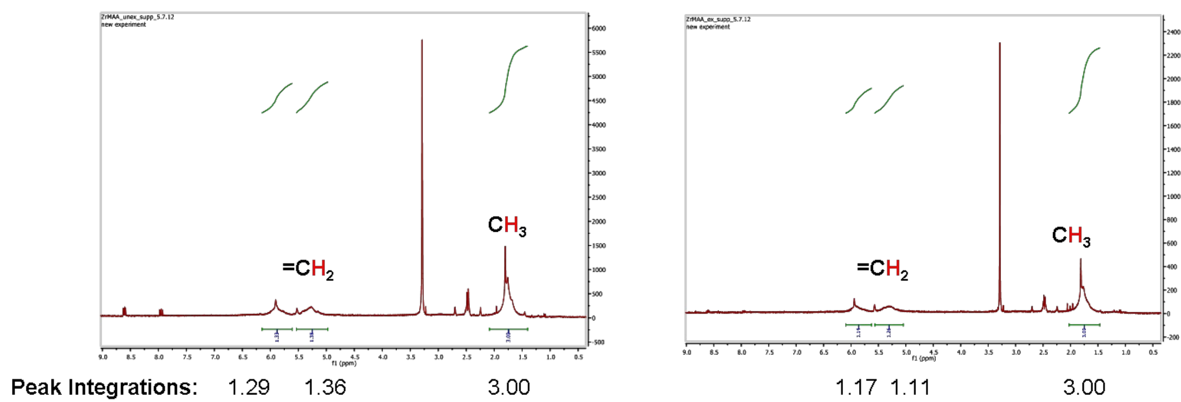

Figure 4.4 ¹H NMR spectra of HfO2 – MAA films a) before and b) after UV exposure

4.3.1.4 In-Film Fourier Transform-Infrared (FT-IR) Spectroscopy Analysis

The previous data shown has indicated that carbon-carbon double bond cross-linking and metal-oxide network formation does not contribute to the patterning mechanism. Therefore, by process of elimination, the solubility change in the nanoparticles must occur at the ligand-core interface. FT-IR is an effective spectroscopy method to observe the changes in chemical bonds upon UV exposure. To replicate the conditions of the resist during lithographic processing, the IR spectra were measured by using a double-sided polished silicon wafer as a substrate. The silicon wafer is transparent to IR wavelengths, and by measuring the IR spectra in the film state, the resist is observed under the same conditions during lithographic processing. Resist solutions containing HfO_2-MAA nanoparticles were spin-coated onto the double-sided polished silicon wafers, some were exposed to UV light, and measured using FT-IR spectroscopy. The IR spectra measured are shown in Figure 4.7. The spectrum on the left was obtained by referencing a blank silicon wafer as the background spectrum, and measuring the unexposed resist film as an example. The image on the right is the spectrum of the exposed resist film. However, instead of referencing a blank silicon wafer as the background, the spectrum of the unexposed resist film was referenced. The peaks in the image on the right indicate changes in the film. The y-axis is measuring absorbance intensity, therefore, peaks that appear in the positive-y direction are bonds that are appearing after UV exposure, and peaks in the negative direction are bonds that are no longer present after UV exposure. As discussed in a previous chapter, the peaks at 1427 and 1576 cm^{-1} correspond to the C-O stretch vibrations of the carboxylic acid. These distinct peaks appear in the negative y-direction, indicating a loss of bound carboxylic acid ligands. The peak present in the positive y-direction is a distinct peak present in the spectrum of unbound methacrylic acid. This data suggests the carboxylic acid ligands are detaching from the surface of

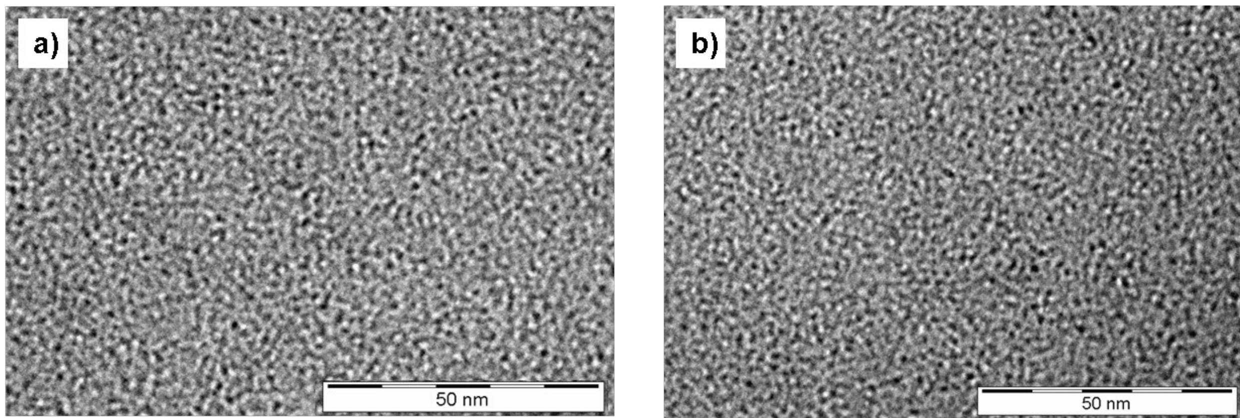

Figure 4.5 TEM images of HfO_2-MAA resist a) before and b) after UV exposure

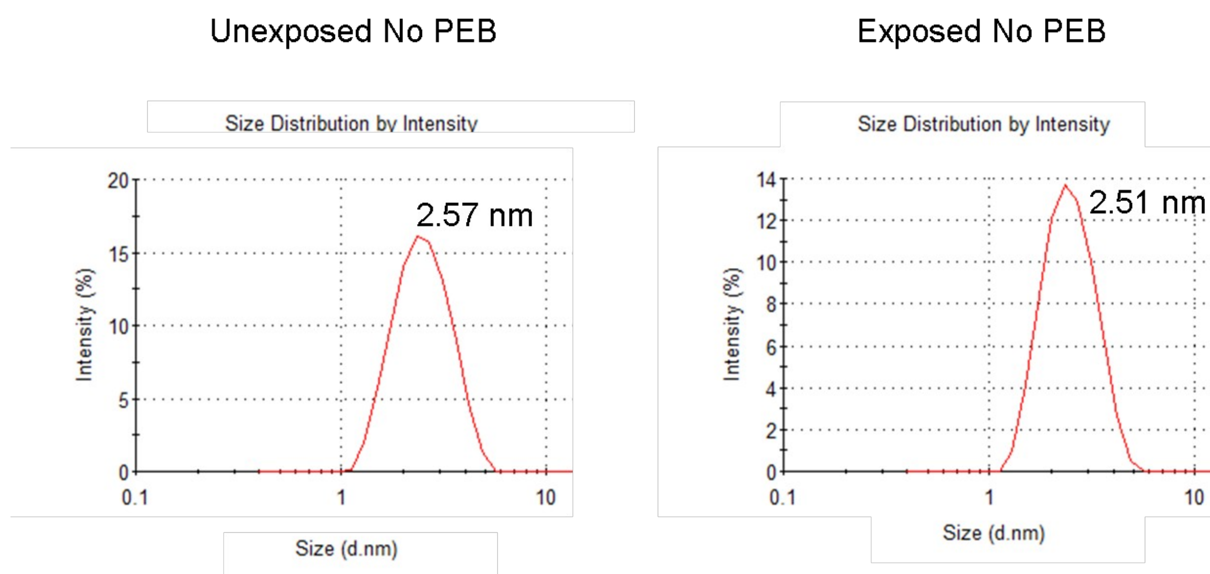

Figure 4.6 Particle size distribution with and without UV exposure as measured by dynamic light scattering

the metal-oxide core during UV exposure. A more complete explanation of the probable cause of the ligand displacement will be discussed later in this chapter.

4.3.2 Investigation of Patterning Mechanism During Post Exposure Bake

4.3.2.1 Thermogravimetric Analysis

As discussed previously, this resist yields negative tone patterns when exposed to UV light and developed in an organic alcohol. However, if the film is subject to a post exposure bake of 130°C for 3 minutes and developed in an aqueous base solution, positive tone patterns are achieved. The thermal treatment after exposure is the key step of the process that changes the tone of the photoresist. If the post exposure bake step is eliminated, both the exposed and unexposed portions of the film dissolve at the same rate. Therefore, the PEB changes the solubility of the unexposed regions in aqueous base.

Initial ^{1}H NMR analysis of films with and without a PEB did not show any significant differences between the two spectra, indicating that a chemical change was not likely occurring during the thermal treatment. Thermal characterization of the films with and without a PEB was used to gain an insight on how the organic content was changing. As described for previous experiments, resist solutions were spin-coated onto silicon wafers. Neither of the wafers was irradiated with UV light, but one of the films was subject to a PEB of 130°C for 3 minutes. This simulates the conditions of the unexposed regions during positive tone processing. The films were removed from the wafers using a razor blade, and the resulting powders were analyzed using thermogravimetric analysis (TGA) (Figure 4.8). The temperature was increased by 10°C/min. up to 600°C. The percentage weight loss up to this point can be used to determine the amount of organic content in the resist be cause all organic material will have decomposed at

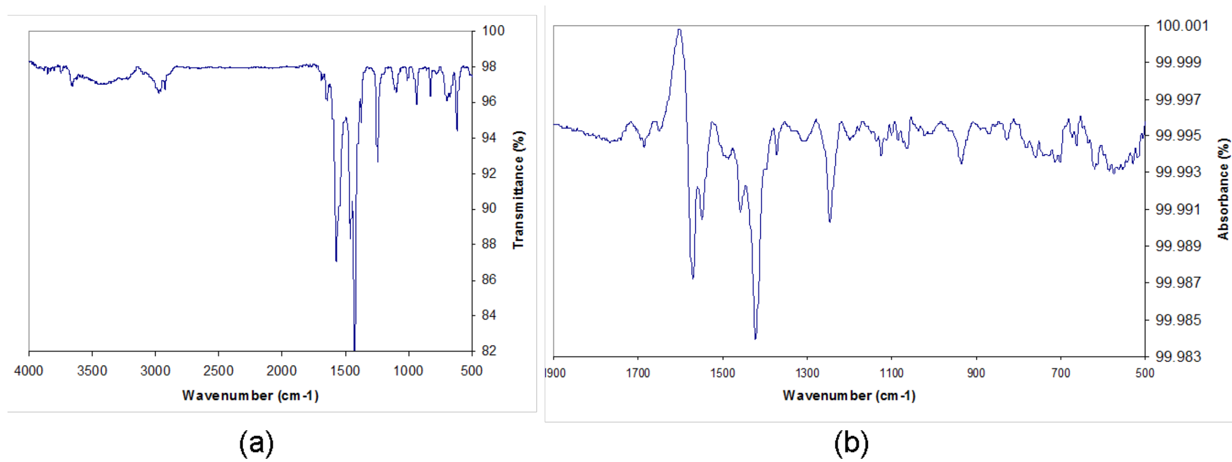

Figure 4.7 a) In-film FT-IR spectrum of HfO_2-MAA resist b) In-film FT-IR spectrum of HfO_2-MAA resist after exposure, referencing the unexposed spectrum as a background

600°C. The unexposed resist without a post exposure bake lost 38% of its mass, while the film with a PEB only lost 33 % of its mass. This indicates that there is less organic content in the film subject to a PEB, suggesting that some organic content was removed during the PEB.

4.3.2.2 In-Film FT-IR Analysis

To further investigate the potential loss of ligands from the film, in-film FT-IR was used. Similar to the experiment above, the resist films were spin-coated onto a polished double-sided silicon wafer. One of the films was exposed to 150 mJ/cm^2 of UV light, while the other film was left unexposed. The spectra of these two films were measured, and then each film was subject to a PEB of 130°C for 3 mins. The films were measured again, using the pre-PEB films as a background reference to observe the changes after PEB. The resulting spectra are shown in Figure 4.9. The y-axis measures transmission intensity, meaning peaks appearing in the positive y-direction are bonds that are disappearing. The C-O stretch peaks are reduced in both the unexposed and exposed region, with a higher intensity leaving the unexposed than the exposed film. In contrast to the FT-IR data shown above, there is no peak at 1600 cm^{-1}, or any other bond forming, indicating that free methacrylic acid is not staying in the film, but is leaving the film. The low intensity of the peaks indicate that a very small amount of methacrylic acid is leaving, though enough to cause a solubility change.

4.3.2.3 Film Thickness Changes After Various Process Steps

The film thickness after various lithographic steps was measured to investigate the possibility of the organic ligands leaving the film during the PEB. The thicknesses were measured with an ellipsometer, and the data tabulated in Table 4.1. The film thickness remains

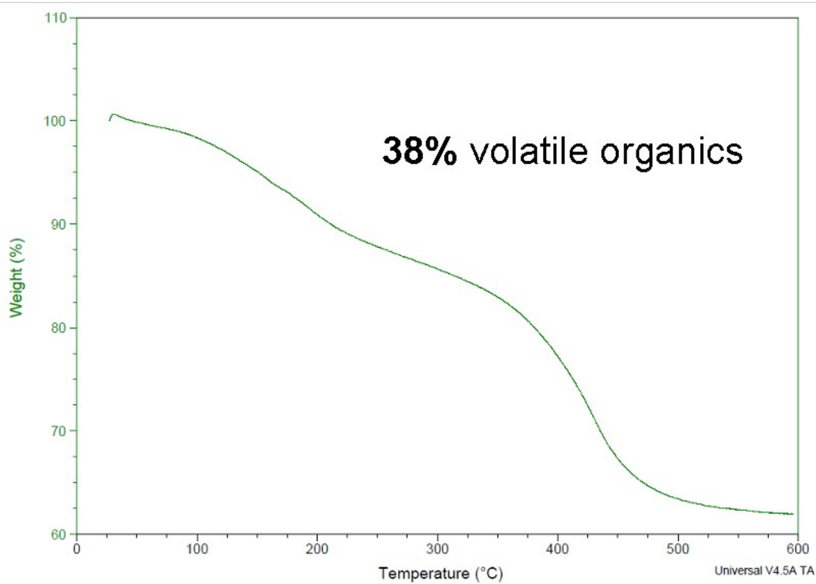

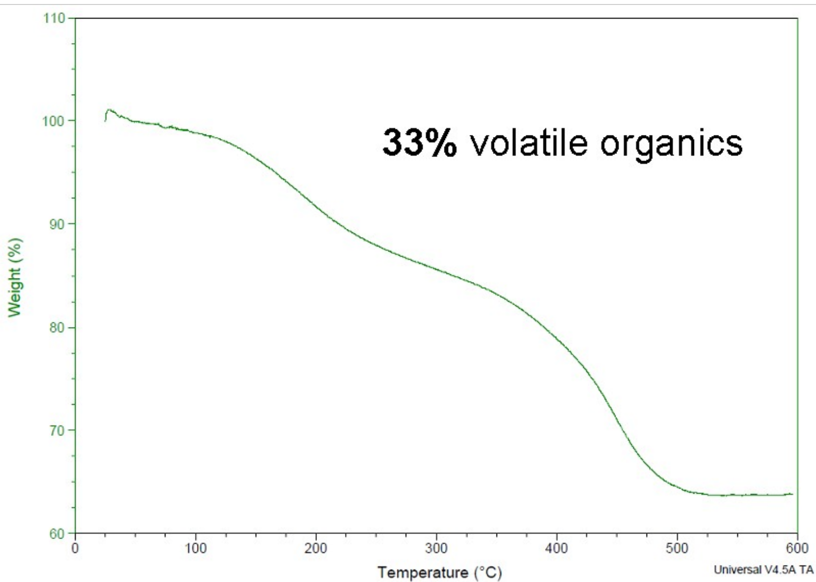

Figure 4.8 Thermogravimetric analysis of unexposed HfO_2-MAA before and after PEB

the same before and after UV exposure, but decreases after the PEB. The unexposed portion shows over twice the amount of film loss than the exposed regions. This is in agreement with the FT-IR data, which shows a higher intensity of C-O bonds lost in the unexposed region that in the exposed region.

4.3.2.4 Particle Size after PEB

To determine whether the metal-oxide core is changing size, DLS was used to measure NP size after the PEB in both the unexposed and exposed regions. The same procedure for sample preparation described above was used. The initial particle size distribution of the unexposed resist film was 2.5 nm. After spin-coating and PEB, the particle size in the unexposed regions grew to 4.2 nm. In the exposed regions, the particles grew to only 3.6 nm. This is a promising result, as the particles remain small after lithographic processing; extremely high resolution features patterned with this material are possible. This data also provides insight to the patterning mechanism, which will be discussed later in the chapter.

4.3.3 Patterning Mechanism

4.3.3.1 Negative Tone Patterning

The data shown for the negative tone mechanism suggests that the carboxylic acid ligands are removed from the surface of the metal oxide core. It is also known that either a photoacid generator or a photoradical initiator is needed to produce the solubility change. The uv exposure mechanisms for the photoradical initiator used, 2,2-dimethyoxy-2-phenylacetophenone (DPAP), and the photoacid generator, n-hydroxynaphthanene triflate, are shown in Figure 4.11.

HfO₂-MAA Unexposed + PEB

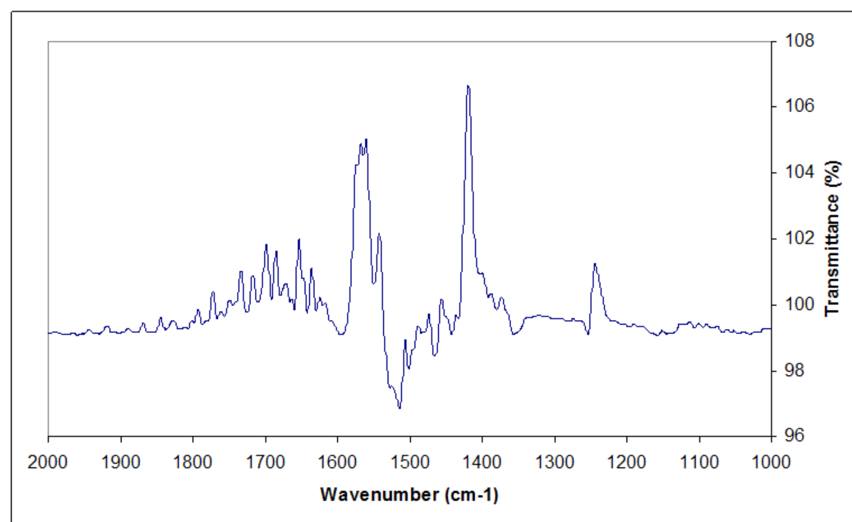

HfO₂-MAA Exposed + PEB

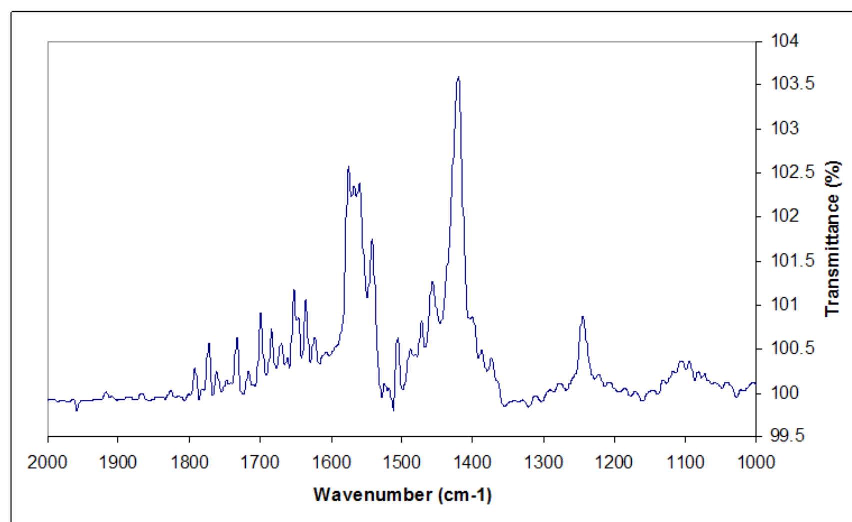

Figure 4.9 In-film FT-IR of unexposed and exposed films after PEB

Table 4.1 Resist film thickness after various lithographic process steps

	Unexposed No PEB	Exposed No PEB	Unexposed With PEB	Exposed With PEB
Film Thickness (nm)	117	117	100	106

When exposed, DPAP generates free-radicals. However, in the presence of water, the benzophenone radical can generate benzoic acid. This benzoic acid, or triflic acid in the case of the PAG, can displace the methacrylic acid ligand upon UV exposure (Figure 4.11). This ligand displacement can alter the solubility of the nanoparticles, making them less soluble in organic alcohols. It is also necessary to consider the number of moles of acid present per mol of methacrylic acid to verify that this is a viable mechanism. Previous work has defined a chemical structure for carboxylic acid-substituted ZrO nanoparticles[34]. Using this chemical structure, and the amount of organic content on the nanoparticles from TGA measurements, the amount of methacrylic acid in 100 mg of resist is 9.68×10^{-5} mol. Typical resist formulations consist of 5 wt % PAG, and 100 mg of resist would therefore contain 1.45×10^{-5} mol PAG. This works out to be roughly 1 acid molecule for every 7 methacrylic acid ligands. This is a reasonable equivalent to consider a solubility change via a ligand exchange.

4.3.3.2 Positive Tone Mechanism

Until the PEB, the process for patterning positive tone features is the same as the negative tone process. The PEB step causes a solubility switch in the unexposed regions, as explained above. Based on the data presented, it is plausible to conclude that the PEB causes the methacrylic acid ligands to detach from the surface of the metal oxide and leave the film (Figure 4.12). In the case of resist formulations containing PAG, the sulfonic acid ligands are more tightly bound to the nanoparticle surface[35], and therefore are unaffected by the PEB conditions. Benzoic acid, though still a carboxylic acid, has a boiling point of 249°C, much higher than the 130°C used to heat the film. This would make the ligand very unlikely to evaporate during the PEB step. In the exposed regions, where the ligand exchange has taken place, there is still

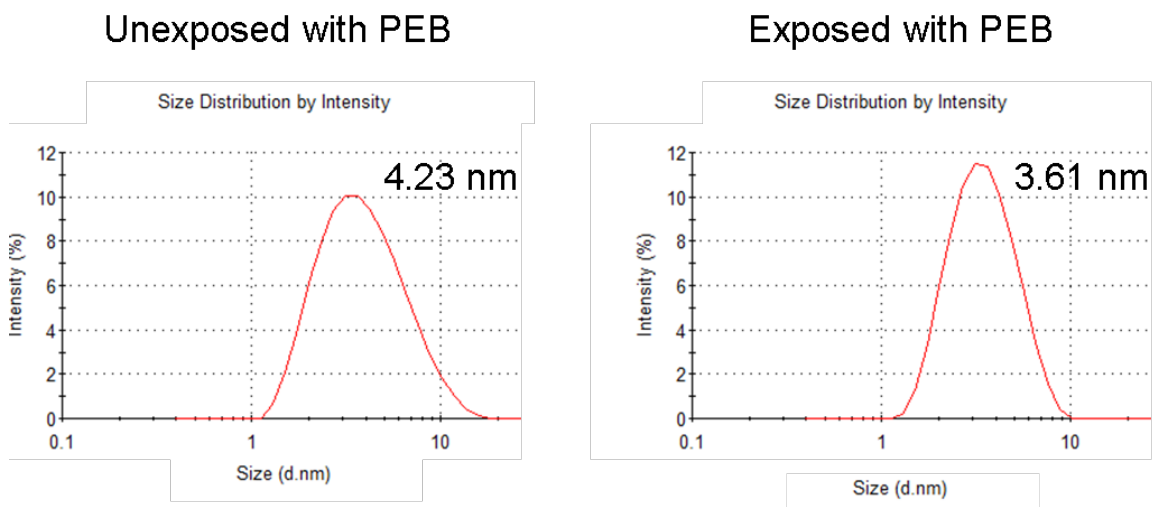

Figure 4.10 Particle size distributions after a post exposure bake with and without UV exposure as measured by dynamic light scattering

residual methacrylic acid both in the film and still bound to the nanoparticles, since there is not enough acid present for a full conversion. This explains the slight film thickness loss and the FT-IR data showing C-O stretch bonds disappearing in the exposed regions. With the loss of ligands, the nanoparticles can aggregate, which can inhibit their solubility in aqueous base solutions. The DLS data shows a slight increase in nanoparticle size after the PEB, indicating such aggregation is occurring.

In lab tests, when adding benzoic acid to the nanoparticle resist, the water solubility was improved. Sulfonic acid NPs have also been synthesized using the procedure detailed above. These particles were readily soluble in water, further supporting the ligand exchange theory, as the exposed portions are dissolved when subject to the positive tone process.

4.4 Conclusions

Using a wide variety of lithographic, spectroscopic and microscopic techniques, the patterning mechanism of the organic-inorganic hybrid nanoparticles was thoroughly analyzed. Through a variety of spectroscopic techniques, it has been verified that free radical cross-linking of C=C double bonds is not a major contributor to the solubility switch that occurs upon exposure. TEM and DLS analysis confirmed that the metal-oxide core size is not changing during exposure, eliminating the possibility of the inorganic core participating in the mechanism. In film FT-IR analysis has confirmed that the methacrylic acid ligands are detaching from the metal-oxide core. TGA, FT-IR and ellipsometry have confirmed that the amount of organic content is reduced in the unexposed regions of the film after post exposure bake. Based on the data presented, a theory of this new patterning mechanism has been established, which involves a ligand exchange during UV exposure, and the loss of methacrylic acid during the PEB. By

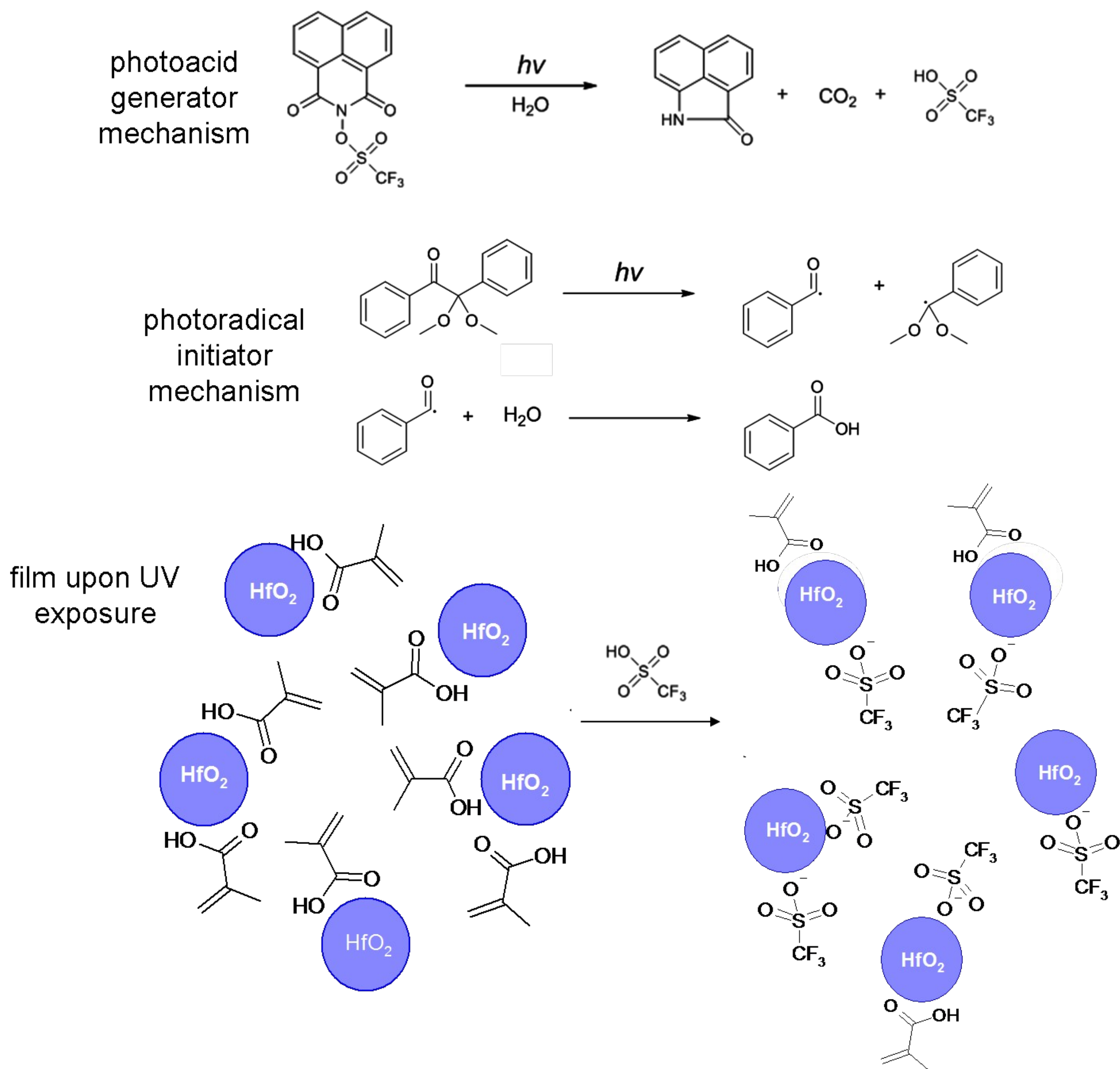

Figure 4.11 Patterning mechanism during UV exposure

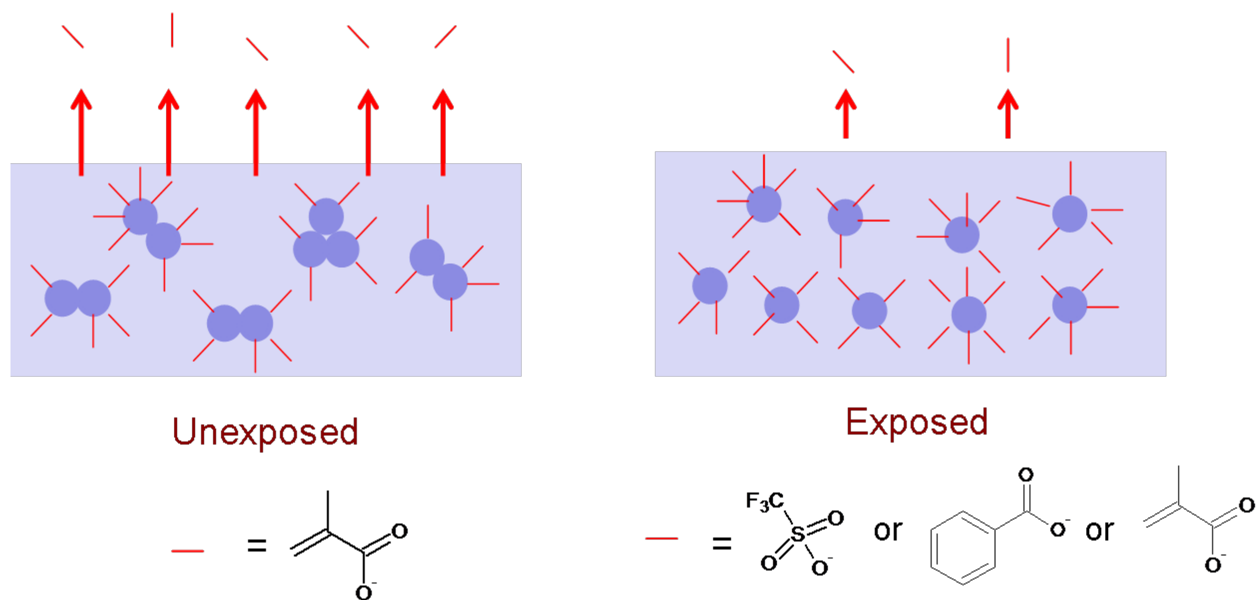

Figure 4.12 Patterning mechanism during the PEB

understanding this dual-tone patterning mechanism, it is possible to further engineer the nanoparticle photoresists to further improve their already excellent patterning capabilities.

Acknowledgements

SEMATECH is gratefully acknowledged for funding, as well as the opportunity to interact and discuss with member companies. The Cornell Nanoscale Science and Technology Facility (CNF) and the Cornell Center for Materials Research (CCMR) are thanked for the use of their facilities. Intel and the Semiconductor Research Corporation Education Alliance (SRCEA) are thanked for providing a fellowship to conduct this research.

REFERENCES

[1] Shi, Z.-G.; Guo, Q.-Z.; Liu, Y.-T.; Xiao, Y.-X.; Xu, L., Drug delivery devices based on macroporous silica spheres. *Materials Chemistry and Physics* **2011,** 126, (3), 826-831.

[2] Liu, Y.; Miyoshi, H., Preparation and characterization of novel drug delivery system of light-sensitive silica nanocapsules with thin shells. *Journal of Biomedical Nanotechnology* **2008,** 4, (1), 25-32.

[3] Othman, S. H.; Abdul Rashid, S.; Mohd Ghazi, T. I.; Abdullah, N., Dispersion and stabilization of photocatalytic TiO2 nanoparticles in aqueous suspension for coatings applications. *Journal of Nanomaterials* **2012,** 718214, 10 pp.

[4] Walker, J. C.; Saranu, S. R.; Kean, A. H.; Wood, R. J. K., Fe nano-particle coatings for high temperature wear resistance. *Wear* **2011,** 271, (9-10), 2067-2079.

[5] Kim, J.-H.; Kim, S.-K.; Nam, K.; Kim, D.-W., Composite proton conducting membranes based on Nafion and sulfonated SiO2 nanoparticles. *Journal of Membrane Science* **2012,** 415-416, 696-70.

[6] Majedi, F. S.; Hasani-Sadrabadi, M. M.; Emami, S. H.; Taghipoor, M.; Dashtimoghadam, E.; Bertsch, A.; Moaddel, H.; Renaud, P., Microfluidic synthesis of chitosan-based nanoparticles for fuel cell applications. *Chemical Communications* **2012,** 48, (62), 7744-7746.

[7] Lismont, M.; Dreesen, L., Comparative study of Ag and Au nanoparticles biosensors based on surface plasmon resonance phenomenon. *Materials Science & Engineering, C: Materials for Biological Applications* **2012,** 32, (6), 1437-1442.

[8] Ghosh Chaudhuri, R.; Paria, S., Core/Shell Nanoparticles: Classes, Properties, Synthesis

Mechanisms, Characterization, and Applications. *Chemical Reviews* **2012,** 112, (4), 2373-2433.

[9] Ferguson, J. B.; Lopez, H.; Kongshaug, D.; Schultz, B.; Rohatgi, P., Revised Orowan Strengthening: Effective Interparticle Spacing and Strain Field Considerations. *Metallurgical and Materials Transactions A: Physical Metallurgy and Materials Science* **2012,** 43, (6), 2110-2115.

[10] Wang, G.; Chen, G.; Wei, Z.; Yu, T.; Liu, L.; Wang, P.; Chang, Y.; Qi, M., A comparative study of TiO2 and surface-treated TiO2 nanoparticles on thermal and mechanical properties of poly(ε-caprolactone) nanocomposites. *Journal of Applied Polymer Science* **2012,** 125, (5), 3871-3879.

[11] Denisyuk, I. Y.; Sobeshuk, N. O.; Burunkova, J. A.; Vorzobova, N. D., Subwavelength microstructures fabrication by self-organization processes in photopolymerizable nanocomposite. *Journal of Nanomaterials* **2012,** 827438, 6 pp..

[12] Kamanina, N. V.; Serov, S. V.; Shurpo, N. A.; Rozhkova, N. N., Photoinduced changes in refractive index of nanostructured shungite-containing polyimide systems. *Technical Physics Letters* **2011,** 37, (10), 949-951.

[13] Philipp, M.; Gervais, P. C.; Sanctuary, R.; Muller, U.; Baller, J.; Wetzel, B.; Kruger, J. K., Effect of mixing sequence on the curing of amine-hardened epoxy/alumina nanocomposites as assessed by optical refractometry. *eXPRESS Polymer Letters* **2008,** 2, (8), 546-552.

[14] Nusser, Klaus; Schneider, Gerald J.; Pyckhout-Hintzen, Wim; Richter, Dieter, Viscosity Decrease and Reinforcement in Polymer-Silsesquioxane Composites. *Macromolecules* **2011,** 44, (19), 7820-7830.

[15] Zhang, W.; Dong, H. N.; Zhang, T.; Guo, J. B.; Wei, J., The effect of monomer structures on photopolymerization kinetics and volume shrinkage behavior for plasma display panel barrier rib, *Journal of Applied Polymer Science* **2012,** 125, 77-87.

[16] Hata, E.; Tomita, Y., Stoichiometric thiol-to-ene ratio dependences of refractive index modulation and shrinkage of volume gratings recorded in photopolymerizable nanoparticle-polymer composites based onstepgrowth polymerization. *Optical Materials Express* 2011, 1, (6), 1113-1120.

[17] Gilman, J. W.; Kashiwagi, Takashi; Giannelis, E. P.; Manias, E.; Lomakin, S.; Lichtenhan, J. D.; Jones, P., Nanocomposites: radiative gasification and vinyl polymer flammability. *Special Publication - Royal Society of Chemistry* **1998,** 224, 203-221.

[18] Bae, W. J.; Trikeriotis, M.; Sha, J.; Schwartz, E. L.; Rodriguez, R.; Zimmerman, P.; Giannelis, E. P.; Ober, C. K., High refractive index and high transparency HfO_2 nanocomposites for next generation lithography. *Journal of Materials Chemistry* **2010,** 20, (25), 5186-5189.

[19] Yoshiiwa, M.; Kageyama, H.; Shirota, Y.; Wakaya, F.; Gamo, K.; Takai, M., Novel class of low molecular-weight organic resists for nanometer lithography. *Applied Physics Letters* **1996,** 69, (17), 2605-2607.

[20] Young-Gil, K.; Kim, J. B.; Fujigaya, T.; Shibasaki, Y.; Ueda, M., A positive-working alkaline developable photoresist based on partially tert-Boc-protected calix[4]resorcinarene and a photoacid generator. *Journal of Materials Chemistry* **2002,** 12, (1), 53-57.

[21] Ueda, M.; Takahashi, D.; Nakayama, T.; Haba, O., Three-component negative-type photoresist based on calix[4]resorcinarene, a cross-linker, and a photoacid generator. *Chemistry of Materials* **1998,** 10, (8), 2230-2234.

[22] De Silva, A.; Ober, C. K., Hydroxyphenylbenzene derivatives as glass forming molecules for high resolution photoresists, *Journal of Materials Chemistry* **2008,** 18, 1903-1910.

[23] De Silva, A.; Lee, J. K.; Andre, X.; Felix, N. M.; Cao, H. B.; Deng, H.; Ober, C. K., Study of the Structure-Properties Relationship of Phenolic Molecular Glass Resists for Next Generation Photolithography. *Chemistry of Materials* **2008,** 20, (4), 1606-1613.

[24] Patsis, G. P.; Constantoudis, V.; Gogolides, E.. Effects of photoresist polymer molecular weight on line-edge roughness and its metrology probed with Monte Carlo simulations. *Microelectronic Engineering* **2004,** 75, (3), 297-308.

[25] Patsis, G. P.; Gogolides, E., Effects of model polymer chain architectures and molecular weight of conventional and chemically amplified photoresists on line-edge roughness. Stochastic simulations. *Microelectronic Engineering* **2006,** 83, (4-9), 1078-1081.

[26] Stowers, J.; Keszler, D. A., High resolution, high sensitivity inorganic resists. *Microelectronic Engineering* **2009,** 86, (4-6), 730-733.

[27] Telecky, A.; Xie, P.; Stowers, J.; Grenville, A.; Smith, B.; Keszler, D. A., Photopatternable inorganic hard mask. *Journal of Vacuum Science & Technology, B: Nanotechnology & Microelectronics: Materials, Processing, Measurement, & Phenomena* 28 **2010**, (6), C6S19-C6S22.

[28] Stowers, J. K.; A. T., Kocsis, M.; Clark, B. L.; Keszler, D. A.; Grenville, A.; Anderson, C. N.; Nalleau, P., Directly patterned inorganic hardmask for EUV lithography. *Proceedings of SPIE* **2011,** 7969, 79691-5.

[29] Lim, Su Hui; Saifullah, M. S. M.; Hussain, Hazrat; Loh, Wei Wei; Low, Hong Yee, Direct imprinting of high resolution TiO_2 nanostructures. *Nanotechnology* **2010,** 21, (28), 285303/1-285303/6.

[30] Ridaoui, H.; Weider, F.; Ponche; A.; Soppera, O., Direct ArF laser photopatterning of metal oxide nanostructures prepared by the sol-gel route, *Nanotechnology* **2010**, 21, (6), 065303/1-065303/10.

[31] Trikeriotis, M.; Rodriguez, R.; Zettel, M. F.; Bakandritsos, A.; Bae, W. J.; Zimmerman, P. A.; Ober, C. K.; Giannelis, E. P., High refractive index nanoparticle fluids for 193-nm immersion lithography. *Proceedings of SPIE* **2009,** 7273, (Pt. 1, Advances in Resist Materials and Processing Technology XXVI), 72732A/1-72732A/6.

[32] Trikeriotis, M.; Bae, W. J.; Schwartz, E.; Krysak, M.; Lafferty, N.; Xie, P.; Smith, B.; Zimmerman, P. A.; Ober, C. K.; Giannelis, E. P., Development of an inorganic photoresist for DUV, EUV, and electron beam imaging. *Proceedings of SPIE* **2010,** 7639, (Pt. 1, Advances in Resist Materials and Processing Technology XXVII), 76390E/1-76390E/10.

[33] Krysak, M.; Trikeriotis, M.; Schwartz, E.; Lafferty, N.; Xie, P.; Smith, B.; Zimmerman, P.; Montgomery, W.; Giannelis, E.; Ober, C. K., Development of an inorganic nanoparticle photoresist for EUV, e-beam, and 193 nm lithography. *Proceedings of SPIE* **2011**, 7972, (Pt. 1,Advances in Resist Materials and Processing Technology XXVIII), 79721C/1-79721C/6.

[34] Puchberger, M.; Kogler, F. R.; Jupa, M.; Gross, S.; Fric, H.; Kickelbick, G.; Schubert, U.. Can the Clusters $Zr_6O_4(OOCR)_{12}$ and $[Zr_6O_4(OOCR)_{12}]2$ Be Converted into Each Other?. *European Journal of Inorganic Chemistry* **2006,** 16, 3283-3293.

[35] Cardineau, B.; Krysak, M.; Trikeriotis, M.; Giannelis, E.; Ober, C. K.; Cho, K. Y.; Brainard, R.. Tightly-Bound Ligands for Hafnium Nanoparticle EUV Resists. *Proceedings of SPIE* **2012,** 8322, 83220V-83220V-10.

CHAPTER 5

USING SMALL MOLECULE RESIST MATERIALS TO INVESTIGATE THERMAL INDUCED BEHAVIORS DURING SUB-MILLISECOND LASER POST EXPOSURE BAKE

Abstract

Control of photoacid diffusion in photoresist films remains a significant challenge to the semiconductor industry. Chemically amplified photoresists require a post exposure bake (PEB), typically performed on a hot plate at 90-150°C for 30-120 seconds, to catalyze the resist deprotection after photoacid generation. This bake step is a primary influence on resist performance as the time/temperature profile controls both the diffusion of photogenerated acids and the deprotection of the resist backbone. Sufficient time must be provided to achieve the level of deprotection required for the solubility switching in a developer, but the seconds timeframe of conventional hot plate PEB leads to an undesirable amount of acid diffusion. A CO_2 laser based scanned heating system is used to achieve sub-millisecond to milliseconds in heating durations with temperatures up to the thermal decomposition limit of the resist. A series of PAGs, of which different components of the acid anion are systematically varied, have been synthesized and studied to gain an insight on how the PAG structure affects the acid diffusion behavior at previously inaccessible higher PEB temperatures. This study has identified PAG structures with sufficient sensitivity and short acid diffusion lengths during laser-PEB, signifying their potential for use with this new heating system. Small molecule resist with low glass transition temperatures (Tgs) have been used to examine the effects of sub-millisecond heating on the reflow behavior of the resist materials. Chemically amplified resists with Tgs as low as 38°C

have produced sub-micron sized features when using laser-PEB as an alternative to hotplate PEB. These results enable previously unpatternable materials to be studied as photoresist systems, broadening the scope of potential resist candidates.

5.1 Introduction

The requirement for smaller feature dimensions continues to drive lithography research forward. In order to meet the requirements of the ITRS roadmap, it is necessary to investigate not only resist materials, but every step of the lithography process as well. By optimizing processing steps, it may be possible to push current materials past their current limit. The post exposure bake (PEB) step in the lithography process has the most effect on the shape and size of the patterns produced[1]. The heat catalyzes the deprotection or cross-linking of chemically amplified resists by mobilizing the photoacid generator (PAG) in the resist matrix. Some diffusion of acid is necessary to start the reaction; however, uncontrollable acid diffusion has been held accountable for limiting resolution and increasing line edge roughness (LER) of patterned resists[2,3]. Controlling acid diffusion by altering resist chemistry has been studied extensively with the creation of polymer-bound PAGs, where the PAG is chemically bonded to the resist chain, thereby limiting its mobility[4,5]. These resists have shown reduced LER, but at the expense of sensitivity[5].

Henderson and co-workers have synthesized single molecule photoresists[6,7]. They consist of a photoacid generator bonded to a molecular glass core functionalized with acid-labile groups. By attaching the PAG directly to the resist, the quantum yield of the system is increased, which has been shown to improve sensitivity[8]. These new resists were hypothesized to reduce LER by

limiting the diffusion of acid while still keeping high sensitivity. LER was improved with the single molecule resists; however, lower sensitivity still remained an issue.

While altering the resist and PAG can enhance photoresist performance, optimizing the heating process can improve lithographic patterns as well. Two important kinetic processes that take place during the PEB include resist deprotection and acid diffusion. These processes are both driven by thermal activation. As long as the activation energy of diffusion is less than that for deprotection, higher temperatures for optimized time durations will result in reduced diffusion[9]. However, traditional hot plate PEB cannot access times shorter than a few seconds. Ober, Thompson and co-workers have developed a CO_2 laser system with a wavelength of 10.6 μm that can spike the temperature of resist films to the hundreds of Celsius degrees for micro- to millisecond temperature dwell times. Boron-doped wafers with a resistivity of 0.01-0.02 ohm/cm^2 are used to absorb the infrared light, as silicon does not absorb in this region. The absorbed energy is converted into heat, effectively baking the resist film on top of the wafer. When used as an alternate PEB method, this laser system can drastically improve both LER and sensitivity, demonstrating the excellent performance capability of the laser[10]. Furthermore, the resists and PAGs tested are stable, even when heated hundreds of degrees beyond their nominal decomposition temperatures[11]. Previous work has demonstrated that both the deprotection and diffusion kinetics change with the transition from hotplate to laser-PEB[12]. Because of this behavioral change, it is necessary to examine the structural effects of resist materials on lithographic performance using laser-PEB in order to fully optimize the system.

The glass transition temperature (Tg) of a resist material is an important parameter to consider when designing a successful resist system. When a material is heated to temperatures above its Tg, it will relax from the glassy state, or reflow. While heating a resist just above its Tg

can smooth standing wave patterns caused during exposure[13,14], heating to temperatures much higher can cause broadening, rounding, or general degradation of the intended features. Much effort has been made to produce photoresists with high glass transition temperatures, using macromolecules such as polymers[15] or small molecule resists, commonly referred to as molecular glasses[16-18]. As small molecules tend to crystallize, these molecules have been designed using bulky, rigid substituents to promote glass formation and a high Tg[19-21]. While many small molecules in the molecular weight range of 200-500 g/mol have proven to be glass formers, their Tg is too low to withstand high temperatures needed in the current lithographic process. The temperatures defined as Tgs are measured in the seconds to minutes timeframe. If the heating time is reduced to small fractions of a second, it may be possible to reach temperatures above the Tg without causing reflow. As previously stated, using a high temperature dwell time on the order of micro- to milliseconds, materials can be heated well above their decomposition temperature without any signs of decomposition[11]. By accessing these short timeframes with laser heating, it will be possible to examine molecular architectures that have not been previously studied as photoresist materials.

This paper investigates a variety of PAGs and the effect of their molecular structure on diffusivity, sensitivity to UV irradiation, and activation energy of the resist films in which they are dispersed. These parameters are examined with the use of both hotplate and laser-PEB and compared to study the effect of PAG structure on lithographic properties with the new heating system. MG resists with low Tgs are used to investigate the effect of a high temperature spike on reflow of the resist material.

5.2 Experimental

5.2.1 Materials

Most starting materials were purchased from Sigma Aldrich and used without further purification. 1-bromo-1,1,2,2,3,3,3-heptafluoropropane was purchased from SynQuest Laboratories. Triphenylsulfonium chloride was purchased from Alfa Aesar. Poly(methyladamantylmethacrylate-co-gammabuytrolactonemethacrylate) was obtained from Mitsubishi Rayon America. Solvents used were anhydrous or HPLC grade unless otherwise noted.

5.2.2 PAG Synthesis and Characterization

The synthesis of TPS-Hf was performed using a previously published protocol[22]. The synthesis and optical characterization of the Series 2 photoacid generators have been described in a previous chapter. The structures of the PAGs are shown in Figure 5.1.

5.2.3 Molecular Glass Resist Synthesis

1,1,1-Tris(4-hydroxyphenyl)ethane was purchased from Sigma Aldrich and used as received. The synthesis of the tri-HPB-mp is described in a previously published procedure[19]. These materials were protected with *tert*-butoxycarbonyl (t-BOC) according to a published procedure[23]. The synthesis of the t-BOC-protected triphenylbenzene derivative is described in a previously published procedure[19]. The structures of the glasses used, as well as their abbreviated names for this paper, can be found in Figure 5.1.

Series 1:

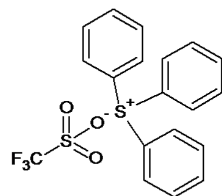

TPS-Tf

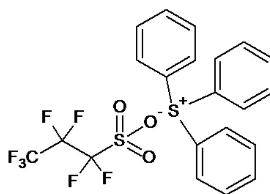

TPS-Hf

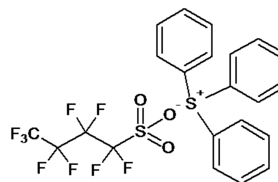

TPS-Nf

Series 2:

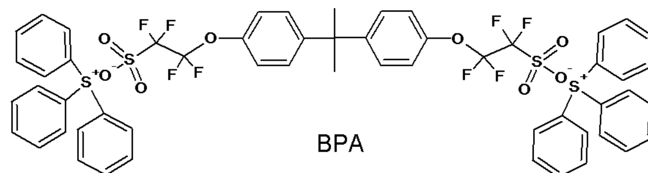

BPA

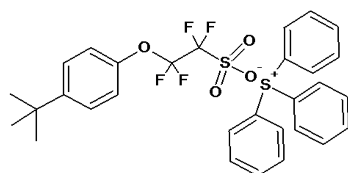

4tbPhenol

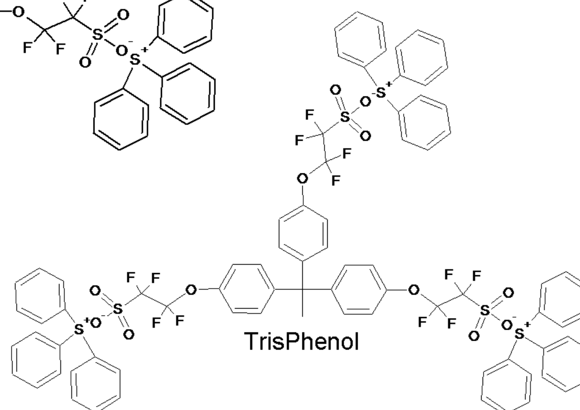

TrisPhenol

MG Resists:

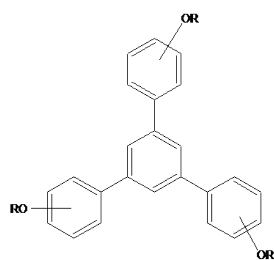

Tri-HPB-mp-t-BOC

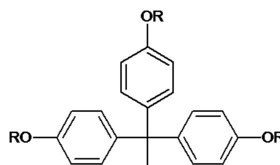

Tris-t-BOC

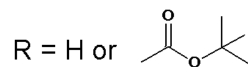

Figure 5.1 PAG and molecular glass resist structures

5.2.4 Characterization

The glass transition temperatures were measured by differential scanning calorimetry (DSC) using a TA Instruments Q1000 Differential Scanning Calorimeter. Three heat/cool cycles were performed, ranging from -50°C to 150°C, with the Tg measured after the second cycle. A TA Instruments Q500 Thermogravimetric Analyzer (TGA) was used to determine the decomposition temperature of the PAG molecules. ^{1}H NMR spectra were recorded on a Varian Inova-400 NMR spectrometer at room temperature. Chemical shifts reported are quoted in parts per million (ppm) and relative to DMSO (δ 2.50 ppm).

5.2.5 Bilayer Fabrication Procedure

The relative acid diffusion lengths of each PAG were measured using a bilayer method[25]. The photoresist and 5 wt % of the appropriate PAG were dissolved in PGMEA and spin-coated onto an HMDS primed wafer at 2000 rpm for 1 minute, and baked at 130°C for 1 minute. The film thickness of this bottom layer was measured with a Woollamm ellipsometer, and then the film set aside. A flexible stamp was made by cross-linking poly-dimethylsilane (PDMS) on top of a silicon wafer to ensure a smooth surface. The cross-linked stamp was then used as a substrate onto which the same photoresist and PAG mixture was spin-coated, using the same procedure was described above. The film was then exposed to UV radiation with an array of doses. The two films were heated at various temperatures for 1 minute, and then the PDMS stamp peeled off. The bilayer was then developed, and the thicknesses of the remaining film at various exposure doses were measured.

5.2.6 Lithographic Processing

Resist solutions were made by dissolving each compound in propylene glycol methyl ether acetate (PGMEA) to make a 5 wt % resist solution. The appropriate PAG was added at various weight % concentrations with respect to the resist. The resulting solution was filtered twice and spin-coated on a hexamethyldisilazane (HMDS) primed silicon wafer at 2000 rpm for 1 minute. The silicon wafer was doped with boron, with a measured resistivity of 0.01-0.02 ohms/cm^2. The film was subject to a post application bake (PAB) of 130°C for 1 minute. The wafer was then exposed using an ABM contact aligner at a wavelength of 254 nm, or a JEOL JBX-9300FS Electron Beam Lithography system operating at 100 keV. The PEB was performed using a traditional hotplate, or a continuous CO_2 laser scanning system with a wavelength of 10.6 µm. This was followed by development in AZ 726-MIF developer (0.26N TMAH) for 1 minute. Scanning Electron Micrographs (SEMs) of patterned images were taken using a Zeiss Ultra 55 scanning electron microscope.

Contrast curves were constructed using the patterning method described above, using a flood exposure dose array when exposing the materials. The PEB and development process is carried out as stated above, and then the film thickness at each exposure dose is measured with a P10 Profilometer.

5.3 Results and Discussion

5.3.1 Series 1 PAGs

5.3.1.1 Acid Diffusion Behavior

To select PAG structures as a starting point for this study, the triphenylsulfonium perfluoro sulfonate salts were mainly chosen because of their success as photoacid generators in

lithographically patterned films. The fluorinated sulfonic acid is one of the strongest organic acids, and therefore can efficiently catalyze the chemical reactions that produce solubility changes. Previous work has shown that there is a significant change in diffusion behavior by simply changing the fluorinated chain length[25]. The length of the fluorinated chain was varied to examine the effect of the chain length on lithographic performance. A model 193 nm resist system, poly(methyladamantylmethacrylate-co-gammabuytrolactonemethacrylate) was chosen because it has been extensively characterized on the laser-PEB system. Three photoresist solutions were made with each of the three Series 1 PAGs, and bilayers of each resist system were fabricated according to the procedure detailed above. The results of the bilayer experiment are summarized in Figure 5.2.

At a PEB temperature of 115°C on the hotplate (1 minute), there was no clear trend observed in acid diffusion length as a function of fluorinated chain length. The method that is used to determine acid diffusion length involved measuring the film thickness change of a layer of unexposed resist and translating this thickness change into diffusion length. Because there are It is important to note that this method cannot determine absolute diffusion lengths, because of a variety of other factors affecting film thickness loss upon development, including dark loss. There are also competing kinetic processes, including resist deprotection, which can affect the amount of film thickness loss. This can account for the seemingly disturbed trend in diffusion length seen with the hotplate PEB. However, this is an effective method to compare diffusion lengths between similar materials, as the only variable between each resist film is the PAG structure.

As shown by the contrast curves in Figure 5.3, the PAGs are extremely sensitive when thermally treated with both the hotplate and the laser. However, the Eo, or dose to clear the resist

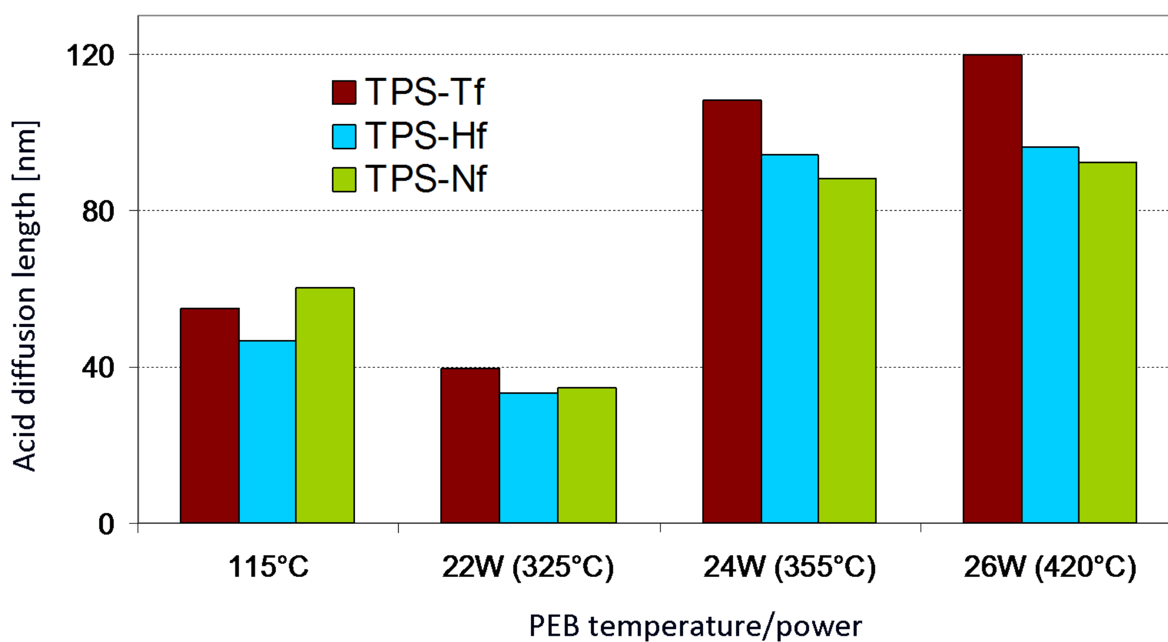

Figure 5.2 Relative acid diffusion length of the Series 1 PAGs after hotplate and laser-PEB

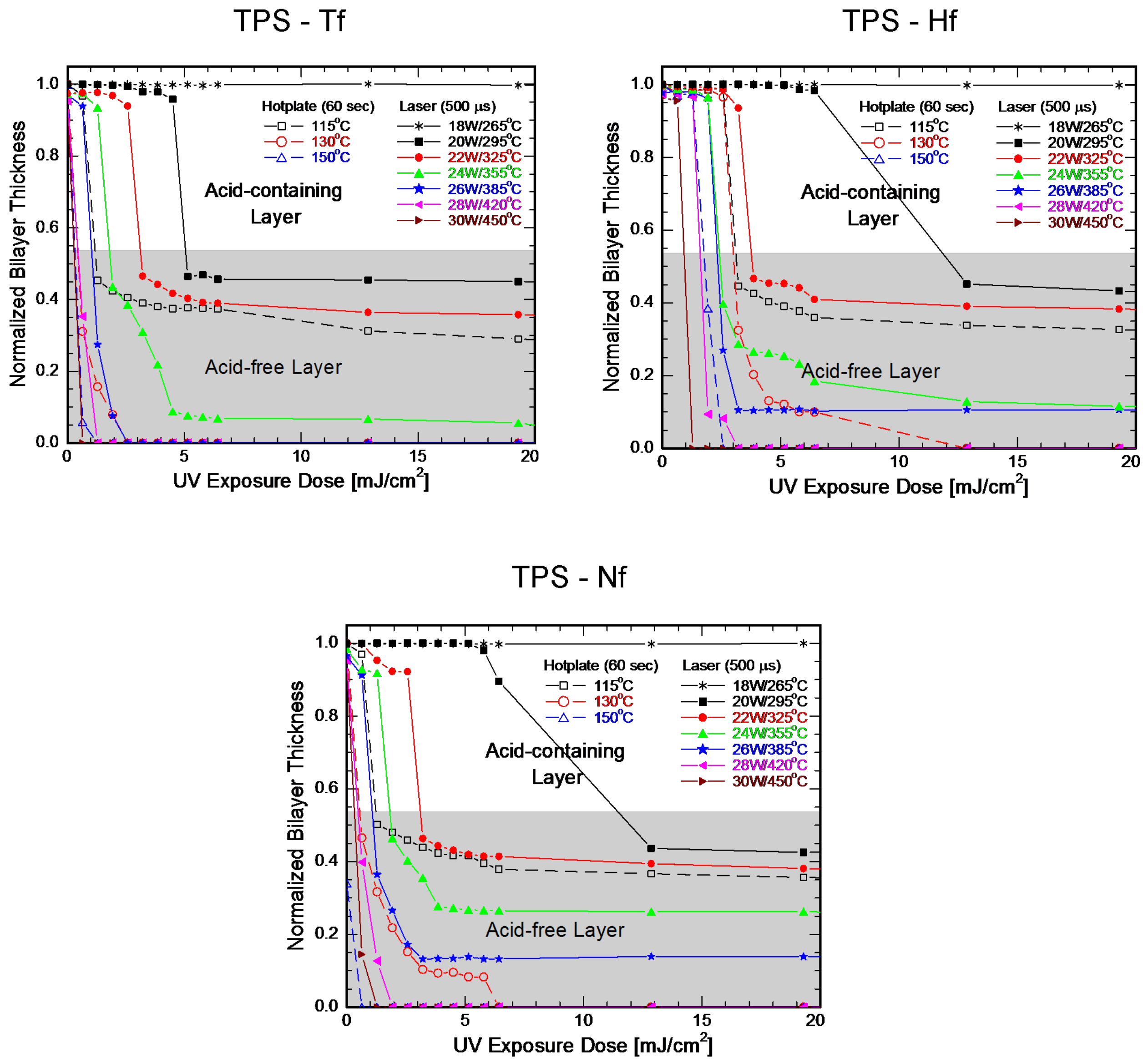

Figure 5.3 Contrast curves of Series 1 PAGs after hotplate and laser PEB

system with each PAG is very similar, as is the diffusion behavior. These similar Eo values can contribute to the lack of a definite trend in diffusion length, as other competing kinetic processes add to the film thickness loss. This series of PAGs exhibited large diffusion lengths during laser-PEB, which can be attributed to the ease of which the flexible fluorinated chain can move through the polymer. These results have indicated the need to re-design the PAG structure to inhibit diffusion of the acid as well as slow the photospeed to effectively study diffusion behavior as a function of PAG structure.

5.3.1.2 Lithographic Performance

The patterning abilities of the Series 1 PAGs were tested, comparing the hotplate and laser-PEB methods. Representative images are shown in Figure 5.4, using the model 193 nm resist polymer and TPS-HF PAG. This resist system was patterned with e-beam lithography, and each wafer was processed identically, except for the PEB method. It is important to note that when using this model resist system, high resolution patterning is not the goal of this experiment, but rather to compare the resist performance at a certain dimension while varying the PEB method. Each image shown is produced using an e-beam dose of 35 $\mu C/cm^2$. The sensitivity of the resist system with e-beam lithography is very similar with both PEB methods, as evidenced by the UV contrast curves shown above. However, the LER has been reduced from 15 nm to 9 nm simply by changing from hotplate PEB to laser PEB.

5.3.2 Series 2 PAGs

The Series 2 PAGs were designed with a bulkier anion, which can prevent the mobility of the PAG through the polymer matrix upon heating. As the anion size was increased, multiple photoacid-generating substituents were added to the structure to increase the quantum yield of

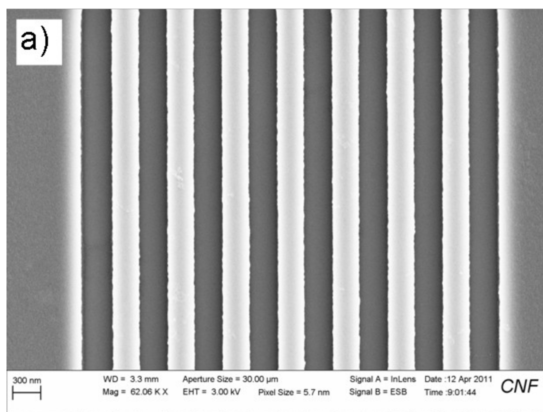

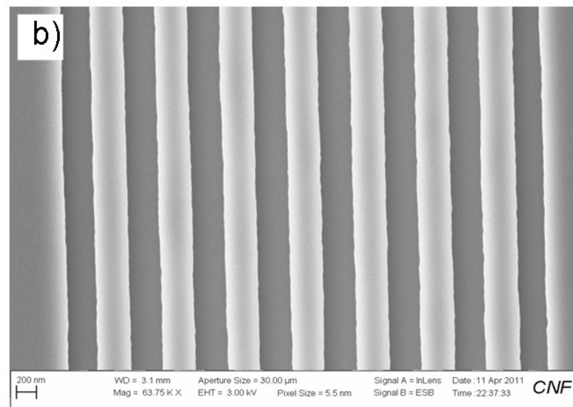

Figure 5.4 SEM images of 200 nm line/space patterns by e-beam lithography using a) hotplate PEB and b) laser PEB

the PAG. The reduced mobility of the PAG can have an adverse effect on sensitivity, and increasing the quantum yield can counteract this effect[26,27].

5.3.2.1 Thermal Characterization

Thermogravimetric analysis was used to determine the decomposition temperature of the synthesized photoacid generators. All of the Series 2 PAGs are stable up to 250°C when heated at a rate of 10°C/min. When heated in the sub-millisecond timeframe, the PAGs will be stable when heated to temperatures hundreds of degrees above this.

5.3.2.2 Lithographic Characterization

Contrast curves generated with exposure to 254 nm UV light were a simple yet effective way to characterize the sensitivity of the Series 2 PAGs relative to each other (Figure 5.6). Each of the contrast curves shown were constructed using laser PEB at various laser powers. In contrast to the Series 1 PAGs, the sensitivity of each of the Series 2 PAGs is very different from one another. The Eo values range from 1.2 to 25 mJ/cm^2. This result was very encouraging, indicting the correct structural modifications were made to access a broader range of diffusion behaviors.

5.3.2.3 Relative Acid Diffusion Behavior

The bilayer experiment was repeated with the Series 2 PAGs as it has been previously described for the Series 1 PAGs, with the results depicted in Figure 5.7. With the wide range of PAG anion sizes, the diffusion behavior is significantly different between each molecule.

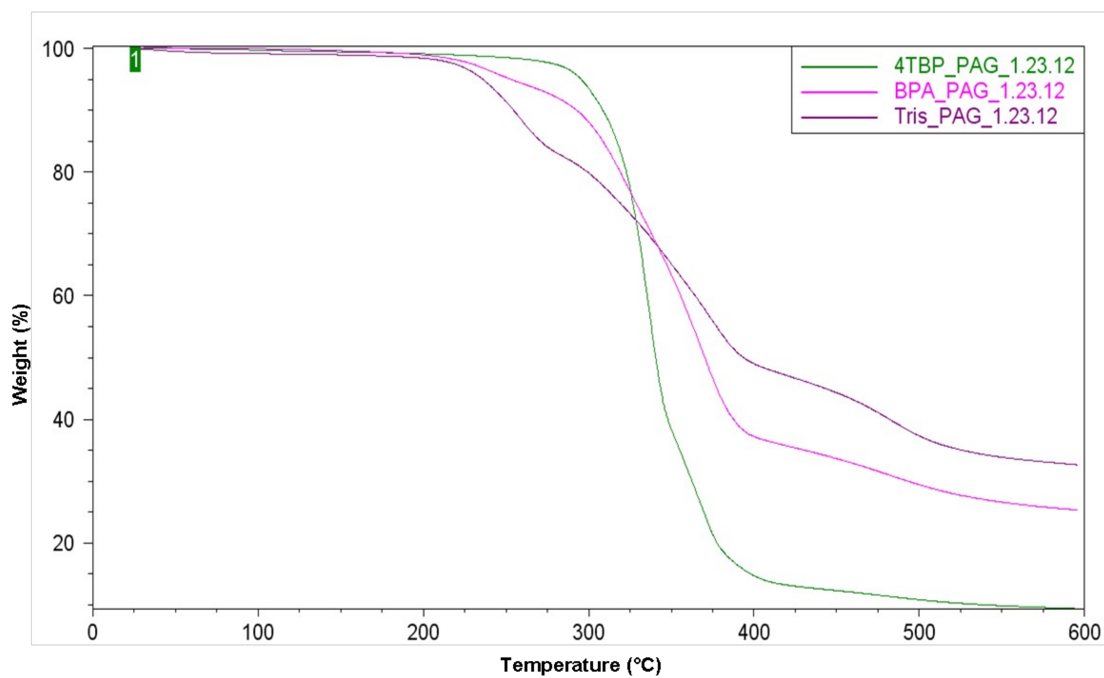

Figure 5.5 Weight loss percentages as a function of temperature of the Series 2 PAGs

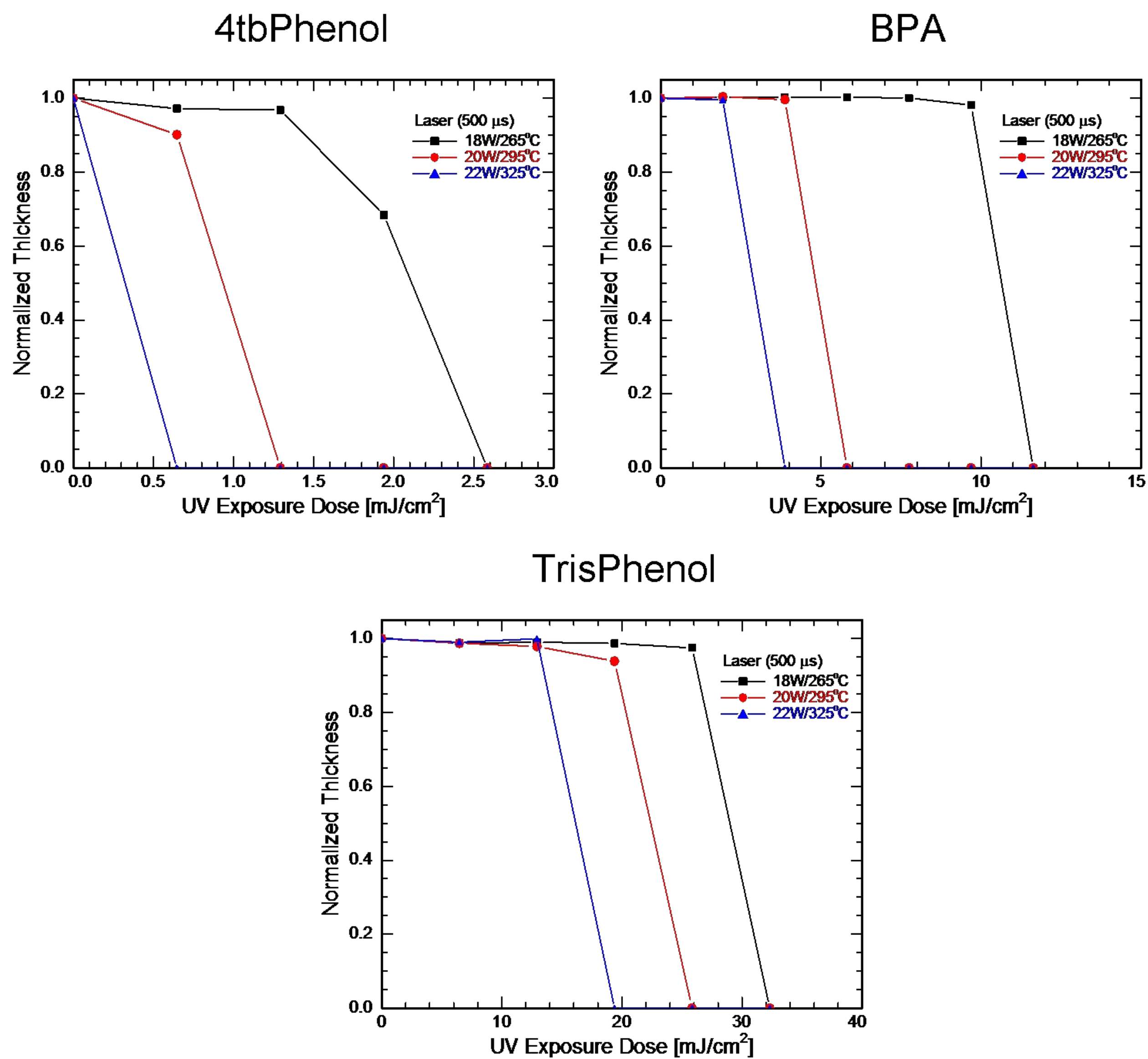

Figure 5.6 Contrast curves of the Series 2 PAGs using laser-PEB

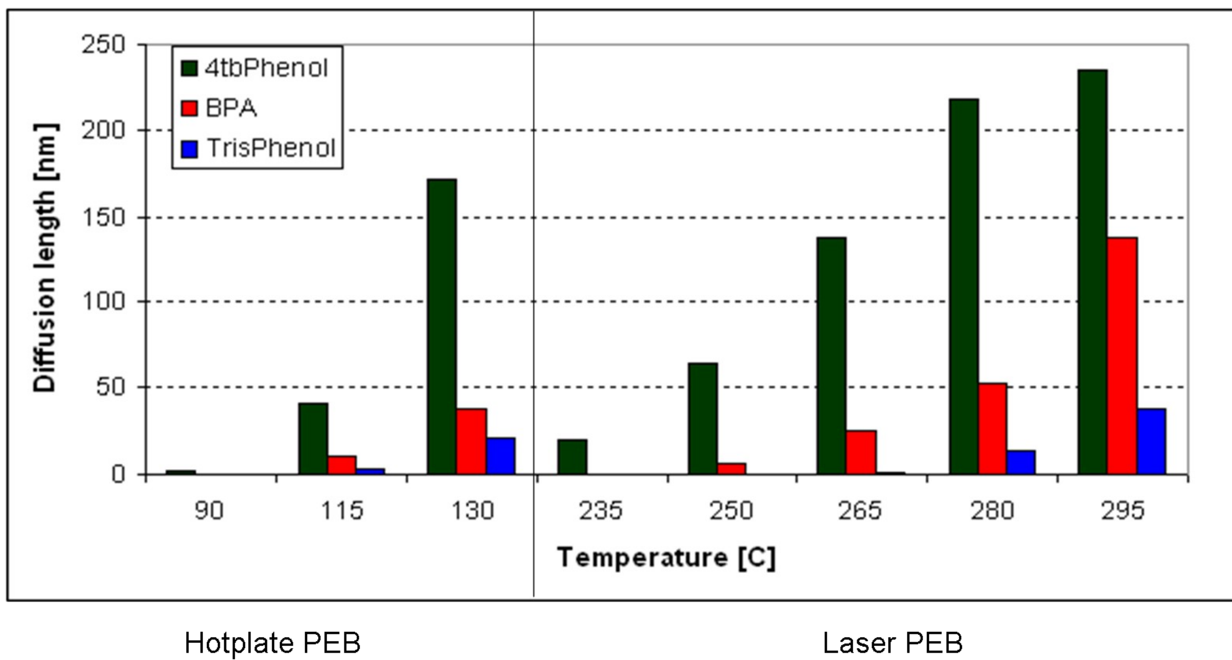

Figure 5.7 Relative acid diffusion behaviors of Series 2 PAGs with hotplate and laser PEB

Another exciting aspect of this result is the relatively small diffusion lengths of the BPA and especially the TrisPhenol PAGs. The bulky aromatics added to the PAG anion have proven to be an effective way to inhibit acid diffusion under laser PEB. The shorter time periods of the PEB duration also limit the acid diffusion at lower laser powers, indicating the PEB method itself can play a role in limiting diffusion.

5.3.2.4 Diffusivity and Activation Energy

The Series 2 PAGs have promising diffusion behaviors, so further analysis on these structures was done to determine the activation energy for these PAGs with both hotplate and laser PEB. The diffusivity is determined from the relative acid diffusion lengths, and is defined by the following equation:

Equation 1

$$D = \frac{\Delta x^{2}}{4t}$$

where D is the diffusivity, Δx is the acid diffusion length, and t is the duration of the PEB

Previous work with this laser system has shown that the diffusion behavior at temperatures near the resist Tg follows the Williams-Landel-Ferry (WLF) model, while at high temperatures, the behavior transitions to the Arrhenius model[12]. To calculate the activation energies of these PAGs, the diffusion model that encompasses the high temperatures achieved with the laser heating system, shown in Equation 2, was used.

Equation 2

$$D_{Total} = D_{Arrhenius} + D_{WLF} = D_0\, exp\left(-\frac{E_A}{kT}\right) + D_{T_g}\, exp\left(-\frac{C_{1g}\cdot(T-T_g)}{C_{2g}+(T-T_g)}\right)$$

where D = diffusivity, E_A = activation energy, $D_0 = 1.4 \times 10^5\ cm^2 \cdot sec^{-1}$, $D_{Tg} = 1.6 \times 10^{-15}\ cm^2 \cdot sec^{-1}$, $C_{1g} = -16.2 \pm 2.7$ and $C_{2g} = 84.7 \pm 27.6$. The constant values are the WLF fit parameters.

The activation energies for the Series 2 PAGs for both hotplate and laser-PEB are summarized in Table 5.1. When switching from hotplate to laser PEB, there is a distinct change in activation energies. For the 4tbPhenol and BPA PAGs, the activation energy barrier is lowered with high PEB temperatures. The activation energy for the TrisPhenol PAG slightly increases with the transition to high temperatures, though the increase is not significant enough to translate to a drastic reduction in sensitivity, as seen in the contrast curves using laser-PEB. As expected, the activation energy increases with the larger PAG size, because of increased molecular weight and bulky size, which will inhibit movement of the acid throughout the resist matrix.

5.3.2.4 Lithographic Patterning

The patterning ability of the TrisPhenol PAG was tested using e-beam lithography. A molecular glass photoresist, CR-15[19] was chosen as the resist system for multiple reasons. Because poor miscibility of the PAG within the photoresist matrix can negatively affect the resist performance[28], a resist with a similar molecular architecture to the PAG structure was chosen to promote miscibility of the resist components. CR-15 has previously shown the capability to pattern high resolution features with Extreme Ultraviolet Lithography (EUV-L).

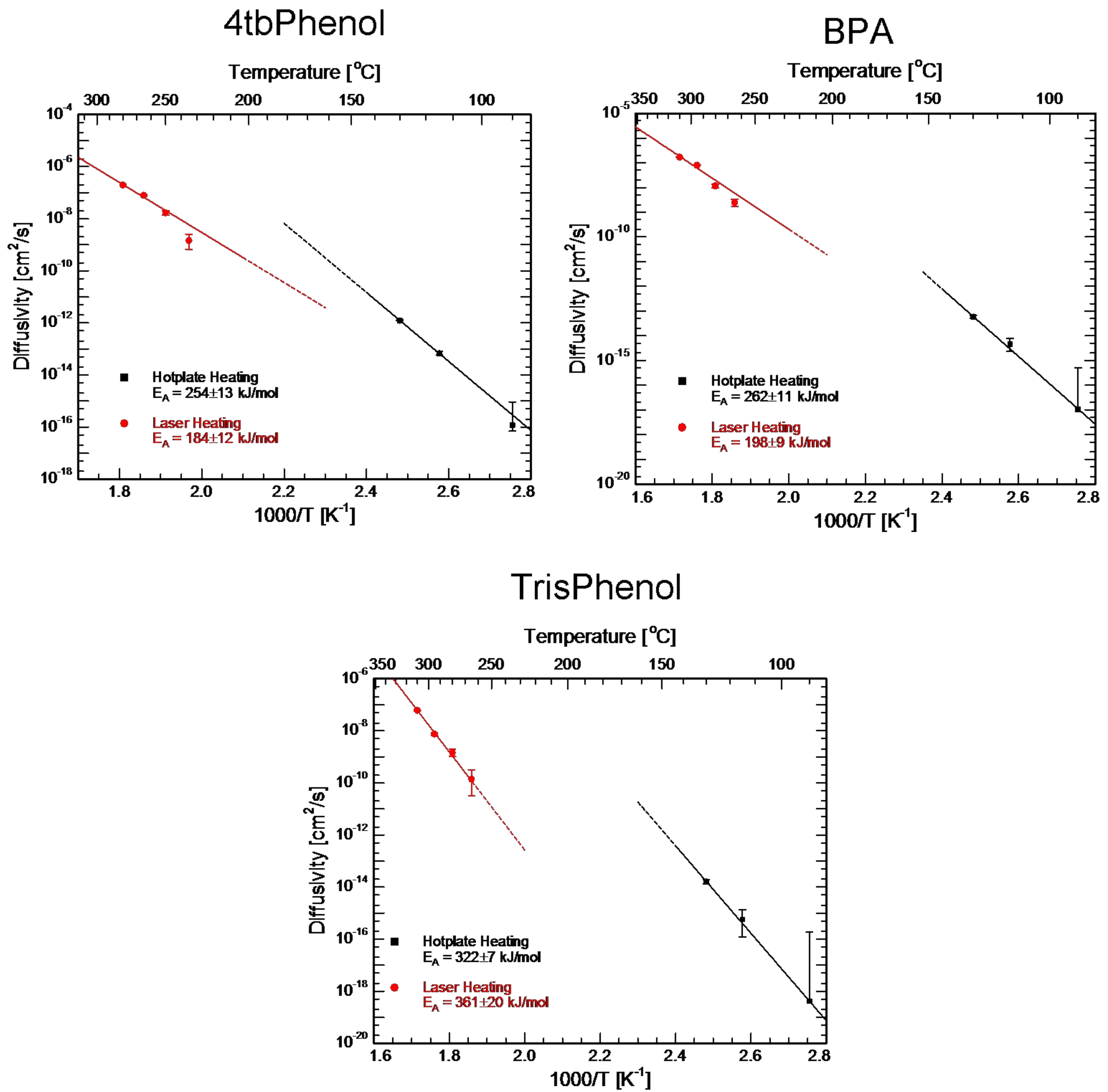

Figure 5.8 Diffusivity as a function of PEB temperature of the Series 2 PAGs using hotplate and laser PEB

Table 5.1 Activation energies of Series 2 PAGs with hotplate and laser PEB

Activation E (kJ/mol)	4tbPhen	BPA	Trisphen
Hot plate 60 sec	254±13	262±11	322±7
Laser 500 μs	184±12	198±9	361±10

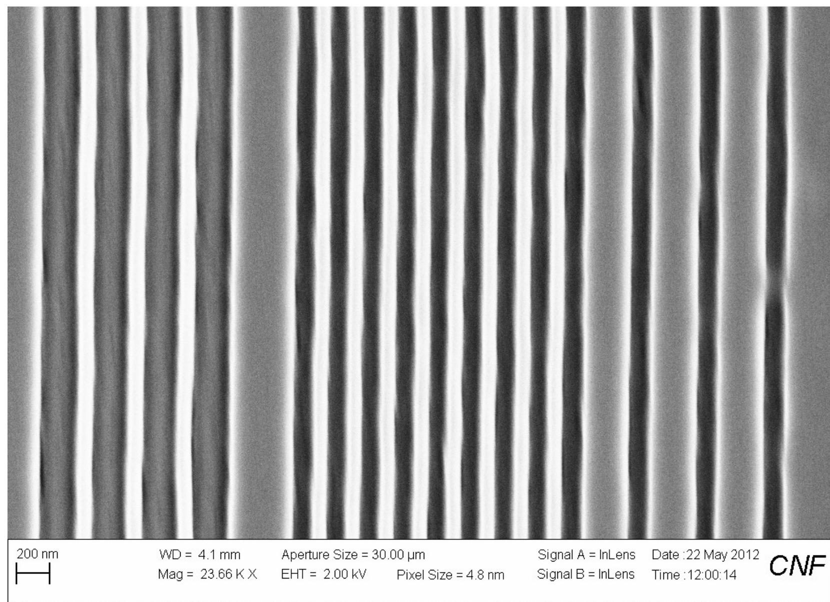

Figure 5.9 SEM image of 100 nm dense and isolated lines of the TrisPhenol PAG and CR-15 resist patterned with e-beam lithography

The TrisPhenol PAG was added at 5 wt % with respect to the CR-15 resist and lithographically patterned in the process described above. The SEM image shown in Figure 5.9 indicates the potential of the TrisPhenol PAG to be used with high resolution resist systems.

5.3.3 Low Tg Molecular Glasses

5.3.3.1 Thermal Decomposition

To test for decomposition of the molecular glass resists, ^{1}H NMR was used. The MGs were spin-coated onto a heavily-doped wafer and subject to heating with the CO_2 laser up to 30 W as described in the experimental section. The film was subsequently removed from the substrate with a razor blade, dissolved in a deuterated solvent and the NMR spectra were measured (Figure 5.11). The spectra obtained for both MGs were clean and identical to their respective NMR spectra before treatment, confirming the assumption that no decomposition occurs during laser-PEB.

5.3.3.2 Lithographic Patterning of Low Tg MG Resists with Laser-PEB

To examine the effect of laser-PEB on the patterning of low Tg MGs, a model resist system was selected. Tris-t-BOC (Figure 5.1), with a 75 % t-BOC protection ratio, has a Tg of 51°C, as measured by DSC. T-BOC is considered a high activation energy protecting group, requiring temperatures of at least 80°C to effectively catalyze the acid-induced deprotection[29]. The resist solution was prepared using tris-t-BOC and 5 wt % (with respect to the resist) of the TrisPhenol PAG. The solution was spin-coated onto two wafers. Both wafers were exposed to 254 nm UV light with an array of doses using an ABM contact aligner. The films were subject to either a hotplate PEB of 80°C for 1 minute, or laser-PEB with an array of laser powers ranging

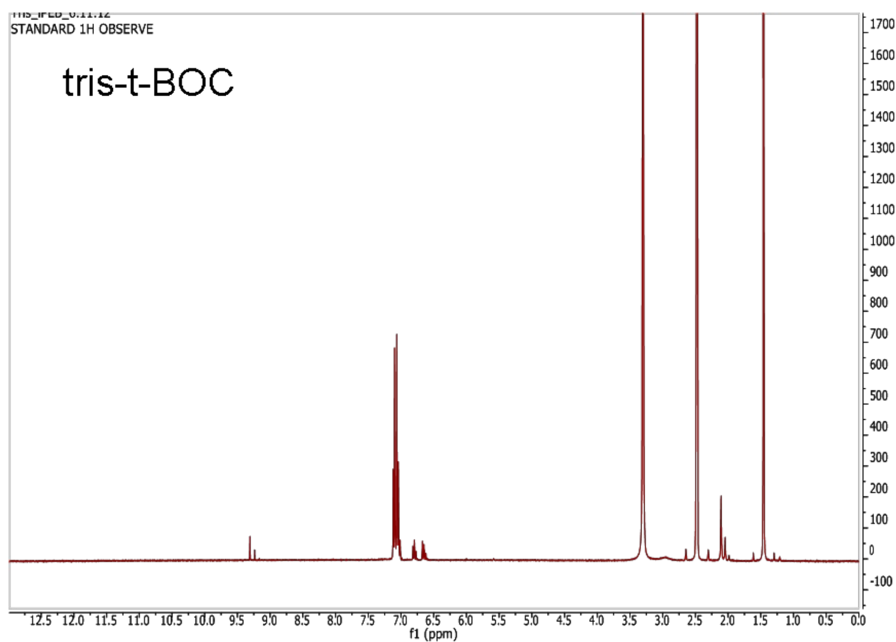

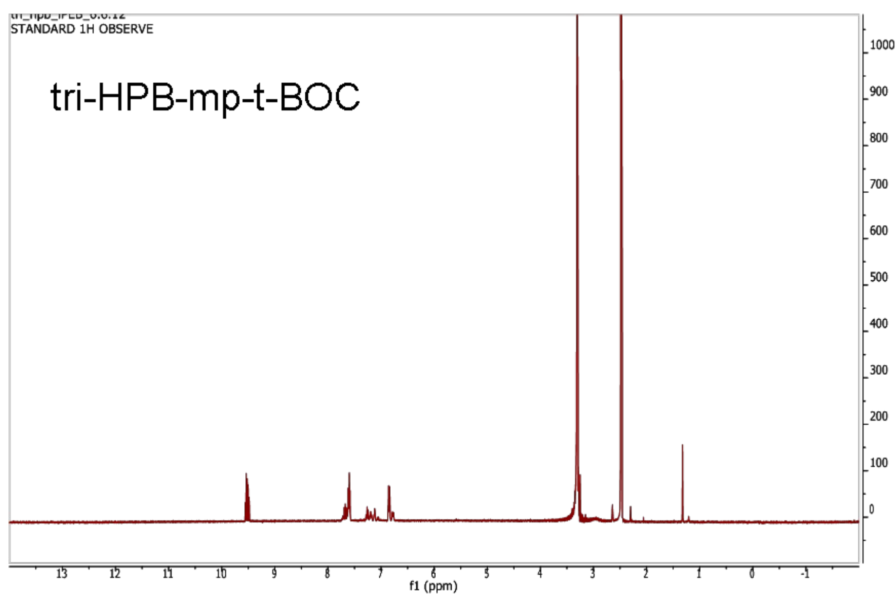

Figure 5.10 ¹H NMR analysis of tris-t-BOC and tri-HPB-mp-t-BOC after thermal treatment with the CO_2 laser

from 12-30 W, all for 500μs. The films were then developed using AZ 726-MIF developer (0.26N tetramethylammonium hydroxide solution) for 1 minute. An optical microscope was used to image the resulting patterns (Figure 5.11). The image on the left shows a representative pattern set in the resist film baked with a hotplate. As expected, the patterns are significantly distorted when heated to a temperature 30°C above the Tg of the resist. The distortions were evident at all exposure doses tested. Using the state of the art lithographic processing this resist system cannot produce well-defined features.

The image on the right shows a representative pattern from the resist film processed with laser-PEB. This film produced clear, well-defined patterns with a 15 W laser power, which heats the film to a maximum temperature of 220°C. This result indicated it is possible to heat a resist well above its Tg in the sub-millisecond timeframe, which is too short under these conditions to allow the polymer to relax from its glassy state.

To further test this hypothesis, e-beam lithography was used to examine the high resolution patterning capability. A representative image of patterned tri-HPB-mp-t-BOC is shown in Figure 5.11. As measured by DSC, the Tg of this material is 38°C, slightly above room temperature. Using a laser power of 15 W and a temperature dwell time of 500 μs, sub-micron sized features were cleanly resolved when patterned with e-beam lithography. With these model systems, we have successfully demonstrated a proof of concept indicating low Tg chemically amplified materials can produce well-defined lithographic patterns with laser-PEB. This discovery opens the door for a whole new class of low molecular weight MGs to be considered as photoresist materials, which can potentially improve resist performance past the current benchmarks.

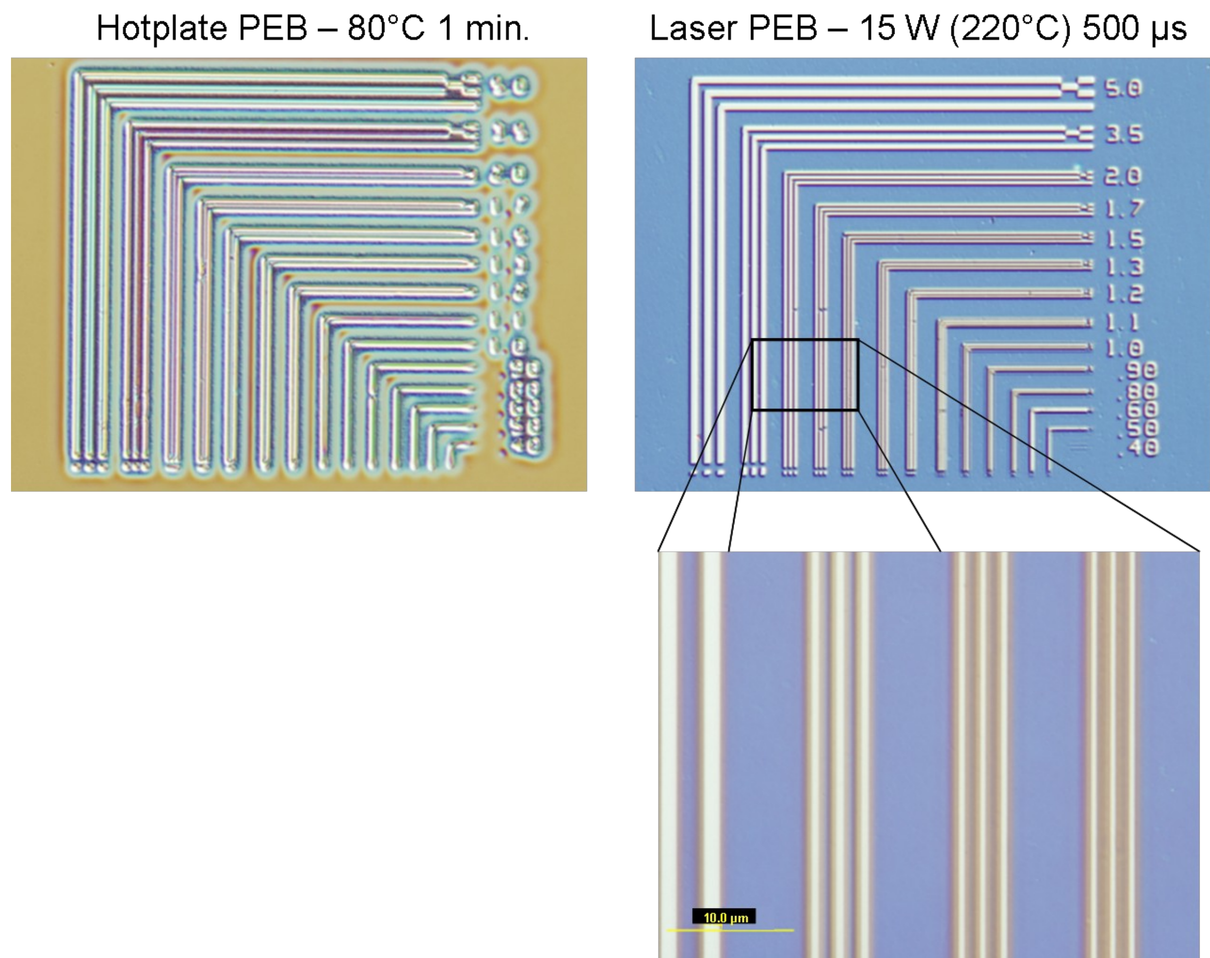

Figure 5.11 Optical images of patterned tris-t-BOC and TrisPhenol PAG with hotplate and laser PEB

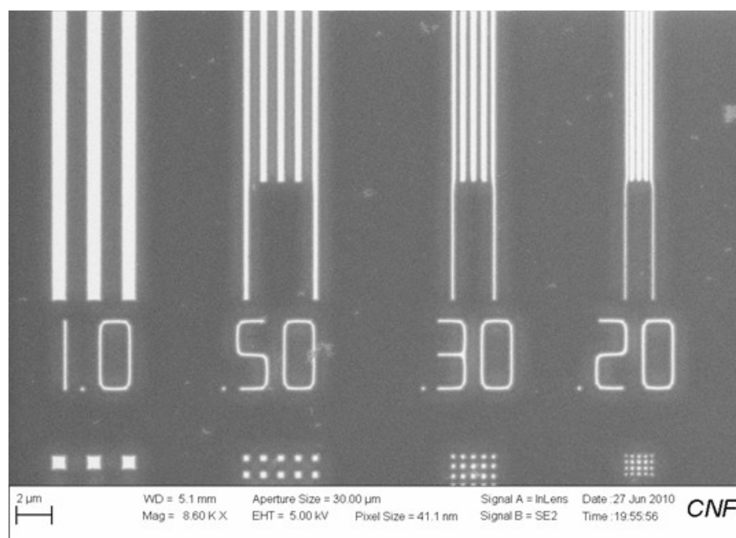

Figure 5.12 SEM image of tri-HPB-mp-t-BOC and TrisPhenol PAG patterned with e-beam lithography using laser-PEB

5.4 Conclusions

This paper has studied a variety of PAG structures for use with the newly developed CO_2 laser heating system. The Series 1 PAGs showed extensive acid diffusion lengths with both hotplate and laser-PEB. Furthermore, simply varying the fluorinated chain length did not provide a large enough contrast to effectively study the diffusion behavior. Series 2 PAGs were designed with bulky aromatic-based anions, which showed a large range of sensitivities when lithographically processed. In particular, the BPA and TrisPhenol PAGs showed significantly decreased acid diffusion lengths when processed with laser-PEB. Using a diffusivity model tailored for the temperature range accessed in this study, the activation energies for these new PAGs have been calculated for both hotplate and laser-PEB. TrisPhenol PAG has shown the ability to produce well-resolved lines with e-beam lithography. This study has also demonstrated the ability to pattern chemically amplified, low Tg MG resists by using the CO_2 laser as an alternate PEB method. Well-resolved patterns were achieved with both UV and e-beam irradiation. These results have broadened the scope of low molecular weight materials that can now be considered as viable candidates for next generation photoresists.

Acknowledgements

This work was funded by a grant from Globalfoundries through the Semiconductor Research Corporation (SRC). Intel and the SRC Education Alliance are gratefully acknowledged for providing a fellowship to support this research. The Cornell Nanoscale Science and Technology Facility (CNF) and the Cornell Center for Materials Research (CCMR) are thanked for the use of their facilities. Prof. Michael Thompson is thanked for use of the CO_2 laser system,

as well as valuable discussions on the data collected in this study. Byungki Jung is acknowledged for assistance with the laser-PEB process, as well as modeling and calculations.

REFERENCES

[1] Walker, E. J., Reduction of photoresist standing-wave effects by post exposure bake. *IEEE Transactions on Electron Devices* **1975,** 22, (7), 464-466.

[2] Itani, T.; Yoshino, H.; Hashimoto, S.; Yamana, M.; Samoto, N.; Kasama, K., A study of acid diffusion in chemically amplified deep ultraviolet resist. *Journal of Vacuum Science and Technology B* **1996,** 14, (6), 4226-4228.

[3] Yoshizawa, M.; Moriya, S., Study of the acid-diffusion effect on line edge roughness using the line edge roughness evaluation method. *Journal of Vacuum Science and Technology B* **2002,** 20, (4), 1342-1348.

[4] Allen, R.D.; Brock, P. J.; Na, Y.; Sherwood, M. H.; Truong, H. D.; Wallraff, G. M.; Fujiwara, M.; Maeda, K., Investigation of polymer-bound PAGs: synthesis, characterization and initial structure/property relationships of anion-bound resists. *Journal of Photopolymer Science and Technology* **2009,** 22, 25-29.

[5] Wang, M.; Gonsalves, K. E.; Rabinovich, M.; Yueh, W.; Roberts, J. M., Novel anionic photoacid generators (PAGs) and corresponding PAG bound polymers for sub-50 nm EUV lithography. *Journal of Materials Chemistry* **2007,** 17, 1699-1706.

[6] Lawson, R.; Lee, C.; Whetsell, R.; Yueh, W.; Roberts, J.; Tolbert, L.; Henderson, C. L., Molecular class photoresists containing photoacid generator functionality: a route to a single molecule photoresist. *Proceedings of SPIE* **2007,** 6519, 65191N-1-10.

[7] Lawson, R.; Lee, C.; Yueh, W.; Tolbert, L.; Henderson, C. L.; Single molecule chemically amplified resists based on ionic and non-ionic PAGs; *Proceedings of SPIE* **2008,** 6923, 69230K-1-10.

[8] Choi, K. W.; Leeson, M. J.; Cao, H. B.; Chandhok, M.; Thompson, G.; Prabhu, V. M.; Lavery, K. A.; Lin, E. K.; Wu, W. L.; Woodward, J. T, Effect of photoacid-generator concentration and developer strength on the patterning capabilities of a model EUV photoresist. *Proceedings of SPIE* **2007,** 6519, 651943-1-9.

[9] Malik, S.; Eisele, J.; Whewell, A.; Ferreira, L.; Holt, T.; Bowden, M., Post-exposure bake temperature considerations for high activation energy resist systems, *Journal of Photopolymer Science and Technology* **2000,** 13, (4), 513-518.

[10] Sha, J.; Jung, B.; Thompson, M. O.; Ober, C. K.; Chandhok, M.; Younkin, T. R., Submillisecond post-exposure bake of chemically amplified resists by CO_2 laser spike Annealing. *Journal of Vacuum Science and Technology B* **2009,** 27, (6), 3020-3025.

[11] Jung, B.; Ober, C. K.; Thompson, M. O., Deprotection reaction kinetics in chemically amplified photoresists determined by sub-millisecond post exposure bake. *Proceedings of SPIE* **2012,** 8325, 83250N-83250N-7.

[12] Jung, B.; Sha, J.; Paredes, F.; Chandhok, M.; Younkin, T. R.; Wiesner, U.; Ober, C. K.; Thompson, M. O., Kinetic Rates of Thermal Transformations and Diffusion in Polymer Systems Measured during Sub-millisecond Laser-Induced Heating. *ACS Nano* **2012,** 6, (7), 5830-5836.

[13] Kim, S.-K., Thermal effects study for a chemically amplified photoresist. *Journal of the Korean Physical Society* **2006,** 49, (3), 1211-1216.

[14] Cho, I. W.; Park, J.-M.; Kim, H.; Hong, J.-Y.; Kim, S.-S.; Cho, H.-K.; Oh, H.-K., Reduction of line width and edge roughness by resist reflow process for extreme ultra-violet lithography. *Proceedings of SPIE* **2009,** 7273, 72732D/1-72732D/8.

[15] Joo, H. S.; Seo, D. C.; Kim, C. M.; Lim, Y. T.; Cho, S. D.; Lee, J. B.; Song, J. Y.; Kim,

K. M.; Park, J. H.; Jung, J. C.; et al, High performance 193 nm photoresist materials based on ROMA polymers: sub-90 nm contact hole application with resist reflow. *Proceedings of SPIE-The International Society for Optical Engineering* **2004,** 5376, 126-133.

[16] Young-Gil, K.; Kim, J. B.; Fujigaya, T.; Shibasaki, Y.; Ueda, M., A positive-working alkaline developable photoresist based on partially tert-Boc-protected calix[4]resorcinarene and a photoacid generator. *Journal of Materials Chemistry* **2002,** 12, (1), 53-57.

[17] Ueda, M.; Takahashi, D.; Nakayama, T.; Haba, O., Three-component negative-type photoresist based on calix[4]resorcinarene, a cross-linker, and a photoacid generator. *Chemistry of Materials* **1998,** 10, (8), 2230-2234.

[18] Chang, S. W.; Ayothi, R.; Bratton, D.; Yang, D.; Felix, N.; Cao, H. B.; Deng, H.; Ober, C. K., Sub-50 nm feature sizes using positive tone molecular glass resists for EUV lithography. *Journal of Materials Chemistry* **2006,** 16, (15), 1470-1474.

[19] De Silva, A.; Ober, C. K., Hydroxyphenylbenzene derivatives as glass forming molecules for high resolution photoresists. *Journal of Materials Chemistry* **2008,** 18, 1903-1910.

[20] De Silva, A.; Lee, J. K.; Andre, X.; Felix, N. M.; Cao, H. B.; Deng, H.; Ober, C. K., Study of the Structure-Properties Relationship of Phenolic Molecular Glass Resists for Next Generation Photolithography. *Chemistry of Materials* **2008,** 20, (4), 1606-1613.

[21] Yang, D.; Chang, S. W.; Ober, C. K., Molecular glass photoresists for advanced Lithography. *Journal of Materials Chemistry* **2006,** 16, 1693-1696.

[22] Ayothi, R.; Yi, Y.; Cao, H.; Wang, Y.; Putna, S.; Ober, C. K., Arylonium photoacid generators containing environmentally compatible aryloxyperfluoroalkanesulfonate groups. *Chemistry of Materials* **2007,** 19, (6), 1434-1444.

[23] Hansen, M. M.; Riggs, J. R., A novel protecting group for hindered phenols. *Tetrahedron Letters* **1998**, 39, 2705.

[24] Vogt, B. D.; Kang, S.; Prabhu, V. M.; Lin, E. K.; Satija, S. K.; Turnquest, K.; Wu, W., Measurements of the Reaction Diffusion Front of Model Chemically Amplified Photoresists with Varying Photoacid Size. *Macromolecules* **2006,** 39, (24), 8311-8317.

[25] Stewart, M. D., Catalyst diffusion in positive-tone chemically amplified photoresists. Ph.D. Thesis, Univeristy of Texas at Austin, 2003.

[26] Van Steenwinckel, D.; Gronheid, R.; Lammers, J. H.; Meyers, A. M.; Van Roey, F.; Willems, P., A novel method for characterizing resist performance. *Proceedings of SPIE-The International Society for Optical Engineering* **2007,** 6519, 65190V/1-65190V/11.

[27] Choi, K.-W.; Prabhu, V. M.; Lavery, K. A.; Lin, E. K.; Wu, W.-l.; Woodward, J. T.; Leeson, M. J.; Cao, H. B.; Chandhok, M.; Thompson, G., Effect of photoacid generator photoresist. *Proceedings of SPIE-The International Society for Optical* Engineering **2007,** 6519, 651943/1-651943/9.

[28] Lawson, R. A.; Henderson, C. L., Mesoscale kinetic Monte Carlo simulations of molecular resists: effects of photoacid homogeneity on resolution, line-edge roughness, and sensitivity. *Journal of Micro/Nanolithography, MEMS, and MOEMS* **2010,** 9, (1), 013016/1-013016/8.

[29] Cameron, J. F.; Ablaza, S. L.; Xu, G.; Yueh, W., Design and chemistry of advanced deep-UV photoresists: the role of the photoacid generator. *Journal of Photopolymer Science and Technology* **1999,** 12, (4), 607-620.

CHAPTER 6

INVESTIGATION OF SINGLE-COMPONENT MOLECULAR GLASSES FOR ALL-DRY LITHOGRAPHY

Abstract

As the semiconductor industry continues its pursuit of Moore's Law, resolution limits are being pushed to the sub-30 nm regime. In order to meet these demands, radical new resist designs and processes must be explored. Today's resists are based on polymers. More recently molecular glass (MG) structures have been examined as alternative photoresist materials. One especially attractive feature of MG resists is their potential for use in all-dry lithographic processing conditions. Physical vapor deposition (PVD) has been used to deposit thin films of MGs onto various substrates, something not possible with polymers. PVD deposits a uniform film of controlled thickness free from impurities that would be introduced by casting solvents used in traditional spin coating methods. Thermal development may be used as an alternative to developing in solvents in order to prevent resist swelling and pattern collapse by capillary forces. MGs have emerged as leading candidates for use with PVD and thermal development because of their small size and high thermal stability. Single-component systems have been synthesized, that contain a benzyl chloride substituent and cross-link upon exposure to UV or electron-beam irradiation. The effects of structure on thermal stability, glass transition temperature (Tg) and various lithographic processing conditions have been examined. This study identified a stable molecular glass structure capable of all-dry lithographic processing.

6.1 Introduction

Spin-coating is a widely accepted method of thin film preparation. This solvent-based process requires materials to be dissolved in a casting solvent, and then deposited on a rotating substrate. The centrifugal force created by high spin speeds will spread the material across the substrate, creating a film of uniform thickness after seconds to minutes of spinning[1]. Thermal treatment is required after spin-coating to remove any residual solvent in the film. While spin-coating can easily create a uniform film over a large area, there are some disadvantages associated with this method. Molecules must be soluble in a spinning solvent with suitable viscosity and thin film forming properties[2]. Traces of residual solvent can be left behind, and solvent impurities are transferred to the film[3]. Physical vapor deposition (PVD) has emerged as a viable method of film deposition that can overcome these issues. Evaporation of resist materials creates a film free from pinhole defects and of a uniform, controlled thickness[4]. Multiple components can be deposited simultaneously by co-evaporation, and with layer-by-layer deposition, can potentially reduce aggregation of different film components[5]. It has also been suggested that vapor deposition may pack the molecules of a film more efficiently and uniformly, thereby creating a denser film than achieved with spin-coating[6]. PVD can eliminate solvent waste generated by spin-coating, making it a more environmentally-friendly and cost-effective deposition method. Schmidt and co-workers have demonstrated improvement in resist sensitivity with films prepared by PVD over those prepared via spin-coating[7].

While wet development is currently the method of choice for the semiconductor industry, there are drawbacks associated with the process. A large amount of solvent waste is generated. Lithographic patterns can collapse from capillary forces pushing on the resist sidewalls when the development solvent is present between the features. Dewetting of the resist film from the

substrate may occur, and the developing solvent can penetrate the insoluble portion of the resist, causing swelling and pattern distortion[8]. Thermal development is a more environmentally friendly technique that could overcome these issues. This method exploits photochemistries that yield products of a much different molecular weight than the starting material, creating a contrast of evaporation temperatures. When thermally treated after exposure, the lower molecular weight portion will evaporate first, leaving the higher molecular weight material behind. Thermal development can potentially improve the line edge roughness of patterned materials[9].

Polymers have been extensively studied as thin films by means of spin-coating because of their amorphous nature and high glass transition temperatures (Tg). However, polymers are poor candidates for evaporation, since their large size will cause the polymer chains to thermally degrade before subliming when heated under vacuum. Molecular glasses (MGs) have been studied as an alternative class of materials to polymers[10-12]. Molecular glasses (MGs) are low molecular weight amorphous compounds that are small in size but still retain the beneficial properties of polymers, including high Tg. The molecular architecture is critical in designing MGs, because small molecules have a tendency to crystallize. Rigid, bulky substituents with asymmetrical structures are known to favor the glassy state[13-17]. Because of the use of high temperatures in both PVD and thermal development, high thermal stability is crucial. The structures that promote glass formation improve the thermal stability of the compounds as well.

The fundamental properties of vapor-deposited MGs have been studied by Ediger and co-workers. The molecular packing of the glasses when vapor-deposited provides uniform kinetic stability and low enthalpy[18]. The time required for stable vapor-deposited glasses to transform to a supercooled liquid greatly exceeds the structural relaxation time[18], further indicating the tight packing and stability of the MGs. The thermal expansion coefficients of vapor-deposited MG

and ordinary MGs have been measured[19]. The vapor-deposited MGs exhibit an expansion coefficient that is 14% lower than that of an ordinary glass. MG films prepared with this method can be thermally processed in layers during transistor fabrication without the concern of distorting previously constructed layers.

A single-layer resist that can be processed via chemical vapor deposition has been designed using plasma-polymerizable methyl silane[20]. Exposure to 248 or 193 nm radiation yields a siloxane network that can be dry-developed using chlorine HBr plasma. While the possibility of all-dry resist processing is promising, it is also necessary to consider alternative, less abrasive development methods, as well as compatible resist structures.

Photoresists that crosslink or de-polymerize upon irradiation can be thermally developed to create negative or positive tone patterns, respectively. MGs that can cross-link upon exposure to UV radiation are ideal candidates for all-dry processing, as their small size allows for successful deposition and evaporation at elevated temperatures. Schmidt and co-workers have shown that molecular glass resists based on coumarin derivatives can photodimerize in the solid state, and these monomers can be evaporated at high temperatures under high vacuum[21,22]. These molecules have successfully produced micron-sized features with exposure to 254 nm UV light. This study successfully demonstrated the all-dry lithography process, though further research is necessary to produce higher resolution patterns in the nanometer regime.

This chapter describes the preparation and characterization of molecular glasses designed for use with physical vapor deposition and high-vacuum thermal development. The effect of structure on thermal stability and patternability is discussed, as well as compatibility and results using an all-dry lithography process.

6.2 Experimental

6.2.1 Synthesis of Molecular Glasses

Reagents were purchased from Sigma Aldrich and used without further purification. HPLC grade solvent were purchased from Fisher Scientific and used without further purification. *p*-chloromethyl-methoxy-calix[4]arene (CM-Calix) was synthesized according to previously published protocols[23,24]. 4-(1-{3-[1,1-bis(4-hydroxyphenyl)ethyl]phenyl}-1-(4-hydroxyphenyl)ethyl)phenol (CR-2) and 4-(1-{3,5-bis[1,1-bis(4-hydroxyphenyl)ethyl] phenyl}-1-(4- hydroxyphenyl)ethyl)phenol (CR-15) were synthesized according to previously published protocols[10].

2-[4-methoxy-2-(naphthalen-2-yl)phenyl]naphthalene

To a 500 mL three-necked round bottomed flask equipped with a nitrogen inlet and a condenser was added 1.50 g (5.64 mmol) 2,4-dibromoanisole, 0.15 g (0.56 mmol) and 1.94 g (11.3 mmol) 1-naphthaleneboronic acid under nitrogen. Toluene (85 mL), methanol (28 mL) and a 2M K_2CO_3 solution (23 mL) were subsequently added. Palladium (II) acetate was then added at 5 mol %. The mixture was stirred at 75°C overnight. Upon completion, the reaction was cooled to room temperature and poured into H_2O. The aqueous layer was extracted x3 with dichloromethane. The organic layers were combined, dried over Na_2SO_4, and concentrated *in vacuo*. Further purification by column chromatography (ether:dichloromethane 1:1) afforded 1.3 g of a white glassy material. Yield = 64% ^{1}H NMR (300 MHz, Chloroform-d) δ 8.25 – 7.13 (m, 17H), 3.75 (s, 3H).

2-[3,5-bis(chloromethyl)-4-methoxy-2-(naphthalen-2-yl)phenyl]naphthalene (CM-Binaphthyl)

To a 500 mL round-bottomed flask was added 1.00 g (2.78 mmol) 2-[4-methoxy-2-(naphthalen-2 yl)phenyl] naphthalene and 2.09 g (69.4 mmol) paraformaldehyde in 134 mL dioxane. While stirring continuously, 11 mL acetic acid, 23 mL HCl and 21 mL phosphoric acid (85 %) were added. The resulting solution was stirred for 8 hours at 100°C. Upon completion, the reaction was poured into ice water. The precipitate was filtered off and redissolved in chloroform. The organic layer was washed until the aqueous layer reached a neutral pH. The organic layer was separated, dried over MgSO4, and concentrated *in vacuo*. Further purification was achieved by washing with hexanes several times to afford 0.45 g of a white powder. Yield = 35%. ^{1}H NMR (300 MHz, Chloroform-d) δ 8.25 – 7.13 (m, 15H), 5.10 (br s, 4H), 3.75 (s, 3H).

1,3-bis[1,1-bis(4-methoxyphenyl)ethyl]benzene

To a 300 mL round-bottomed flask equipped with a nitrogen inlet and condenser was added 0.64 g (15.9 mmol) NaH (60 % oil dispersion) and a stirbar. 20 mL anhydrous hexane was added under nitrogen, and the mixture stirred for 20 minutes. The hexane was then decanted, and 15 mL anhydrous THF was added. 1.0 g (2.00 mmol) of CR-2 was added slowly, and then 4.0 mL (63.7 mmol) MeI was added dropwise via a syringe. The mixture was stirred overnight at reflux. After completion of the reaction, the mixture was cooled, and then diluted with a 4:1 ether:water mixture. The organic layer was separated and washed twice with H_2O. The organic layer was separated, dried over $MgSO_4$, and the solvent removed by rotary evaporation. The crude product was purified by recrystallization in n-butanol. Yield = 90%. ^{1}H NMR (300 MHz, Chloroform-d) δ 6.99 – 6.64 (m, 20H), 3.77 (s, 12H), 1.24 (s, 6H).

CM-CR2

^{1}H NMR (300 MHz, Chloroform-d) δ 7.05 – 6.74 (m, 16H), 4.53 (d, J = 8.5 Hz, 5H), 3.89 – 3.65 (m, 9H), 1.24 (s, 6H).

1,3,5-tris[1,1-bis(4-methoxyphenyl)ethyl]benzene

^{1}H NMR (300 MHz, Chloroform-d) δ 6.85-6.61 (m, 27H), 3.77 (s, 11H), 1.93 (s, 9H).

CM-CR15

^{1}H NMR (300 MHz, Chloroform-d) δ 6.95-6.62 (br m, 22H), 4.52 (s, 10H), 3.89 – 3.67 (m, 18H), 1.93 (s, 9H).

6.2.2 Characterization

^{1}H NMR spectra were recorded on a Varian Inova-300 NMR spectrometer (300 MHz) at room temperature. Chemical shifts reported are quoted in parts per million (ppm) and relative to $CHCl_3$ (δ 7.26 ppm). FT-IR spectrum were recorded on a Mattson Instruments Galaxy 2020 FT-IR spectrometer. The decomposition temperature for each MG was measured on a TA Instruments Q500 Thermogravimetric Analyzer, and their glass transition temperatures (Tg) were measured on a TA instruments Q1000 Modulated Differential Scanning Calorimeter. High Performance Liquid Chromatography was performed with an Agilent 1100 series with a Zorbax Bonus RP 4.6 x 150 mm column. The elution solvent was a THF/water (60/40) mixture, with a flow of 1 mL/min. Detection was performed at 254 nm.

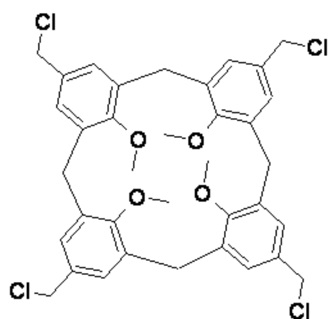

CM-Calix

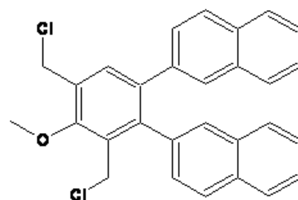

CM-Binaphthyl

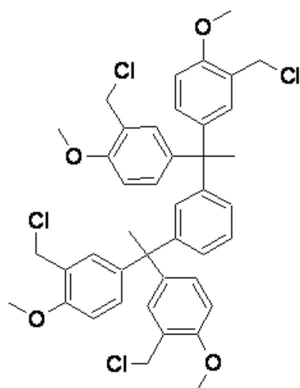

CM-CR2

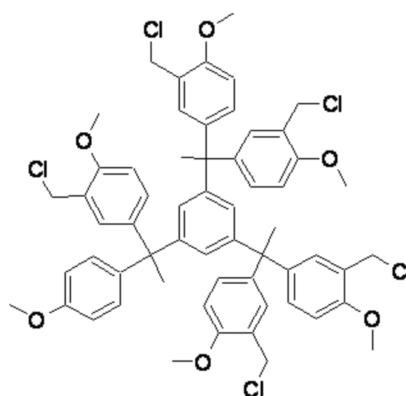

CM-CR15

Figure 6.1 Molecular glass structures

6.2.3 Film Deposition

6.2.3.1 Vapor Deposition

Prior to deposition, the silicon wafers were cleaned via O_2 plasma etching and then primed with a 20 wt % hexamethyldisilazane (HMDS) solution in PGMEA. The wafer was then placed in the substrate holder and the desired MG was placed in a heatable source in the PVD tool. The chamber was placed under vacuum at a pressure of 7×10^{6} mbar. Two shutters, one below the substrate and one above the source are used to control film deposition. Once the shutter above the source was open, the source was slowly heated until a slow, steady rate of evaporation of 0.2 Å/s was reached. The rate of evaporation was measured by oscillating quartz crystals positioned near the substrate holder. Once the evaporation rate was constant, the shutter below the substrate was opened, allowing a film of even thickness to be deposited on the substrate. The substrate is rotated during the evaporation process to ensure a uniform film deposition.

6.2.3.2 Spin-coating

The resist powder was dissolved in 2-butanone to make a 5 wt % solution. The solution was filtered twice using a filter with a 0.2 μm pore size. The filtered solution was spin-coated onto a silicon wafer primed with a 20 vol % hexamethyldisilazane (HMDS) solution in propylene glycol methyl ether acetate (PGMEA) at a spin speed of 2000 rpm for 60 seconds. The film was then baked at 100°C for 60 seconds to remove any residual spinning solvent.

6.2.4 Lithographic Processing

The films were exposed with an ABM contact aligner or a Leica VB6 electron-beam lithography system operating at 100 keV. The films were either solvent developed by submerging the wafer in various organic alcohols, or dry developed by placing the wafer in a high vacuum chamber and heating it to various temperatures. The resulting patterns were imaged using a Zeiss Ultra 55 Scanning Electron Microscope.

6.2.5 Dissolution Rate Measurements

The dissolution rates of the resists were measured with a quartz crystal microbalance (QCM). A thin resist film was spun on a quartz crystal resonator using the same procedure detailed above. The films that were exposed were irradiated with 254 nm UV light using an ABM contact aligner. The crystal was then attached to the microbalance and dipped into a beaker in which developer was stirring continuously. The apparatus was quickly placed into the developer and anchored into place, taking care to ensure it was disturbed as little as possible during the process. The microbalance measures the frequency change of the resonator during the development process, which is directly proportional to the mass of the crystal, as shown in Sauerbrey's equation (Equation 1). Using this equation, the changes in frequency are converted into film thickness.

Equation 1

$$\Delta F = -\frac{2 f_0^2}{A\sqrt{\rho_q \mu_q}} \Delta m$$

where ΔF = frequency change, f_0 = resonant frequency (Hz), A = area, ρ_q = quartz density (2.65 $g \cdot cm^{-3}$), μ_q = quartz shear modulus (2.95×10^{11} $g \cdot cm^{-2} \cdot s^{-2}$), and Δm = mass change

6.3 Results and Discussion

6.3.1 Design Strategy and Synthesis

In order for a molecule to be a strong candidate for successful all-dry lithography, illustrated in Figure 6.3, it must fulfill certain structural requirements. The compound must have a low molecular weight, as heavier materials will reach their thermal decomposition temperature before subliming. Along with a robust core, the side arms of the material must be strongly bound to prevent a loss of functional groups during heating. Flexible arms can also lower the Tg, which will promote reflow of the material in subsequent heating steps in the lithographic process. The cores chosen for this study are dense, low molecular weight glass formers. Branched, twin and ring structures have previously shown high thermal stability as well as the ability to form amorphous materials[13-15]. The hydroxyl moieties of these cores have been fully protected by methylation. The methoxy group is a stable functional group, and acts as a directing group during the addition of the benzyl chloride. The chloromethyl groups will attach either *ortho* or *para* to the methoxy[21]. The short, halogenated side arm can produce a free radical upon exposure to e-beam radiation, and cross-link with neighboring radicals. The formation of a cross-linked aromatic network provides the solubility change needed to create patterns after development.

Each molecule was synthesized in a similar manner. CR-2 and CR-15 were synthesized using an acid-catalyzed condensation reaction with phenol and the appropriate aldehyde. The hydroxyls of calix[4]arene, CR-2 and CR-15 were then methylated using a Williamson ether synthesis, and subsequently the aromatics were directly chloromethylated by using proton acids. CM-Binaphthyl was synthesized via a Suzuki coupling reaction, followed by chloromethylation(Figure 6.2). Careful purification afforded pure compounds verified by NMR analysis.

6.3.2 Thermal Analysis

The separate thermal decomposition curves exhibit similar decomposition behavior, with two distinct temperatures where significant weight loss occurs, Figure 6.2. The initial weight loss can be attributed to the loss of the chloromethyl groups, which are the least thermally stable substituents on the compounds. The second weight loss step corresponds to the degradation of the methoxy groups, as well as the MG core.

CM-Binaphthyl showed intriguing thermal properties. The structure exhibits a high decomposition temperature of 282°C, because of its compact size and the rigidity of the naphthalene substituents. Its relatively high Tg of 70 °C can be attributed to the bulky naphthalene groups as well as molecular asymmetry. Its low molecular weight gives it a strong potential for vapor deposition. However, the chloromethylation reaction employed only allows for substitution at the ortho position with respect to the methoxy group, limiting the resist to only two cross-linking sites. The effect of this on the lithographic properties will be discussed later in this chapter.

CM-CR15 has a sufficiently high Tg of 50°C, but showed a much lower decomposition temperature than the other compounds tested. The larger asymmetrical structure can contribute to its lower thermal stability. With a high number of benzyl chlorides, it has the potential to create a dense network upon exposure to e-beam radiation.

CM-Calix showed a combination of high thermal stability and a high Tg, due to its rigid ring structure. The chloromethyl groups are located at the *para* position with respect to the methoxy groups, which improves the ability to cross-link to neighboring molecules.

Figure 6.2 Synthetic schemes for CM-Binaphthyl and CM-CR2

6.3.3 Vapor Deposition

The molecules were vapor deposited with a custom built vapor deposition tool, with which the evaporation rate was measured with a quartz crystal microbalance. At 110-140°C, a small amount of evaporation for the CM-Calix molecule was detected, which was most likely due to volatile impurities. At 170°C, evaporation began at a steady rate. When the material reached a temperature of 195°C, a spontaneous drop in the evaporation rate was observed. This can be attributed to the sintering of the material in the source. Temperatures above 203°C caused bumping, or the release of thermally degraded volatile components.

HPLC was used to verify that the CM-calix molecule was successfully vapor deposited with no decomposition, shown in Figure 6.4. To study the patterning properties of this compound, CM-calix was co-evaporated with diphenyl(2,4,6-trimethylbenzoyl)phosphine oxide (TPO), a photoradical initiator, to aid in the cross-linking during exposure. In Figure 6.3, the vapor deposited sample, shown in red, only exhibits the peaks seen in the unheated source material, indicating that no thermal degradation took place during the deposition.

6.3.4 Dissolution properties

The dissolution kinetics of the CM-CR15 resist was studied to gain an insight on the behavior of the material during development. The dissolution rate of the unexposed areas is an important parameter in controlling the lithographic performance of a resist[25]. Monitoring the film thickness change in the exposed regions can reveal important information about the swelling behavior in various developers. During development, the solvent can penetrate the cross-linked network, distorting the shape of the patterned features. This is more likely to occur when the solubility change is based on a difference in molecular weight rather than a polarity change, as

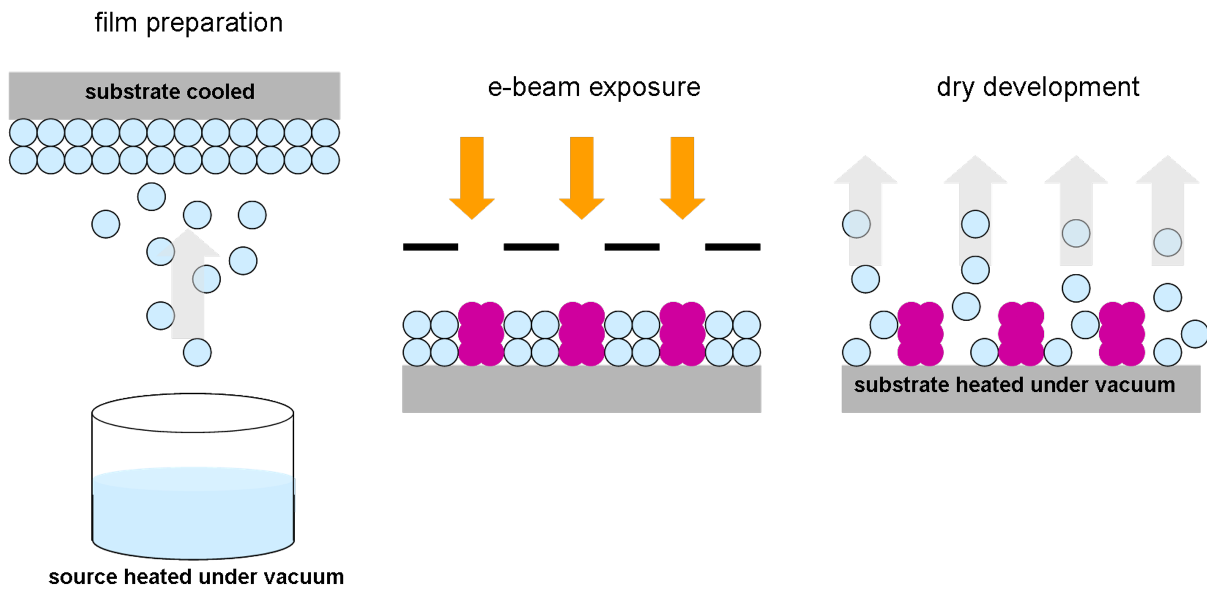

Figure 6.3 All-dry lithography process

Table 6.1 Thermal Characterization of Molecular Glasses

Resist	Molecular Weight (g/mol)	Decomposition Temperature	Tg
CM-Binaphthyl	457.0	282°C	70°C
CM-CR2	726.8	178°C	48°C
CM-CR15	994.3	130°C	53°C
CM-Calix	673.8	250°C	50ºC

the developer still has an affinity for the cross-linked material. Resist swelling has been documented as the cause of line snaking, rounding and increased roughness[26, 27].

A variety of organic alcohols with a range of polarities were tested as developers (Figure 6.5). The solubility of CM-CR15 improved as the developer became less polar. This is expected, as the CM-CR15 molecule is quite hydrophobic. Isopropanol enabled a slow, controlled dissolution rate, with complete development occurring after 100 seconds. CM-CR15 is substantially more soluble in 2-methyl-2-butanol, as the film was dissolved in 22 seconds. 1-butanol and 1-hexanol were both extremely fast developers, dissolving the resist in about 10 seconds. None of the developers showed a significant increase in film thickness, indicating that resist swelling is not an issue with this resist and the various developers.

6.3.5 Lithographic patterning with solvent developer

The goal of this study has been to develop single-component molecular glasses as resists for vapor deposition and high-vacuum dry development. Electron-beam lithography was chosen to obtain high-resolution images of CM-CR15. A range of doses were tested from 100-1000 $\mu C/cm^2$. As expected, the low number of cross-linking sites on the CM-Binaphthyl compound hindered its ability to act as an effective photoresist material. Irradiation with e-beam doses up to 1000 $\mu C/cm^2$ failed to produce patterns when developed in the range of developers tested above. Similar behavior was observed with CM-CR2, with which a contrast was not seen upon exposure and solvent development. In-film studies, discussed in the next section, were performed to gain an insight on the cross-linking behavior.

With a high number of cross-linking sites, CM-CR15 showed a solubility change when exposed to e-beam radiation. Feature sizes down to 35 nm could be imaged after development in

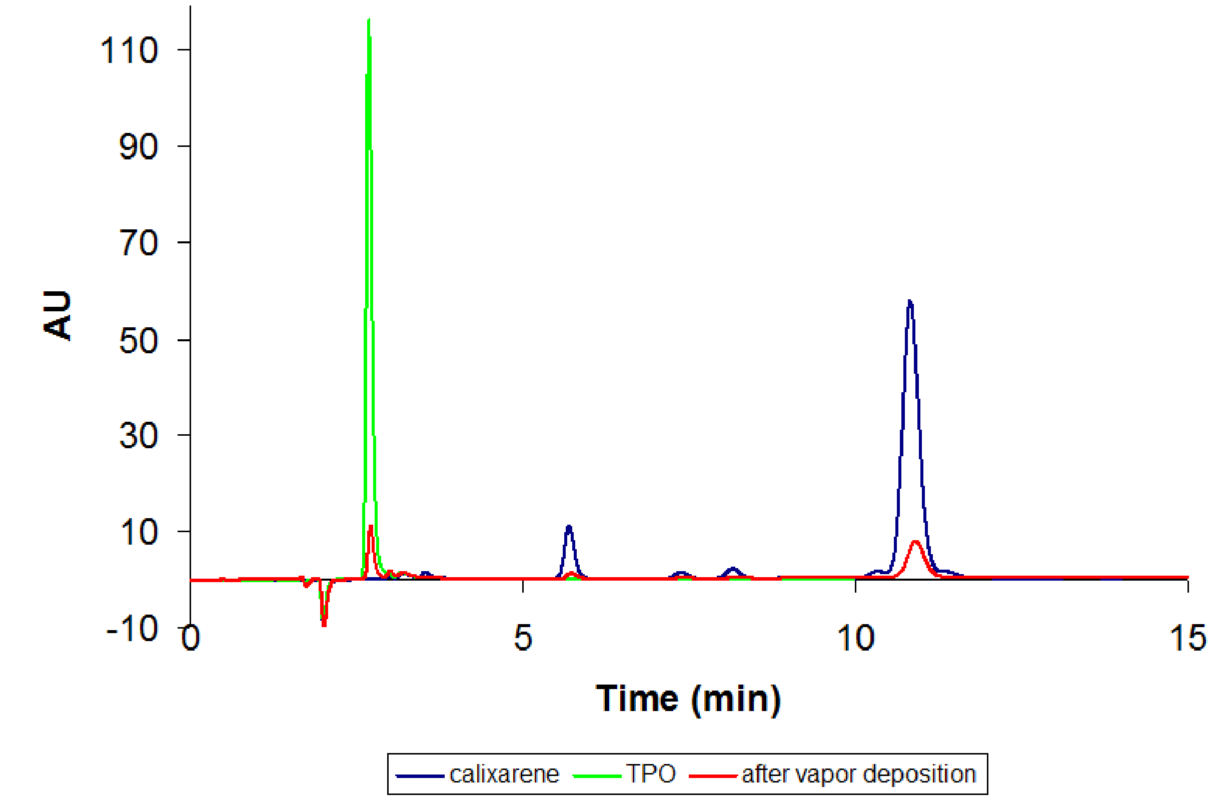

Figure 6.4 HPLC graph of CM-calix and TPO before vapor deposition and the resulting film after co-deposition of the materials

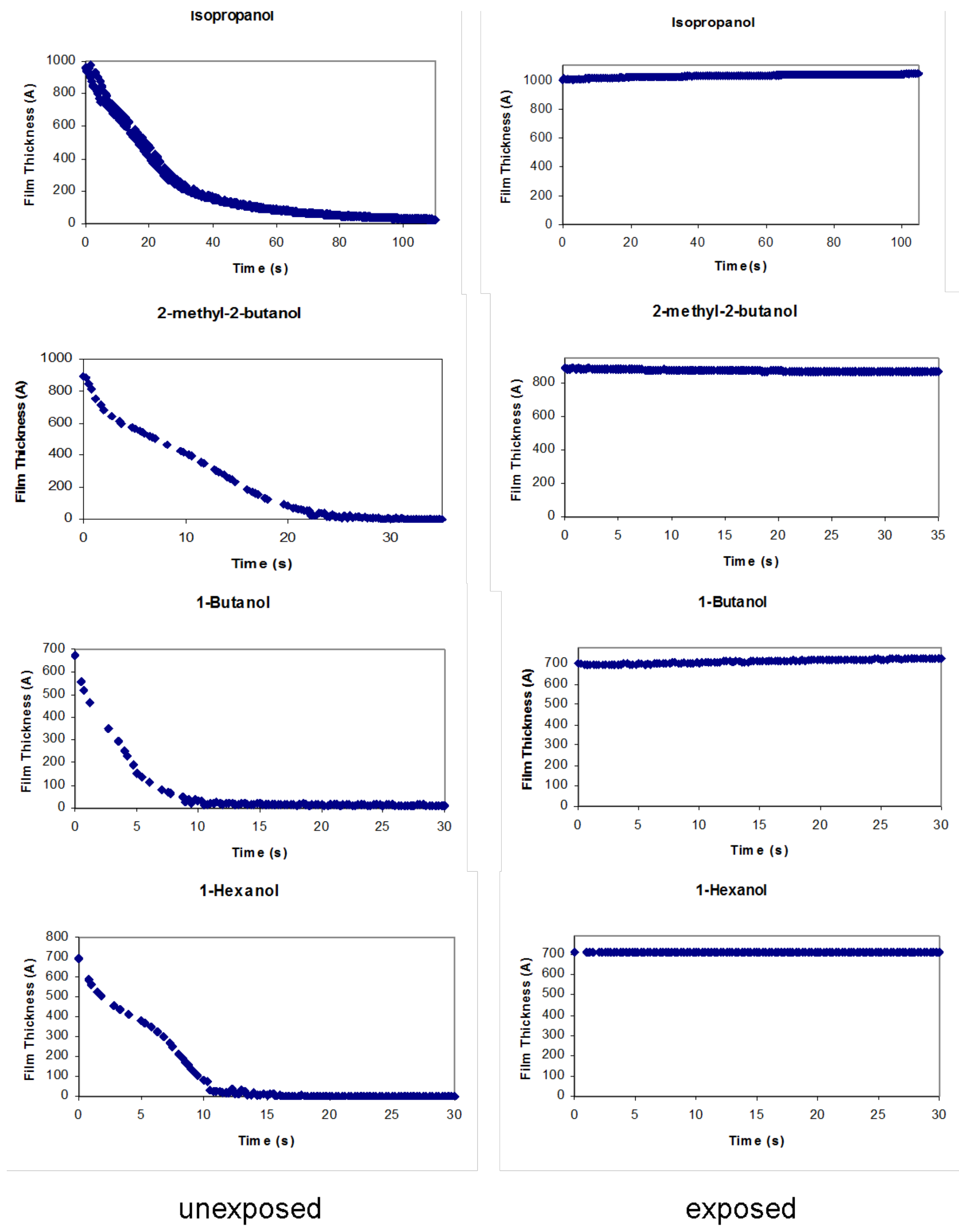

Figure 6.5 Dissolution rates of CM-CR15 in various developers

isopropanol(Figure 6.6). With all solvent developers, however, residue in the unexposed areas was observed post-development. This is most likely due to re-deposition of insoluble, partially

cross-linked material onto the substrate. While CM-CR-15 is capable of producing high resolution patterns, this study suggests solvent development may not be the most suitable candidate for glasses using this type of free-radical cross-linking mechanism.

6.3.6 In-film investigation of cross-linking reaction

When the chloromethylated resist is exposed to electron-beam radiation, this provides sufficient energy to break the carbon-chlorine bond, which will generate a free-radical. These free-radicals will then cross-link, creating a high molecular weight network which is insoluble in the organic alcohol developers. The formation of free-radicals can be followed as a function of exposure dose by monitoring the carbon-chlorine stretching mode with FT-IR spectroscopy.

While e-beam radiation is the most efficient way to cross-link the benzyl chlorides, UV irradiation will also generate free-radicals[24]. In an effort to examine the inability of CM-CR2 to produce patterns, CM-Calix and CM-CR2 were both spin-coated onto double-sided polished silicon wafers and monitored via FT-IR after exposure to various doses. A single film was used for the entire range of exposure doses. The C-Cl stretch peak occurs around 690 cm^{-1} for both molecules (Figure 6.7). As the exposure dose increases, the intensity of the C-Cl peak in the CM-Calix spectrum decreases with respect to the neighboring constant peaks, indicating a loss of C-Cl bonds. The C-Cl peak of the CM-CR2 also decreases with a higher exposure dose, which is evidence of the free-radical formation. However, the location of the benzyl chloride on CM-CR2 may not allow for a high density network to form, resulting in the solubility of the exposed portion of the resist. This result indicates that the number and location of benzyl chloride

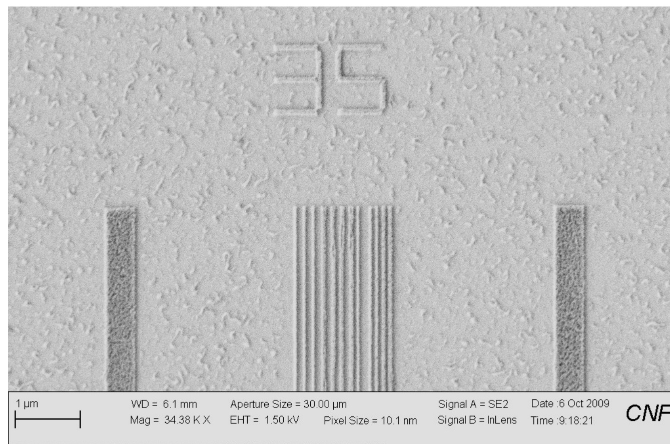

Figure 6.6 SEM image of high resolution patterns obtained by e-beam lithography of CM-CR15 with a dose of 200 μC/cm^2 and development in isopropanol

substitution is crucial to the formation of lithographic patterns. Photo-labile sites must be present on all sides of the molecule, enabling a 3D network formation to give an effective solubility contrast.

6.3.7 All-Dry Lithographic Processing

The patternable resists were tested with the all-dry lithography process. The small size and rigid architecture of the CM-Calix molecule provides the thermal stability necessary to withstand the high temperatures used in both the deposition and development processes. A range of development times and temperatures were tested, with results shown in SEM images in Figure 6.8. The image on the left shows 100 nm line/space patterns from high temperature development at 300°C for 3 min. The right image also shows 100 nm features, but with a lower temperature development of 165°C for 5 hours. Both development methods were able to resolve nanometer scale patterns with smooth line edges and uniform line widths. As evidenced by the ispropanol-developed image in Figure 6.6 and the image of features produced by the all-dry process, dry development can significantly reduce the rough line edges seen with solvent-based development. This method of lithographic processing shows promise to produce well-resolved, high-resolution features.

6.4 Conclusions

This study reports the synthesis and characterization of a class of chloromethyl-functionalized aromatic molecular resists. The thermal properties were investigated to identify potential candidates for physical vapor deposition and all dry lithographic processing. The UV-catalyzed free-radical cross-linking reaction was monitored in-situ via FT-IR analysis. The core

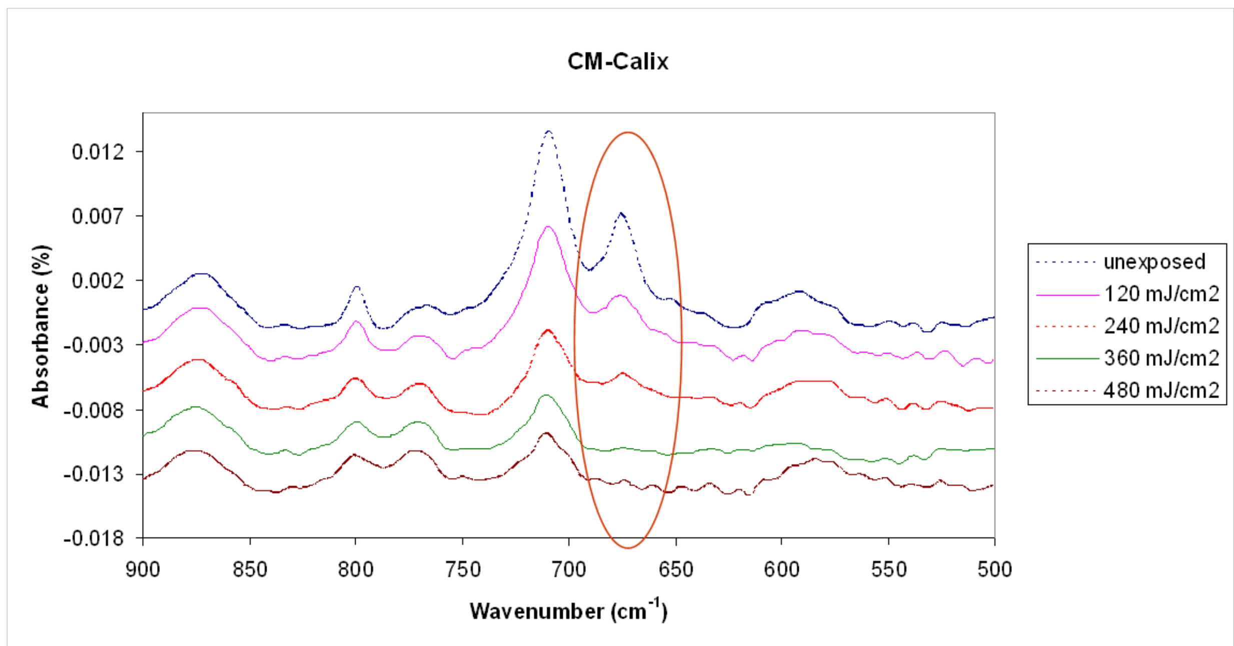

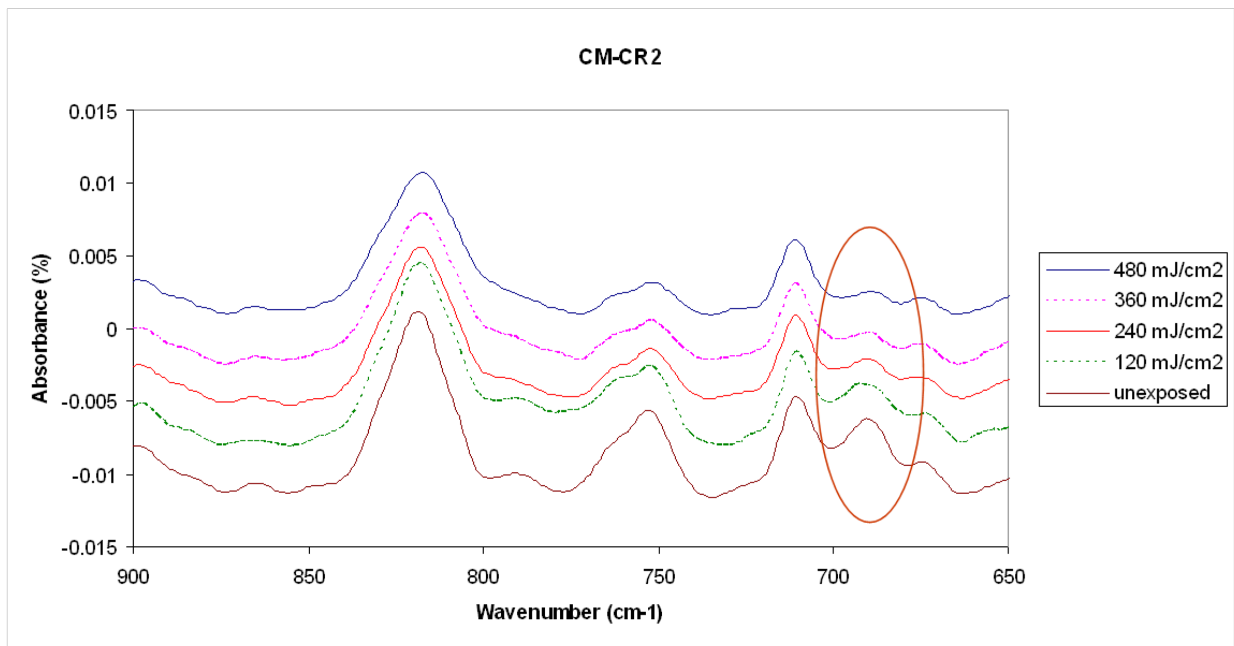

Figure 6.7 In-film IR spectra of CM-Calix and CM-CR2

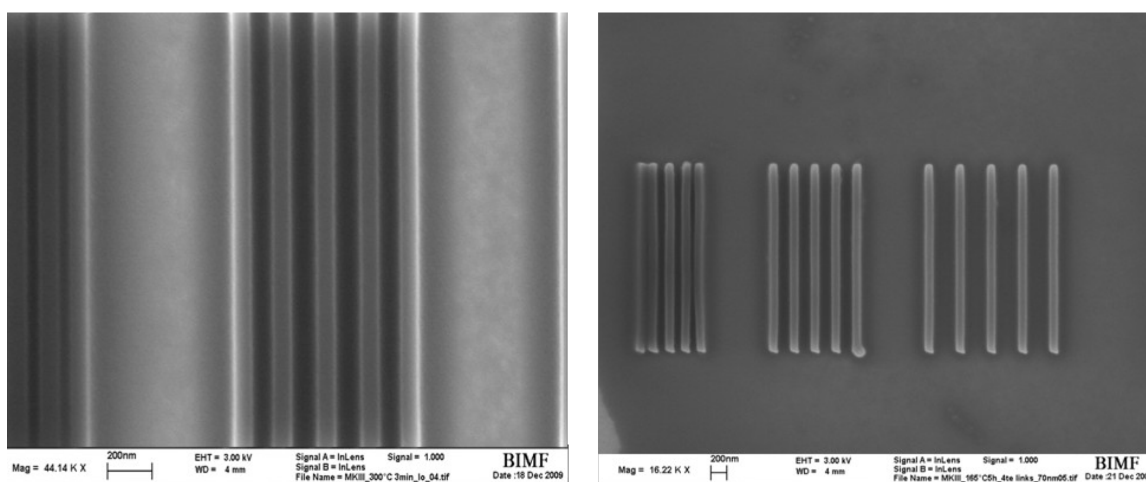

Figure 6.8 SEM of 1:1 (left) and 1:2 and 1:3 (right)100 nm line/space patterns obtained after all-dry e-beam lithographic processing of CM-Calix

structure as well as location and number of chloromethyl substituents were observed to have an effect on the decomposition temperature, Tg and patterning ability of the resists. The patternable MGs were successfully vapor deposited onto silicon substrates, and patterned with electron-beam lithography. Various methods of development were examined, including both wet and dry development. This research has helped identify a compound capable of all-dry lithographic processing and producing well-resolved patterns.

Acknowledgements

This work was funded by the Semiconductor Research Corporation (SRC). Prof. Hans-Werner Schmidt, Christian Neuber and Tristan Kolb are gratefully acknowledged for their guidance and use of the physical vapor deposition tool. The Cornell Nanoscale Science and Technology Facility (CNF) and the Cornell Center for Materials Research (CCMR) are thanked for use of their facilities.

REFERNCES

[1] Norman, K.; Ghanbari-Siahkali, A.; Larsen, N. B., Studies of Spin Coated Polymer Films. *Annual Reports on the Progress of Chemistry, Section C: Physical Chemistry* **2005,** 101, 174–201.

[2] Schubert, D. W.; Dunkel, T., Spin coating from a molecular point of view: its concentration regimes, influence of molar mass and distribution. *Materials Research Innovations* **2003,** 7, 314–321.

[3] VanderHart, D. L.; Prabhu, V.; Lavery, K. A.; Dennis, C. L.; Rao, A. B.; and Lin, E. K., Thin-film solid-state proton NMR measurements using a synthetic mica substrate: Polymer Blends. *Journal of Magnetic Resonance* **2009,** 201, (1), 100-110.

[4] Sato, M.; Iijima, M.; Takahashi, Y., Fabrication of polyurea resists by vapor deposition polymerization for all dry process. *Journal of Photopolymer Science and Technology* **1995,** 8,(1), 137-140.

[5] Neuber, C.; Bate, M.; Thelakkat, M.; Schmidt, H.-W.; Hansel, H.; Zettl, H.; Krausch, G., Combinatorial Preparation and Characterization of Thin-Film Multilayer Electro-Optical Devices. *Review of Scientific Instruments* **2007,** 78, 72216 1-11.

[6] Kearns, K. L.; Still, T.; Fytas, G.; and Ediger, M. D., High-Modulus Organic Glasses Prepared by Physical Vapor Deposition. *Advanced Materials* **2010,** 22, (1), 39-42.

[7] Kolb, T.; Neuber, C.; Krysak, M.; Ober, C. K.; Schmidt, H.-W., Multicomponent Physical Vapor Deposited Films with Homogeneous Molecular Material Distribution Featuring Improved Resist Sensitivity. *Advanced Functional Materials* **2012,** accepted.

[8] Felix, N.; Tsuchiya, K.; and Ober, C. K., High-Resolution Patterning of Molecular Glasses

Using Supercritical Carbon Dioxide. *Advanced Materials* **2006,** 18,(4), 442-446.

[9] Auzelyte, V.; Langner, A.; Solak, H. H., Thermal Development of a Calixarene Resist. *Journal of Vacuum Science & Technology B: Microelectronics and Nanometer Structures* **2009,** 27, (6), 2990-2992.

[10] De Silva, A.; Ober, C. K., Hydroxyphenylbenzene derivatives as glass forming molecules for high resolution photoresists, *Journal of Materials Chemistry* **2008,** 18, 1903-1910.

[11] De Silva, A.; Lee, J. K.; Andre, X.; Felix, N. M.; Cao, H. B.; Deng, H.; Ober, C. K., Study of the Structure-Properties Relationship of Phenolic Molecular Glass Resists for Next Generation Photolithography. *Chemistry of Materials* **2008,** 20, (4), 1606-1613.

[12] Yang, D.; Chang, S. W.; Ober, C. K., Molecular glass photoresists for advanced Lithography. *Journal of Materials Chemistry* **2006,** 16, 1693-1696.

[13] Shirota, Y., Organic materials for electronic and optoelectronic devices. *Journal of Materials Chemistry* **2000**, 10, 1-25.

[14] Shirota, Y., Photo- and electroactive amorphous molecular materials—molecular design, syntheses, reactions, properties, and applications. *Journal of Materials Chemistry* **2005,** 15, 75-93.

[15] Strohriegel, P.; Grazulevicius, J. V., Charge Transporting Molecular Glasses. *Advanced Materials* **2002,** 14, (20), 1439-1452.

[16] Wang, S.; Oldham, W. J. Jr.; Raymond, J.; Hudack, A.; Bazan, G. C., Synthesis, Morphology, and Optical Properties of Tetrahedral Oligo(phenylenevinylene) Materials. *Journal of the American Chemical Society* **2000,** 122, (24), 5695-5709.

[17] Reichert, V. R.; Mathias, L. J., Expanded Tetrahedral Molecules from 1,3,5,7-Tetraphenyladamantane. *Macromolecules* **1994,** 27, (24), 7015-7023.

[18] Dawson, Kevin; Kopff, Laura A.; Zhu, Lei; McMahon, Robert J.; Yu, Lian; Richert, Ranko; Ediger, M. D., Molecular packing in highly stable glasses of vapor-deposited tris-naphthylbenzene isomers. *Journal of Chemical Physics* **2012,** 136, (9), 094505/1-094505/11.

[19] Dalal, Shakeel S.; Sepulveda, A.; Pribil, Greg K.; Fakhraai, Zahra; Ediger, M. D., Density and birefringence of a highly stable α,α,β-trisnaphthylbenzene glass. *Journal of Chemical Physics* **2012,** 136, (20), 204501/1-204501/10.

[20] Nault, M.; Weidman, T.; Sugiarto, D.; Mui, D.; Lee, C.; Yang, J. Single-layer chemical vapor deposition photoresist for 193 nm deep-ultraviolet photolithography. *Journal of Vacuum Science & Technology, B: Microelectronics and Nanometer Structures* **1998,** 16, (6), 3730-3733.

[21] Pfeiffer, F.; Felix, N. M.; Neuber, C.; Ober, C. K.; Schmidt, H.W., Towards Environmentally Friendly, Dry Deposited, Water Developable Molecular Glass Photoresists. *Physical Chemistry Chemical Physics* **2008,** 10, 1257-1262.

[22] Pfeiffer, F., Neuber, C., and Schmidt, H.W., All-dry photoresist systems: physical vapor deposition of molecular glasses. *Proceedings of SPIE* **2008**, 6923, 69231F/1-69231F/8.

[23] Gutsche, C. D.; Dhawan, B.; Levine, J. A.; No, K. W.; Bauer, L. J., Conformal Isomers of the Ethers and Esters of Calix[4]arenes. *Tetrahedron* **1983,** 39, (3), 409-426.

[24] Nagasaki, T. Sisido, K.; Arimura, T.; Shinkai, S., Novel Cornformational Isomerism of Water Soluble Calix[4]arenes. *Tetrahedron* **1992,** 48, (5), 797-804.

[25] De Silva, A.; Sundberg, L. K.; Ito, H.; Sooriyakumaran, R.; Allen, R. D. and Ober, C. K., A Fundamental Study on Dissolution Behavior of High-Resolution Molecular Glass Photoresists. *Chemistry of Materials* **2008,** 20 (23), 7297-7300.

[26] Glendinning, W. B.; Helbert, J. N., Handbook of Vlsi Microlithography: Principles,

Technology, and Applications. *Noyes Publications* **1991,** 1-1003.

[27] Yu, X.; Subramani, C.; Yang, X; Kim, C.K.; Rotello, V.M., Photooxidation of Nanopatterned Poly(chloromethylstyrene): Direct Formation of Crosslinked Aldehyde-Functionalized Films for Chemical Functionalization and Bioconjugation. *Macromolecular Rapid Communications* **2010,** 31, (9-10), 910-914.

SUMMARY AND FUTURE WORK

This thesis has focused on the development of new small molecule resist materials for high resolution patterning with both state of the art and emerging lithographic processes. Chapters two, three and six describe the synthesis, characterization and lithographic performance of molecular glass (MG) photoacid generators, MG resists and inorganic-organic hybrid nanoparticle photoresists. Chapter four investigates the patterning mechanism of the nanoparticle resists, demonstrating that a new patterning mechanism has been used to create high resolution patterns. Chapters five and six describe alternative lithographic processing techniques, sub-millisecond laser heating and vapor deposition. This work focused on the preparation of new materials for use with these new techniques.

Chapter two describes the synthesis and characterization of MG photoacid generators (PAGs). The large anion sizes of the PAGs were found to reduce the acid diffusion length, and the addition of multiple PAG functionalities to a single core was found to increase the quantum yield of the PAG. This research helped establish design guidelines for PAGs to reduce acid diffusion during post exposure bake while maintaining high sensitivity. E-beam patterning using the PAGs confirmed their ability to pattern high resolution features.

Chapter three discusses the synthesis and characterization of the new inorganic-organic hybrid materials. Various ligands and inorganic cores were characterized, which established design guidelines for the nanoparticle resists. Lithographic characterization of these materials revealed the materials are capable of producing sub-30 nm patterns with extremely high sensitivity and low line edge roughness when using EUV exposure. In addition, the inorganic

core provides excellent dry etch resistance, enabling the use of thin films to prevent pattern collapse.

As the nanoparticle system is a new concept in resist design, chapter four provides an in-depth analysis of the patterning mechanism. The resist is dual tone, capable of producing both positive and negative tone patterns, indicating a complex patterning mechanism. A wide variety of spectroscopic and lithographic techniques were applied to probe the patterning chemistry, and it was determined that a ligand exchange is occurring during UV exposure with the resist and the photogenerated acid, which changes the solubility of the nanopartcles. The post-exposure bake used to produce positive tone patterns is responsible for detaching the ligands from the nanoparticle surface in the unexposed regions, which prevents solubility in aqueous base.

Chapter five describes the characterization of acid diffusion during sub-millisecond laser heating using the MG PAGs characterized in chapter 2. A transition from the Willians-Landel-Ferry model of diffusion to an Arrhenius model is observed with the transition to shorter heating periods with higher temperatures. The MG PAGs have shown reduced acid diffusion lengths with laser heating, as well as the capability to pattern high resolution features, indicating these structures are favorable for use with laser-post exposure bake. The short duration of the heating cycle has been proven to limit the effects of heating over the glass transition temperature. MGs with low glass transition temperatures were not previously patternable with hotplate PEB, due to reflow during exposure to high temperatures on the hotplate. However, with laser heating, well-resolved sub-micron sized patterns were produced with MGs exhibiting a Tg as low as 38°C.

Chapter six outlines the design of small, rigid MG resists for use with vapor deposition. The thermal properties were analyzed, establishing a guideline for optimal resist architecture for high thermal stability. The lithographic performance of the MGs was compared using vapor

deposition and spin coating, as well as solvent and dry development. The all-dry processed resist was shown to produce 100 nm lines with very low line edge roughness. The MG resists used have shown the capabilities of the vapor deposition and dry development techniques as promising candidates for use in high resolution patterning.

The nanoparticle resists are some of the leading candidates for next generation patterning. The discovery of the patterning mechanism has provided a detailed understanding of this system, and can be used to further engineer the resists to further improve the lithographic properties. With the design guidelines established for the nanoparticles, as well as the MG resists and PAGs, the structures can be further optimized to improve their patterning qualities. The acid diffusion behavior under laser post exposure bake was well characterized, and the techniques used can be applied to screen resist materials for use with the laser heating technique. The discovery of the use of laser heating to produce patterns with low Tg resists enables a whole new class of materials that can be characterized as potential resists. As Tg is correlated with molecular size, smaller materials can now be considered, potentially improving resolution and line edge roughness of the lithographic patterns.